Reduced-Complexity Wireless Transceiver Architectures and Techniques for Space-Time Communications

Tsakalaki, Elpiniki

Publication date:
2012

Document Version
Early version, also known as pre-print

Reduced-Complexity Wireless Transceiver Architectures and Techniques for Space-Time Communications

Elpiniki Tsakalaki
Department of Electronic Systems
Aalborg University

A Dissertation Submitted to the Department of Electronic Systems and the Committee on Graduate Studies of Aalborg University in Partial Fulfillment of the Requirements for the Degree of Doctor of Philosophy

October, 2012

Assessment committee:

- Professor emeritus **Jørgen Bach Andersen**, Department of Electronic Systems, Aalborg University, Denmark (Chairman)
- Professor **Ralf R. Müller**, Department of Electronics and Communications, University of Science and Technology, Trondheim, Norway
- Professor **John Thompson**, School of Engineering, University of Edinburgh, United Kingdom

Abstract

The dissertation sheds light on the performance gains of multi-antenna systems when the antenna aspects and the associated signal processing and coding aspects are integrated together in a multidisciplinary approach, addressing a variety of challenging tasks pertaining to the joint design of smart wireless transceivers and communication techniques. These tasks are at the intersection of different scientific disciplines including signal processing, communications, antennas and propagation. Specifically, the thesis deals with reduced-complexity space-time wireless transceiver architectures and associated communication techniques for multi-input multi-output (MIMO) and cognitive radio (CR) systems as well as wireless sensor networks (WSNs). The low-complexity architectures are obtained by equipping the wireless transceiver with passive control ports which require the minimum amount of RF hardware while enhancing the communication and spectrum sensing performance under non-ideal propagation conditions. The combined signal and antenna models derived throughout the dissertation are generic with respect to their applicability to any kind of reconfigurable, adaptive, parasitic and tunable RF systems.

In the context of point-to-point MIMO communication, the passive control ports are employed for counteracting the near-field impairments represented by the local coupling and impedance mismatch, and the far-field impairments expressed by the spatial correlation and the diversity branch power imbalance. The communication RF ports are on the other hand employed for signal multiplexing. By this way, it is possible to obtain the optimal trade-off between correlation, coupling, antenna efficiency and spatial multiplexing gain over different channel scenarios.

In a multiuser scenario, the control ports are employed for synthesizing weakly-correlated virtual antennas out of single-radio user terminals, thus achieving the multiuser diversity gains with low user populations.

The thesis also addresses the CR design challenges in size and cost constrained devices. The concept of *spatial-spectrum sensing* is proposed and enabled via low-complexity agile and steerable single-radio reactance-assisted antennas. In this context, the control ports are employed for altering both the frequency and the spatial response of the antenna. The thesis further examines the spectrum sensing performance enhancement using such reconfigurable antenna systems, via switched diversity and analogue beamforming in clustering propagation environments. Last but not least, analogue interference suppression is enabled by emulating conventional baseband zero-forcing (ZF)

transceivers using a single-feed parasitic array.

In the last part of the thesis we propose novel space-time diversity techniques, such as the modified-Alamouti code, tailored for single-radio array architectures mounted on energy-constrained wireless sensor nodes. The proposed systems demonstrate significant total energy savings within simple *non-cooperative* communication setups compared to traditional cooperative diversity solutions under different realistic propagation conditions.

Acknowledgements

I would like to gratefully acknowledge the Aalborg University / Center for Teleinfrastructur (CTIF) and Athens Information Technology (AIT) collaboration for the joint offering of the doctoral program. My research work was funded by the Future and Emerging Technologies (FET) Programme within the Seventh Framework Programme (FP7) for Research of the European Commission, under FET-Open grant CROWN-233843 (Cognitive Radio Oriented Wireless Networks).

Deep gratitude is due to the doctoral thesis advisors, professors Constantinos Papadias and Ramjee Prasad, and associate professor Elisabeth de Carvalho for the valuable encouragement throughout the duration of the project.

Special thanks are conveyed to Dr. Osama Alrabadi for the collaborative research and the fruitful discussions which have been inspiring for my thesis project.

Many thanks are also to Jens Erik Pedersen, Dorthe Sparre, Iben Bondegaard Andersen, Chrysanthi Efstathiou for the invaluable help and assistance.

Last but not least, I cordially thank my beloved family for their continuous support during the three years of my doctoral study.

List of Acronyms and Abbreviations

Table 1: Acronyms and Abbreviations

Acronym / Abbrev.	Meaning
2D	2-dimensional
3D	3-dimensional
ADC	Analogue-to-Digital Converter
AoA	Angle of Arrival
AoD	Angle of Departure
AS	Angle Spread
ASVP	Anti-Series Varactor Pair
ATSC	Advanced Television Systems Committee
AWGN	Additive White Gaussian Noise
BER	Bit Error Rate
BPSK	Binary Phase-Shift Keying
BS	Base Station
CDF	Cumulative Distribution Function
CDI	Channel Distribution Information
CR	Cognitive Radio
CSIT	Channel State Information at the Transmitter
DAC	Digital-to-Analogue Converter
DMN	Decoupling and Matching Network
DPC	Dirty Paper Coding
DSP	Digital Signal Processor
EGC	Equal Gain Combining
ESPAR	Electronically Steerable Parasitic Array Radiator / Receptor
E3SPAR	Electronic Spatial Spectrum Sensing Passive Array Receptor

Table 1 Acronyms and Abbreviations (continued from previous page)

Acronym / Abbrev.	Meaning
FPGA	Field-Programmable Gate Array
FBR	Front-to-Back Ratio
GSM	Global System for Mobile Communications
IF	Intermediate Frequency
i.i.d.	Independent and Identically Distributed
LNA	Low Noise Amplifier
MAMP	Multi-Active Multi-Passive
MIMO	Multi-Input Multi-Output
MMSE	Minimum Mean Square Error
ML	Maximum Likelihood
MoM	Method of Moments
MRC	Maximum Ratio Combining
NLOS	No Line Of Sight
NTSC	National Television System Committee
MQAM	M-ary Quadrature Amplitude Modulation
SIMO	Single-Input Multi-Output
OB	Opportunistic Beamforming
OC	Optimum Combining
OSA	Opportunistic Spectrum Access
OSIC	Ordered Successive Interference Cancellation
PAS	Power Angle Spectrum
PAR	Peak-to-Average Ratio
PCB	Printed Circuit Board
PIFA	Planar Inverted-F Antenna
PILA	Planar Inverted-L Antenna
PDF	Probability Density Function
PU	Primary User
PIN	Positive Intrinsic Negative
PSD	Power Spectral Density
QoS	Quality of Service
RF	Radio Frequency
SC	Selection Combining
SIMO	Single-Input Multi-Output
SINR	Signal-to-Interference-plus-Noise Ratio

Table 1 Acronyms and Abbreviations (continued from previous page)

Acronym / Abbrev.	Meaning
SISO	Single-Input Single-Output
SM-HE	Spatial Multiplexing-Horizontal Encoding
SNR	Signal-to-Noise Ratio
SU	Secondary User
SPDT	Single Pole, Double Throw
STBC	Space-Time Block Code
S-PA	Switched Parasitic Array
S-UCA	Switched Uniform Circular Array
TS STC	Time-Switched Space-Time Code
UCA	Uniform Circular Array
UMTS	Universal Mobile Telecommunications System
UT	User Terminal
V-BLAST	Vertical-Bell Laboratories Layered Space Time
WiMAX	Worldwide Interoperability for Microwave Access
WSN	Wireless Sensor Network
ZF	Zero Forcing

Notations and Symbols

Throughout the PhD thesis, a bold small letter designates a vector and a bold capital letter designates a matrix of the specified size. Moreover, the following notations and symbols are used:

Table 2: Notations and Symbols

Symbol	Meaning
$(\cdot)^*$	Conjugate operator
$(\cdot)^{\mathrm{T}}$	Transpose operator
$(\cdot)^{\mathrm{H}}$	Conjuage transpose (Hermitian) operator
$(\cdot)^{-1}$	Inversion operator
$\mathbb{E}$	Mean value operator
$\lvert\cdot\rvert$	Amplitude of complex number
$\lVert\cdot\rVert$	Euclidian norm
$\lVert\cdot\rVert_{\mathrm{F}}$	Frobenius norm
$\langle\cdot\rangle_i$	The ith entry of a vector
$\langle\cdot\rangle_{ij}$	The (i,j) entry of a matrix
$\lambda_{\min}(\cdot)$	The minimum eigenvalue of a square matrix
$\mathbf{I}_R$	An identity matrix of size R
j	Imaginary unit
$\mathbb{C}$	The set of complex numbers
$\mathbb{R}$	The set of real numbers
$\Re\{\cdot\}$	The real part of the enclosed complex number
$\det(\cdot)$	Determinant of a matrix
$\mathrm{diag}(\cdot)$	A (square) diagonal matrix with the elements of the enclosed vector laid across the main diagonal of the matrix
ϑ, θ	Elevation angles
φ, ϕ	Azimuth angles
Ω	Solid angle

Table 2 Notations and Symbols (continued from previous page)

Symbol	Meaning
λ	Free-space carrier wavelength
$\kappa = 2\pi/\lambda$	Wavenumber

List of Figures

LIST OF FIGURES

List of Tables

LIST OF TABLES

Contents

1

Introduction

The area of smart multi-antenna systems is in the forefront of wireless research, largely due to their potential of improving radio communications by achieving high-rate data access for last-mile deployment, increased capacity of mobile services, enhanced quality of service (QoS), improved radio-frequency (RF) spectrum usage, and extended battery life in portable units. In this context, several solutions based on smart antenna technology have been proposed for next generation communication systems in order to solve heterogeneous problems related to coverage, throughput, spectral efficiency and energy consumption.

- Beamforming and spatial multiplexing systems: Multi-antenna systems are generally employed as power-focusing (beamforming) systems when operating in narrow clustering channels or in a low power regime, or else as spatial multiplexing systems when enough scattering in the surrounding environment exists. Specifically, the goal of smart antenna systems during initial stages of deployment was to improve link signal-to-noise ratios (SNRs) through directional array gain. This has been achieved via beamforming, the communication technique within which the array beams its signal in certain favored directions while minimizing the leaked power in other directions [BFBS02]. On the other hand, the demand for increased capacity in wireless networks has motivated recent research toward the development of algorithms and standards that exploit the spatial dimension available in multi-input multi-output (MIMO) systems [GF98; Tel99]. The MIMO technology enables spatial multiplexing where multi parallel data streams are communicated by equipping the transmitter and the receiver with multiple antennas, without sacrificing extra bandwidth or transmit power. Thanks to scattering environments that make the separation of the transmitted mixture of signals possible by decoding their unique spatial signatures, the data rate achieved by each individual antenna can be added up so that the multiple antennas act as a data-rate multiplier.

- Multiuser diversity systems: To cope with the increasing demands for high cell throughput, multi-antenna systems have also shown a great potential in over-

coming the difficulties related to the management of user mobility by providing the capability of exploiting the spatial diversity of the users themselves. Within the so-called multiuser diversity cellular systems, the users having the best link with respect to a random beamforming precoding are selected by the serving multi-antenna base station thus offering significant average cell throughput for moderate to large user populations [VTL02; SH05].

- Cognitive radio: The wide concept of cognitive radio (CR) has also been recently introduced so as to provide wireless systems with self-configuration capabilities, in particular for effectively detecting and exploiting the so-called "spectrum holes" (i.e., the underutilized spectrum bands) and maximizing the wireless network throughput [Hay05]. Multi-antenna systems play a significant role across different aspects of cognition. First, multiple antennas are employed to improve the spectrum sensing performance, so that spectrum holes are detected accurately and reliably [ZLPH09; ZLLZ10; YA09]. Moreover, smart antenna systems offer cognitive beamforming capabilities ensuring that the transmission among peer cognitive radios does not cause any harmful interference to unintended licensed spectrum / primary users (PUs) [GJMS09].

- Cooperative space-time processing: In distributed wireless systems, cooperative diversity can harness the advantages of multi-antenna systems without using many antennas on the same receive or transmit device. For distributed networks this is motivated by the need for simple, inexpensive nodes with limited processing power and few transmit or receive antennas per node. Space-time techniques have been employed to groups of energy-constrained single-antenna radios (e.g., wireless sensor nodes) forming a virtual antenna array at transmission or at reception. By utilizing such cooperative space-time schemes, it has been shown that significant energy savings can be realized compared to traditional node-to-node communication [CGB04; LCL05; Jay06].

Conventionally, multi-antenna systems refer to a set of active antenna elements where each element is connected to a separate RF chain. The intelligence is performed in the baseband stage where complex signal processing tasks are handled. Although multi-antenna systems are utilized to face the rising expectations in the performance of modern wireless networks, having proved to enhance wireless communications by theory and experimentation, they suffer from the following limitations:

- RF hardware complexity: The explosion in the antenna dimension where each antenna has its separate RF chain [including its own analogue-to-digital converter (ADC), digital-to-analogue converter (DAC), low-noise amplifier (LNA), power amplifier and intermediate frequency (IF) / RF filters] incurs a hardware implosion. The RF complexity is proportional to the number of antennas since each antenna has its separate RF frontend for independently modulating and demodulating the signals.

- Inter-chain interference: The use of non-ideal (dirty) RF components will result in a leakage (cross talk) among the parallel RF chains leading to reduced system performance [JM05].

- Circuit energy consumption: It refers to the DC power consumption of the power amplifier, the DAC, the mixer, the active filters in the transmit chain, the frequency synthesizer, the LNA, the IF amplifier, the ADC and the active filters in the receive chain. Circuit energy consumption increases as radios are added to the multiple antenna system while being critical to energy-constrained systems like small portable devices and wireless sensor nodes [CGB04].

- Synchronization requirements: Space-time communication implemented via node cooperation requires accurate synchronization among the cooperating radios in terms of carrier frequency, carrier phase, symbol timing, and timing phase [LCL05]. This requires proper equalization methods dealing with the time and frequency asynchronous issues (e.g., [VG06]). However such techniques are prohibited for terminals with limited processing power capabilities such as wireless sensor nodes.

On top of these limitations, the ongoing trend toward miniature, compact, and highly integrated telecommunication devices, typically limits the area devoted to the antennas. The following important challenges are introduced to multi-antenna devices under size constraints:

- Spatial correlation: Closely spaced antennas emit signals of correlated spatial signatures, resulting in reduced spatial diversity performance and channel capacity. For the system to achieve the performance promised by the celebrated MIMO capacity under rich scattering conditions, the antenna elements need to have a typical inter-element spacing of half the carrier wavelength [TLV05], thus leading to large array realizations.

- Antenna system efficiency: The strong mutual coupling among the closely spaced antenna elements, alters the input impedance seen by the RF ports, thus leading to a mismatch loss (i.e., some of the incident power is reflected back to the source). Moreover, some of the power that is supposed to be radiated in the space is dissipated in the real part of the neighboring antennas' terminations [MKAL06]. Such phenomena result in an overall poor antenna matching efficiency leading to a significant number of dropped service occurrences and limiting the overall system capacity.

These practical challenges entail that the performance of multi-antenna systems is especially sensitive to the antenna design, propagation environment and a host of other factors that were less significant in single-antenna designs. This places more emphasis on the proper modeling and understanding of such systems. Although many studies have given considerable attention to the performance analysis of multi-antenna systems in the context of coding and signal processing architectures, the investigation of the antenna aspect is mainly limited to the impact of the number of antenna elements with

little consideration on their radiation characteristics as well as the array geometry. Furthermore, conventionally deployed as time-invariant systems, the traditional multi-active antennas are not able to alter the propagation channel conditions. Adaptation to the channel, as it naturally changes over time or frequency, merely comes from smart signal processing at the digital baseband.

This work is motivated by the fact that there is an additional room for exploitation of the theoretical gains of multi-antenna systems when the antenna aspects and the associated signal processing and coding aspects are integrated together in a multidisciplinary approach. This dissertation addresses the limitations of multi-active antennas by introducing hybrid array topologies of (multi)-active multi-passive (MAMP) antenna systems and associated communication techniques suitable for such antenna architectures. The passive antenna ports are terminated with switched or tunable reactive loads that alter the boundary conditions of the antenna structure and, therefore, the propagation conditions. Firstly, this incurs advantages in terms of the antenna real-estate since the passive terminations are attached to low-cost switches / loads rather than to full RF chains; it should also be noted that in many of the proposed systems a single active port is maintained and yet we are able to provide the functionality of the conventional multi-antenna system through a smart reconfiguration of the passive port terminations. Furthermore, the antenna system is now able to alter the propagation channel by altering its radiation properties. This degree of freedom that does not exist in conventional antenna implementations permits us to treat the array configuration and its radiation properties as an additional component in the joint optimization of the system performance, thus allowing the system to approach its theoretical performance limits.

Side by side to the reduced-complexity hybrid MAMP systems, associated communication techniques fitting such antenna architectures are also proposed. The dissertation follows a holistic approach where the antenna model is integrated with the signal model and explains how to employ such systems for enhancing the system performance. The system performance ranges from ergodic / outage rate in point-to-point MIMO and average cell throughput in multiuser systems, to total energy consumption in wireless sensor networks (WSNs) and sensing performance via probability of detection in CR applications.

1.1 Multi-Port Network Model

The dissertation mainly deals with reactance-assisted (parasitic) antennas as a class of reduced-complexity MAMP arrays. The analysis throughout the thesis is kept tractable by mapping every network port to a separate radiator where all the radiators are physically identical. The radiators themselves are simplified by principally considering theoretical models of dipoles or monopoles. The far-field of such ideal antennas can be expressed analytically whereas, with other non-ideal structures, full-wave electromagnetic simulation is required in order to extract the active port patterns [Orp08; PDL06].

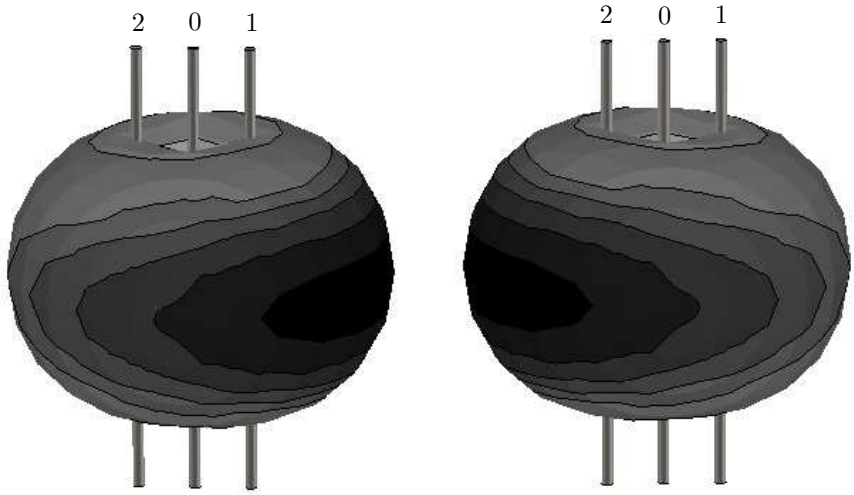

Beampattern A Beampattern B

Figure 1.1: A 3-element MAMP antenna structure comprised of three antenna elements (a central active dipole and two parasitic dipoles) and two swapped beampatterns. (The darker the color on contour map, the higher the beampatttern directivity.)

Nonetheless, the MAMP array model is quite general in the sense that it applies to any kind of reconfigurable, switched, tunable or adaptive antenna structure. It should be noted that, although the reduced-complexity antennas and the associated techniques proposed for improving different performance criteria are mainly analyzed using such theoretical antenna systems, in many cases we also provide examples of practical designs with non-ideal integrated antennas.

To illustrate the concept of the general MAMP network model, Figure 1.1 shows a 3-element MAMP antenna structure comprised of three dipole antennas. The central dipole is the active element (designated as port 0) and the other two dipoles are passive (ports 1 and 2). The coupling model of such antenna system is expressed as

$$\mathbf{w}_{\text{eq}} = (\mathbf{Z} + \mathbf{X})^{-1}\mathbf{u}, \tag{1.1}$$

where $\mathbf{u} = [1\ 0\ 0]^{\text{T}}$ and $\mathbf{Z} \in \mathbb{C}^{3\times 3}$ is the (standard) mutual impedance matrix[1] while $\mathbf{X} \in \mathbb{C}^{3\times 3}$ is a diagonal loading matrix. The vector $\mathbf{w}_{\text{eq}} \in \mathbb{C}^{3\times 1}$ is termed as the "equivalent weight vector" and represents the contribution of each dipole to the radiation pattern synthesis. The equivalent weight vector expresses the fact the antenna elements are controlled indirectly, thanks to the mutual interactions among the antenna ports, via

[1] $\mathbf{Z}$ is the impedance matrix obtained when terminating the ports with the standard terminations (generally 50 Ohm terminations).

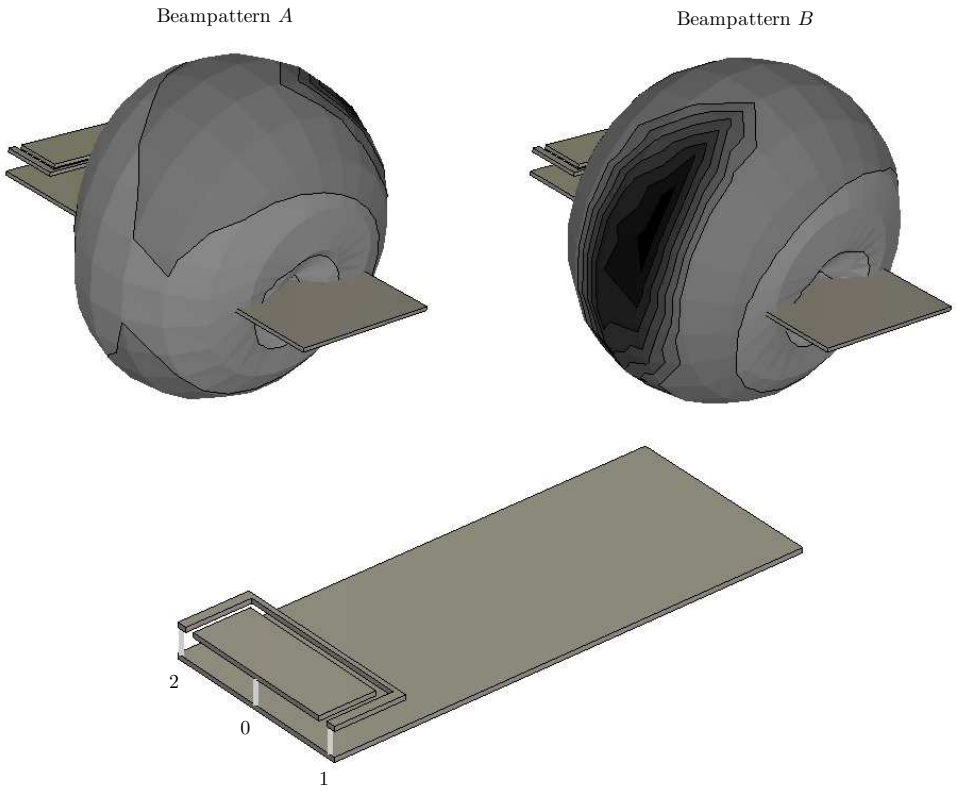

Figure 1.2: A 3-port MAMP antenna structure (comprised of a central active port and two passive ports) and two swapped beampatterns. (The darker the color on contour map, the higher the beampatttern directivity.)

the passive load terminations. In the absence of mutual coupling, $\mathbf{Z}$ becomes diagonal and $\mathbf{w}_{\text{eq}}$ collapses to the vector $\mathbf{u}$ (up to a scalar), thus the ability to control the array no longer exists.

By swapping the loads of the passive terminations, the MAMP beampattern is swapped (Beampatterns A and B in Figure 1.1) and the channel observed by the central active port is altered. The same network and coupling model [equation (1.1)] as well as the same control mechanism is valid for the (internal) mobile antenna shown in Figure 1.2. However, the passive antenna terminations in Figure 1.2 (ports 1 and 2) are attached physically to the same radiating structure which is geometrically different from the active radiating structure. Unlike Figure 1.1, the far-field of the antenna system in Figure 1.2 is a bulky superposition of the 3D complex port patterns (where each port pattern has two polarized components) requiring full-wave electromagnetic simulation.

Consequently, our choice on simple ideal antenna arrays is favored for avoiding overly complex analysis.

1.2 Related Work

The implementation challenges of multi-antenna technology have prompted the wireless communications community to actively research on reducing the complexity of space-time, CR and cooperative diversity systems. The work in the literature that is found related to the topic of this thesis is summarized below.

Beamforming

- Spatial combining / analogue beamforming: In this reduced-complexity approach the multi-antennas are simultaneously attached to a single RF chain. By controlling the time / phase delay and gain of the signals in each antenna path independently in the analogue domain (using RF phase shifters and attenuators), the multi-antenna system can improve the signal-to-noise-plus-interference ratio (SINR) by properly steering the beam gain and null whereas requirements on the power amplifiers can be also relaxed through spatial power combining [LPL06]. The spatial combining can be used as analogue beamformer, however having RF components in the path of every antenna increases the cost, RF complexity and more importantly the RF insertion losses. Moreover, this technique does not result in altering the antenna's boundary conditions and thus the channel properties. Both drawbacks are addressed by the following alternative analogue beamforming approach.

- Reactance-assisted analogue beamforming: The work in [OG00] introduced a single-radio parasitic antenna array known as electronic steerable parasitic array radiator (ESPAR) antenna. The ESPAR antenna is a smart antenna system that presents a significant advantage over its predecessors (like the Yagi-Uda antenna): it is able to control the beam patterns as any smart antenna system, while being implemented using a single active antenna element and a number of parasitic elements placed around the active element. The parasitic elements are short-circuited and loaded with variable reactors (varactors) that control the imaginary part of the parasitic elements input impedances. By adjusting the varactors response, the radiation pattern of the ESPAR antenna system can be controlled to direct its beams and nulls towards certain directions in an adaptive or predefined fashion [SHOK04]. In the present work, we expand this approach by utilizing similar systems for a) enhancing the selection combining performance of multiuser diversity systems, b) offering space-frequency agility to CR spectrum sensing antenna systems, and c) nulling the interference toward a set of unwanted receivers via a novel analogue orthogonal precoding scheme. Moreover, we utilize compact sized antenna systems for achieving the aforementioned tasks, thus the antenna matching efficiency plays an important role when optimizing the different performance criteria.

Spatial Multiplexing

- Analogue / single-radio MIMO: The doctoral study in [Alr11] introduced the concept of MIMO with a single-feed antenna array where spatial multiplexing is enabled by smartly encoding the different datastreams onto a set of parasitic elements loaded with passive reactances. Thus, the information is embedded within the angular variations of the beampatterns. However, such systems are limited to low-order PSK modulation whereas the implementation complexity increases dramatically for high order modulations and OFDM signaling. In the MIMO part of this thesis, we largerly address a modulation-independent approach by keeping the multiple radios (for spatial multiplexing) whereas the passive antenna terminations are exploited so as to offer antenna state reconfiguration. In this way, the antenna system can adapt itself to the propagation environment and combat the system and channel limitations that are critical to the performance of compact MIMO systems, such as the coupling and the spatial correlation.

Diversity

- Adaptive MIMO antenna (AdaM): [SPM06; Pin07] introduced an adaptive MIMO system comprising a set of active antennas coupled to a set of passive radiators closed on (i.e., terminated with) complex loads. However, the design was mainly intended for pattern diversity, by changing the passive radiators' loading conditions using PIN diodes, and operated at base stations where size and complexity are affordable. On the other hand, in this thesis we keep the antenna implementations compact thus addressing the size constraints of modern wireless devices. Moreover, unlike the electromagnetic modeling approach in [SPM06; Pin07], our models explicitly highlight the relation between the performance optimization criteria and the controllable passive terminations.

- State selection: It describes the technique in which the transceiver connects via a switching network to the state(s) corresponding to the strongest channel(s), where the state can refer to an antenna element, mode, port or polarization. Therefore, fewer RF chains are utilized and a simpler RF frontend architecture of reduced hardware complexity is achieved. In case of transmit state selection, a feedback path informing the transmitter which state(s) to select will be required. The most common approach in MIMO systems is antenna selection [SN04]. Traditionally implemented, antenna selection requires large spacing among the antennas so as to ensure uncorrelated (orthogonal) diversity branches. Nonetheless, our approach requires the passive antennas to be closely spaced to the active ones for effectively altering their radiation properties, following the seminal work of R. Vaughan [Vau98]. This naturally leads to compact antenna implementations where the passive antennas can be properly controlled to ensure the desired diversity branch orthogonality.

Spatial Oversampling

- In [WIK04; IWF02] the authors propose a reduced-complexity receiver architecture by oversampling the linear mixture of the received signals using a number of antennas and a single RF chain. The collected spatial-temporal samples permit demultiplexing the signal components at the receiver side without loss of information. On the other hand, the oversampling approach in [Bai08] using a rotating receive antenna is intended to maximize the link capacity in the general sense, i.e., no specific reception technique was targeted. However, sampling at a rate higher than the symbol rate leads to bandwidth expansion making the receiver sensitive to adjacent channel interference. It should be noted that in our work, antenna system reconfiguration happens at a much lower rate, e.g., according to the slow-varying channel statistics, leading to simpler control circuit designs.

Simultaneous space-frequency control

- Frequency-agile small smart antenna: The publication in [LGL10] deals with a space-steerable frequency-agile ESPAR antenna in a study parallel and independent to our work on a similar system concept [TAPP10d; TAPP10c]. However, unlike [LGL10], our work includes full antenna modeling highlighting the new concept of spatial-spectrum sensing.

Cooperative communication

- The last chapter of the thesis suggests energy-efficient non-cooperative space-time diversity schemes and associated transceiver architectures for WSNs that do not require cooperation strategies that require sharp time and frequency synchronization. In the literature, there has been proposed an asynchronous approach based on selection cooperation [BA08]. It refers to a technique where a source node communicates with a destination node using the "best" relay node among a pool of relays. The best relay node is the relay with the best instantaneous relay-destination channel. This scheme requires no time and frequency synchronization and achieves good performance in terms of outage probability for networks with more than three relays. However, the requirement of the additional best relay node increases the circuit energy and thus the total system energy consumption. On the contrary, our proposed non-cooperative diversity schemes are applied to simple single-RF antenna source and destination nodes and thus come at no additional circuit energy cost.

1.3 Thesis Outline

The rest of the thesis is organized as follows:

- Section 1.4: The last section of Chapter 1 summarizes the papers published within this PhD study.

- Chapter 2: In this chapter the hybrid MAMP antenna structures are employed to address the limited performance of MIMO terminals in realistic non-ideal channel conditions. The MAMP antenna is capable of reconfiguring according to the structure of the RF propagation channel: the antennas transmission parameters (transmit covariance and antenna efficiency) can be properly adjusted via parasitic (passive) radiators attached to tunable loads based on the long-term channel statistics. The hybrid MAMP array is tractably analyzed using the active element response and current vectors, all being functions of the parasitic loading. The MAMP arrays target at maximizing the ergodic or the outage rate of MIMO links (Section 2.1) as well as the average throughput performance of multiuser diversity systems (Section 2.2). The proposed antenna systems can be limited to practical dimensions whereas the passive antennas require no extra RF hardware, thus meeting the cost, space and power constrains of the users mobile terminals. Design examples and performance evaluation are provided for point-to-point MIMO and multiuser diversity systems under realistic poor scattering environments and compactness constraints.

- Chapter 3: Within the CR paradigm, this part of the thesis addresses the major design challenges of antenna systems intended for CR transceivers under compactness constraints. A new approach is proposed based on parasitic antenna theory via the ESPAR antenna which is a type of MAMP architecture with a single active element described in Section 3.1. The approach aims at making spatial spectrum sensing feasible for compact lightweight terminals. The idea developed in Section 3.2 is to replace the wideband antenna required for sensing over a large bandwidth by a tunable narrowband antenna for both sensing and communication purposes. The flexibility of the proposed antenna system lies in its capability to scan both the frequency and spatial resource dimensions simultaneously via a single RF chain within a miniaturized antenna system. This is done by properly tuning a set of reactive loads connected to a group of parasitic elements closely coupled to the driven element. By doing so, the operational frequency subband leaps to another subband (frequency tuning). Moreover, at every subband, circular permutations of the reactive loads rotate the narrowband beam pattern to different angular positions, giving the cognitive transceiver the capability of sensing over various segments of the space. Further, the work in Section 3.3 shows that beampattern directionality leverages the performance of spectrum sensing algorithms like energy detection by enhancing the receive SNR, whereas the selection combining across the weakly correlated beampatterns gives rise to a diversity action further boosting the probability of sensing detection. Finally, Section 3.4 presents an ESPAR-based analogue interference cancellation method for nulling the interference toward a number of licensed spectrum users with highly reduced RF complexity.

- Chapter 4: In this chapter, the thesis exploits recent advances in smart-antenna wireless sensor transceiver prototypes enabling the existence of more than one

antenna within single-radio transceiver architectures. Exploiting such capability, the thesis proposes simple non-cooperative space-time techniques for single-RF switched-antenna systems that reduce significantly both the transmission and the circuit energy consumption in WSNs. The energy savings of the suggested schemes are shown not only against conventional single-input single-output (SISO) systems, but also against cooperative diversity schemes in Rayleigh and log-normal shadowed Rayleigh fading channels with distance-based path loss.

- Chapter 5: The last chapter summarizes the basic conclusions of the thesis.

1.4 Publications

1.4.1 Thesis Publications

The work of the doctoral project has resulted in the following publications:

Journal papers:

- Elpiniki Tsakalaki, Osama N. Alrabadi, Constantinos B. Papadias, Ramjee Prasad, "Reduced complexity radio architecture for enhanced receive selection combining in multiuser diversity systems," *International Journal of Antennas and Propagation, Special Issue on MIMO Antenna Design and Channel Modeling*, vol. 2012, Article ID 454210, 2012. [TAPP12b]

- Elpiniki Tsakalaki, Osama N. Alrabadi, Antonis Kalis, Constantinos B. Papadias, Ramjee Prasad, "Non cooperative space-time communication for energy efficiency in sensor networks," *IEEE Transactions on Communications*, vol. 60, no. 1, pp. 48-54, January 2012. [TAPP12a]

- Elpiniki Tsakalaki, Osama N. Alrabadi, Constantinos B. Papadias, Ramjee Prasad, "Adaptive reactance-controlled antenna systems for MIMO applications," *IET Microwave Antennas & Propagations Journal, special issue on RF/Microwave Commun. Subsystems for Emerging Wireless Technologies*, vol. 5, no. 8, pp. 975-984, June 2011. [TAPP11a]

- Elpiniki Tsakalaki, Osama N. Alrabadi, Constantinos B. Papadias, Ramjee Prasad, "Spatial spectrum sensing for wireless handheld terminals: design challenges and novel solutions based on tunable parasitic antennas," *IEEE Wireless Communications Magazine, special issue on Dynamic Spectrum Management in Wireless Networks*, vol. 17, no. 4, pp. 33-40, August 2010. [TAPP10d]

Conference papers:

- Elpiniki Tsakalaki, David Wilcox, Elisabeth de Carvalho, Constantinos B. Papadias, Tharmalingam Ratnarajah, "Spectrum sensing using single-radio switched-beam antenna systems," To Appear, *7th International ICST Conference Cognitive Radio Oriented Wireless Networks and Communications (Crowncom)*, Stockholm, Sweeden, June 2012. [TWdCR12]

- Elpiniki Tsakalaki, Osama N. Alrabadi, Constantinos B. Papadias, Ramjee Prasad, "Analogue orthogonal precoding using reduced complexity transceivers," *IEEE International Symposium on Antennas and Propagations (APSURSI)*, pp. 2845-2848, Spokane, Washington, July 2011. [TAPP11b]

- Elpiniki Tsakalaki, Osama N. Alrabadi, Constantinos B. Papadias, Ramjee Prasad, "An adaptive reactance-assisted antenna system for the MIMO uplink," *17th IEEE International Conference on Electronics, Circuits, and Systems (ICECS)*, pp. 1228-1231, Athens, Greece, December 2010. [TAPP10a]

- Elpiniki Tsakalaki, Osama N. Alrabadi, Constantinos B. Papadias, Ramjee Prasad, "Enhanced selection combining for compact single RF user terminals in multiuser diversity systems," *21st Annual IEEE International Symposium on Personal, Indoor and Mobile Radio Communications (PIMRC)*, pp. 951-954, Istanbul, Turkey, September 2010. [TAPP10b]

- Elpiniki Tsakalaki, Osama N. Alrabadi, Constantinos B. Papadias, Ramjee Prasad, "Spatial spectrum sensing for cognitive radios via miniaturized parasitic antenna Systems," *5th International ICST Conference Cognitive Radio Oriented Wireless Networks and Communications (Crowncom)*, pp. 1-5, Cannes, France, June 2010. [TAPP10c]

These publications relate to the PhD thesis chapters as shown in the following table:

Table 1.1: Thesis chapters and corresponding publications

Chapter / Section		Publication
Chapter 2	Section 2.1	[TAPP11a],[TAPP10a]
	Section 2.2	[TAPP12b],[TAPP10b]
Chapter 3	Section 3.2	[TAPP10d],[TAPP10c]
	Section 3.3	[TWdCR12]
	Section 3.4	[TAPP11b]
Chapter 4		[TAPP12a]

Other publications were done in parallel to the doctoral study. The work therein is not directly related with the material presented in this thesis but has extended the author's knowledge in the field of digital beamforming for (base station) antenna arrays.

Journal paper:

- Osama N. Alrabadi, Elpiniki Tsakalaki, Howard Huang, Gert Pedersen, "Beamforming via large and dense antenna arrays above a clutter," *2nd Round Review, Journal on Selected Areas in Communications (JSAC) - Special Issue on Large-Scale Multiple Antenna Wireless Systems*, 2013.

Conference paper - this work was conducted during the author's internship in the Innovation Center at Nokia Siemens Networks, Madrid, Spain:

- Elpiniki Tsakalaki, Luis Ángel Maestro Ruiz de Temiño, Tomi Haapala, Javier López Román, Miguel Arranz Arauzo, "Deterministic beamforming for enhanced vertical sectorization and array pattern compensation," *6th European Conference on Antennas and Propagation (EuCAP)*, pp. 2789-2793, Prague, Czech Republic, March 2012.

1.4.2 Communication of Scientific Knowledge

Aside from the conference presentations of the aforementioned conference papers, the research work was also communicated in the following lectures / seminars / tutorials:

- Elpiniki Tsakalaki, "Spectrum sensing using single-radio switched-beam antenna systems," Research Seminar, Athens Information Technology, Athens, Greece, 15 February 2012.
- Constantinos B. Papadias, Antonis Kalis, Elpiniki Tsakalaki, "Single-radio antenna arrays for reduced transmission power and circuit energy consumption," Technical Presentation, *2nd International Workshop on Wireless Green Networks, GREEN Networks: Achievements and challenges*, GREENTIC, Casablanca, Morocco, 2 November 2011.
- Elpiniki Tsakalaki, "Reduced-complexity transceiver architectures for cognitive radio systems," Technical Presentation, *1st International Workshop on Compact Antennas (COMPASS), IET Antennas & Propagation Network*, Athens, Greece, 1 March, 2011.
- Constantinos B. Papadias, Osama N. Alrabadi, Elpiniki Tsakalaki, "Compact antenna systems," Tutorial, *3rd International Symposium on Applied Sciences in Biomedical and Communication Technologies (ISABEL)*, Italy, Rome, 7-10 November 2010.

2

Multi-Active Multi-Passive Antenna Arrays for MIMO and Multiuser Diversity Systems

This chapter addresses the limited performance of MIMO systems under the real-life effects of spatial correlation and antenna mutual coupling. For this reason, in Section 2.1 we propose an adaptive MAMP antenna system capable of changing its transmission parameters via passive radiators attached to tunable loads, according to the structure of the RF propagation channel. The hybrid MAMP array structure is tractably analysed using the active element response vector (instead of the classical steering vector) and the active element current vector (all being functions of the variable loading). The adaptive MAMP system targets at maximising tight MIMO ergodic and outage rate bounds, relying on partial channel knowledge when tuning to a different loading state for optimising the rate of communication. The proposed adaptive MAMP system can be limited to practical dimensions whereas the passive antennas require no extra RF hardware, thus meeting the cost, space and power constraints of the users' mobile terminals. The simulation results show that the adaptive MAMP system, thanks to its 'adaptivity', is able to achieve satisfactory performance even in poor scattering environments whereas a significant part of the mutual information that is lost owing to the spatial correlation and the electromagnetic coupling is successfully retrieved.

Section 2.2 then deals with the problem of the poor performance of antenna selection for compact user terminals in multiuser diversity systems. Although antenna selection is a simple and efficient technique for enhancing the downlink performance of multiuser diversity systems, the large antenna inter-element spacing required for achieving spatial diversity is prohibitive for user terminals due to size restrictions. In order to allay this problem, we propose miniaturized switched-beam MAMP receiver designs assisted by low-cost passive reflectors. Unlike conventional spatial receive diversity systems, the proposed angular diversity architectures occupy a small volume whereas the antenna system properties are optimized by controlling the strong reactive fields present at small dimensions. The systems are designed for maximum antenna efficiency and low inter-

beam correlation, thus yielding K *practically uncorrelated* receive diversity branches. The simulation results show that the proposed enhanced diversity combining systems improve the average throughput of a multiuser network outperforming classical antenna selection especially for small user populations and compact user terminal size.

2.1 Adaptive reactance-controlled antenna systems for MIMO applications

MIMO systems have received great focus recently as they achieve remarkable spectral efficiencies. The exceptional MIMO capacity promised by the celebrated log-det formula increases almost linearly with the number of transmit-receive antennas [GF98]. However, in real-life propagation, many factors may affect the performance of MIMO communication systems. The two major factors[1] are the spatial correlation [TLV05] among the channels and the mutual coupling among the antenna elements [RS01]. The spatial correlation is determined by both the antenna system (e.g. antenna topology, inter-element spacing and termination [WJ04]) as well as the RF propagation channel (distribution of the scatterers, distance between the transmitter and the receiver, etc). On the other hand, the cross-talk between the closely-spaced antenna elements, referred to as mutual coupling, may be unavoidable when considering small portable lightweight terminals with limited physical area. The two factors (spatial correlation and mutual coupling) are not independent from each other. For example, it was first noted in [EYT91] that the mutual coupling may decorrelate the received signals. However, the mutual coupling also results in impedance mismatch and thus degrades the maximum average power the antenna system can extract from the field [LOKM05]. The negative effects of the spatial correlation and the mutual coupling can be jointly mitigated by incorporating a decoupling and matching network just before the antenna system [HSB+06], within what is referred to as multi-port conjugate matching or bilateral Hermitian matching [WJ04]. However, such a sophisticated network is difficult to design when considering many antenna elements, besides its negative impact on the system bandwidth [MKAL06]. Consequently, the classical uncoupled matching techniques like a) the characteristic impedance (or Z_o) termination, which is the simplest type of termination, and b) the self-impedance termination which is optimal under no mutual coupling, are preferred for their simple deployments though they provide suboptimal performance. An alternative optimal single-port matching technique was proposed in [FFLT08] where the ports of the antenna system are matched *individually* without any shunt connections. However, in [FFLT08] *matching the antenna system for the maximum average rate can be optimized only for a specific channel distribution rather than being dynamic to different channel distributions* expressed by the time-varying power angle spectrum (PAS) seen by the transceiver. It is the subject of this work to tackle this limitation by proposing a novel adaptive MAMP antenna system capable of

[1] Other factors include the mutual interference among the parallel RF chains as well as the near-field losses raised by the user's hand and head.

controlling its correlation and coupling properties based on the distribution of the scatterers within the channel (long-term channel statistics). Specifically, we terminate the active antennas with the simplest type of termination, i.e., the Z_o termination, while controlling the spatial correlation and coupling according to the time-varying PAS seen by the transceiver, via external *passive tunable radiators* that require no extra RF hardware. By this way, we keep the implementation simple and allow the antenna system to *adapt to a dynamic PAS*.

It should be noted that adaptive MAMP systems assisted with reactance-loaded radiators have gained great attention in recent years [BB82]-[AKPP09b]. In [BB82], adaptive tuning using varactor diodes was introduced in order to increase the operational frequency bandwidth of mictrostrip patch antennas. [RHR96] and [HKCK97] describe dynamic matching for microstrip patch antennas using varactor diodes in order to combat the detuning from the desired resonant frequency caused by the interaction of the antenna with its local environment (e.g., antenna mounting and effects of user's hand or body). In [OG00] and [SHOK04], a smart antenna system, known as the 7-element ESPAR, composed of 6 tunable passive radiators surrounding a central active one, has been presented for analogue beam / null steering. The 7-element ESPAR was mainly proposed for wireless routers and laptops due to its large size and the complexity of its control circuitry. [SPM06] introduced an adaptive MIMO (AdaM) system comprising a set of active antennas coupled to a set of passive radiators closed on (i.e., terminated with) complex loads. The design was mainly intended for pattern diversity, by changing the passive radiators' loading conditions using PIN diodes, and operated at base stations where size and complexity are affordable. Further, a polarized Yagi-Uda array with 4 driven (active) ports has been proposed for multi-antenna terminals employing spatial multiplexing in [HNT+07]. In [APK+09; AKPP09b], the authors proposed analogue MIMO transmission techniques via a single active transmit antenna strongly coupled to two closely-spaced passive radiators used for directly encoding PSK symbols on the antenna far-field. The adaptive MAMP system proposed herein is different from its predecessors (ESPAR, AdaM and Yagi-Uda-based antenna systems) in the sense that:

- Unlike prior art, the proposed adaptive MAMP antenna system exploits the multiple active antennas for spatial multiplexing, and the multiple passive antennas for obtaining dynamic diversity (according to the time-varying PAS). This is in accordance with the trend of the future standards [lte] regarding the MIMO uplink where a subset of the available antennas may be used for transmission (this is intended for reducing the number of costly power amplifiers in the transmit RF chains). The proposed adaptive MAMP system is welcome in the sense that it exploits the already non-utilized antennas as tunable radiators.

- The current approach relies on partial channel knowledge, and thus the channel distribution information (CDI) represented by the PAS can be provided to the transmitter via a low-rate feedback channel (it should be noticed that the previous antenna systems require full channel state information to operate).

- The proposed adaptive MAMP system can be operated at lightweight user terminals thus addressing the cost, DC power and size constraints of small handheld devices. This is because the passive radiators do not require any RF hardware [Vau98] and need to be closely-spaced to the active transmit antennas for better control.

2.1.1 Adaptive MAMP Antenna System Description

We propose a transmit adaptive MAMP system capable of controlling the spatial correlation via a set of passive radiators based on the slow changing channel statistics. The passive radiators are attached to tunable imaginary loads and tuned via a simple DC control circuit, e.g., by properly reverse biasing a varactor diode (or a configuration of varactor diodes), a specific reactance can be obtained across the terminals of the diode. Under the assumption that the transmitter is equipped with the proposed adaptive MAMP system, we start by deriving the equivalent transmit spatial covariance matrix as a function of the adaptive array loading. Moreover, we express the transmit efficiency seen by the active antenna elements also as a function of the array loading. For the tractability of our analysis, we assume the kth active antenna attached to the characteristic impedance $Z_k = Z_\mathrm{o}$, whereas the kth passive radiator attached to an imaginary impedance $Z_k = \mathrm{j}X_k$.

2.1.1.1 Transmit Covariance

The spatial correlation and the average power imbalance across the channels on the transmitter side can be both accounted for by calculating the transmit covariance matrix. The transmit covariance matrix, which is a non-normalized correlation matrix, can be obtained by cross-correlating the active element responses of the corresponding active antennas [Ree02], [Fei08]. In order to calculate the active antenna response [Poz94], we first define an array of $\mathcal{K}$ antenna elements, out of which $\mathcal{K}_\mathrm{T}$ are active and the rest are passive. The total array far-field can be expressed as

$$\mathcal{B}_\mathrm{tot}(\varphi) = \boldsymbol{\alpha}^\mathrm{T}(\varphi) \underbrace{(\mathbf{Z}+\mathbf{X})^{-1}\mathbf{v}}_{\mathbf{i}_\mathrm{tot}}, \tag{2.1}$$

where $\boldsymbol{\alpha}(\varphi) \in \mathbb{C}^{\mathcal{K}\times 1}$ is the steering vector obtained from the local geometry of the antenna system, φ is the angle of departure (AoD) in the azimuth plane, $\mathbf{Z} \in \mathbb{C}^{\mathcal{K}\times\mathcal{K}}$ is the mutual impedance matrix and $\mathbf{X} \in \mathbb{C}^{\mathcal{K}\times\mathcal{K}}$ is a diagonal matrix whose (k,k) entry is $\langle\mathbf{X}\rangle_{kk} = Z_\mathrm{o}$ if the kth element is active, and $\langle\mathbf{X}\rangle_{kk} = \mathrm{j}X_k$ if the kth element is passive. $\mathbf{v}$ is the $\mathcal{K}\times 1$ vector of excitations, whose kth entry is $\langle\mathbf{v}\rangle_k = v_k \in \mathbb{C}$ if the kth element is active, and $\langle\mathbf{v}\rangle_k = 0$ if the kth element is passive, and $\mathbf{i}_\mathrm{tot} = (\mathbf{Z}+\mathbf{X})^{-1}\mathbf{v} \in \mathbb{C}^{\mathcal{K}\times 1}$ is the total current vector, i.e., the vector of currents induced on the $\mathcal{K}$ elements. The hybrid antenna structure within which some antenna elements are active and some are passive complicates the analysis of the MIMO system. In order to work around this problem, we reformulate the far-field as a linear superposition of the active element

responses onto which the transmit voltage signals are mapped, thus we rewrite (2.1) as

$$\mathcal{B}_{\text{tot}}(\varphi) = \boldsymbol{\mathcal{B}}^{\text{T}}(\varphi)\mathbf{v}_{\text{s}}, \tag{2.2}$$

where $\mathbf{v}_{\text{s}}$ is a $\mathcal{K}_{\text{T}} \times 1$ vector of the non-zero entries of $\mathbf{v}$ (i.e., the complex data symbols to be transmitted) and $\boldsymbol{\mathcal{B}}(\varphi)$ is a $\mathcal{K}_{\text{T}} \times 1$ vector of the active element responses, whose kth entry is obtained from (2.1) as

$$\langle \boldsymbol{\mathcal{B}}(\varphi) \rangle_k = \mathcal{B}_{\text{tot}}(\varphi)|_{\mathbf{v}=\mathbf{u}_k}, \tag{2.3}$$

where $\mathbf{u}_k$ is a $\mathcal{K} \times 1$ vector of all zeros except a unity voltage signal at the position of the kth active antenna element. Since $\mathcal{B}_{\text{tot}}(\varphi)$ is function of the variable loads $\text{j}X_k$, we get $\boldsymbol{\mathcal{B}}(\varphi)$ as a function of the array loading as well. The $\mathcal{K}_{\text{T}} \times \mathcal{K}_{\text{T}}$ transmit covariance matrix can now be directly obtained from (2.3) as [Ree02]

$$\mathbf{R}_{\text{T}} = \int_{-\pi}^{+\pi} \boldsymbol{\mathcal{B}}(\varphi)\boldsymbol{\mathcal{B}}^{\text{H}}(\varphi)\mathcal{A}(\varphi) \cdot d\varphi, \tag{2.4}$$

where $\mathcal{A}(\varphi)$ is the PAS of the channel and $\frac{1}{2\pi}\int_{-\pi}^{+\pi} \langle \boldsymbol{\mathcal{B}}(\varphi) \rangle_k \langle \boldsymbol{\mathcal{B}}(\varphi) \rangle_k^* \cdot d\varphi = 1$. Notice that the *mutual coupling is inherently taken into consideration within the active element response calculation*. By this way, the array has the ability to control its transmit covariance matrix as well as the electromagnetic coupling among the active antennas, by properly tuning its imaginary loads based on the knowledge of the PAS.

2.1.1.2 Transmit Efficiency

The efficiency of a given antenna system is the ratio of the total power transmitted by the antenna system (denoted by P_{T}) to the total power fed into the antenna system (denoted by P_{I}). The efficiency calculation of a hybrid MAMP antenna structure is facilitated by accommodating the active current vectors [RK05]. Knowing the coupling matrix $(\mathbf{Z}+\mathbf{X})^{-1}$, we can set up the equation for the vector of induced currents on the antenna elements $\mathbf{i}_k \in \mathbb{C}^{\mathcal{K}\times 1}$ when the kth active element is excited while terminating the rest of the elements with their corresponding source/load impedances as

$$\mathbf{i}_k = \mathbf{i}_{\text{tot}}(\varphi)|_{\mathbf{v}=\mathbf{u}_k}. \tag{2.5}$$

By changing the imaginary loads of the passive antenna elements, a mismatch between the source impedance and the input impedance seen by every active antenna may take place. The input impedance $Z_{\text{in},k}$ of the kth active element and the corresponding reflection efficiency due to impedance mismatch can be respectively written as

$$Z_{\text{in},k} = \langle \mathbf{Z} \rangle_{kk} + \frac{1}{\langle \mathbf{i}_k \rangle_k} \cdot \sum_{j\neq k,\ j\in\{1,\ldots,\mathcal{K}\}} \langle \mathbf{Z} \rangle_{kj} \langle \mathbf{i}_k \rangle_j \tag{2.6}$$

and

$$\Delta_{\mathrm{ref},k} = 1 - |\Gamma_k|^2, \quad 0 \leq \Delta_{\mathrm{ref},k} \leq 1, \quad \text{where } \Gamma_k = (Z_{\mathrm{in},k} + Z_{\mathrm{o}})^{-1}(Z_{\mathrm{in},k} - Z_{\mathrm{o}}), \quad (2.7)$$

and $\Delta_{\mathrm{ref},k}$ is the reflection efficiency at the kth active element. On the other hand, the total power dissipated in the loads of the elements when the kth active one is excited is given by $P_k = Z_{\mathrm{o}} \sum_{j \neq k,\ j \in \{1,\ldots,\mathcal{K}\}} |\langle \mathbf{i}_k \rangle_j|^2$ and the corresponding absorption efficiency is

$$\Delta_{\mathrm{abs},k} = 1 - \frac{Z_{\mathrm{o}} \sum_{j \neq k,\ j \in \{1,\ldots,\mathcal{K}\}} |\langle \mathbf{i}_k \rangle_j|^2}{\Re\{Z_{\mathrm{in},k}\} |\langle \mathbf{i}_k \rangle_k|^2}, \quad 0 \leq \Delta_{\mathrm{abs},k} \leq 1 \quad (2.8)$$

Now, assuming negligible ohmic and dielectric losses, we can write the radiation efficiency corresponding to the kth active element as [RK05]

$$\Delta_k = \Delta_{\mathrm{ref},k}\, \Delta_{\mathrm{abs},k}, \quad 0 \leq \Delta_k \leq 1 \quad (2.9)$$

and define the antenna efficiency matrix $\mathbf{\Delta}_{\mathrm{T}}$ as a $\mathcal{K}_{\mathrm{T}} \times \mathcal{K}_{\mathrm{T}}$ diagonal matrix whose (k,k) entry is equal to $\langle \mathbf{\Delta}_{\mathrm{T}} \rangle_{kk} = \Delta_k$. From (2.1) and (2.5), $\mathbf{i}_k$ is function of the variable loads $\mathrm{j}X_k$. Thus, we get $\mathbf{\Delta}_{\mathrm{T}}$ as a function of the array loading as well. As a result, the efficiency of the adaptive MAMP system can be controlled via adaptively tuning the system's passive loads.

It should be noted that the coupling matrix $(\mathbf{Z}+\mathbf{X})^{-1}$ in (2.1) constitutes a *natural* precoder [CO07] operating on the transmit signals which is *nonlinear* with respect to the variable antenna loading (due to the matrix inverse). Unlike conventional baseband precoding techniques which simply map the signals from one space into a different signal space [VP07], *the proposed precoder has the additional capability of controlling the fundamental characteristics of the antenna system represented by the electromagnetic coupling and the antenna efficiency.*

2.1.1.3 Reactance Considerations

Each parasitic element of the adaptive MAMP system is terminated with a variable reactive load. A specific reactance value can be obtained by impressing a certain voltage on the terminals of a varactor diode or a configuration of varactor diodes. Employing varactor diodes in practice yields certain design considerations for a rigorous analysis of which the reader may refer to [Sch04]. In general, varactor diodes are nonlinear elements, thus, the transmit adaptive MAMP system may drive the varactors into non-linearity creating harmonic distortion. This can potentially lead to transmission power degradation as well as to unlicensed spectrum pollution unless special filtering is applied. The harmonic distortion effect can be mitigated by distributing the transmit power over multiple varactors, e.g., using the anti-series varactor pair (ASVP) configuration equivalent of a single varactor [Sch04, Figure 6.4]. Furthermore, varactor diodes are purely capacitive loads, thus only negative reactance values can be generated. In order to improve the feasible reactance range, transmission lines could be included.

For example, using a 3 parallel varactor loaded 50 Ohm transmission line arrangement [Sch04, Figure 6.5], the feasible reactance range spans all possible values. Notice that a transmission line arrangement can be combined with ASVP configuration for additional harmonic distortion suppression benefits.

2.1.2 Adaptive Loading

In this section, we define the optimal adaptive MAMP system loading as the set of loads that maximizes the ergodic or the outage rate of communication based on the CDI. For this reason, elegant bounds on the ergodic and the outage capacity which are already proposed in the literature are slightly modified to account for the transmit efficiency, and redefined in the sense that the transmit covariance matrix includes the effect of the mutual coupling, all being functions of the $\mathrm{j}X_k$ variables. The bounds serve as useful optimization criteria when operating the proposed adaptive system in a channel of a known structure.

We consider a narrowband, flat-fading, quasi-static, point-to-point communication link where the unit-energy signals $\mathbf{v}_\mathrm{s}$ are transmitted using the $\mathcal{K}_\mathrm{T}$ active antennas and received using a uniform-linear array (ULA) of $\mathcal{K}_\mathrm{R}$ antennas. Generally, the kth active antenna transmits $\sqrt{a_k P_\mathrm{T}}\,\langle \mathbf{v}_\mathrm{s}\rangle_k$, where $P_\mathrm{T} = \Delta_k P_\mathrm{I}$ is the transmit power, P_I is the input power and a_k, $0 \leq a_k \leq 1$ is the portion of power allocated to the kth active antenna such that $\sum_{k=1}^{\mathcal{K}_\mathrm{T}} a_k = 1$. Obviously, a_k can be treated as an additional degree of freedom when optimizing the rate of communication. For a uniform power distribution across the transmit antennas, we simply have $a_k = (\mathcal{K}_\mathrm{T})^{-1}$. Let $\mathbf{A}_\mathrm{T}$ be a $\mathcal{K}_\mathrm{T} \times \mathcal{K}_\mathrm{T}$ diagonal matrix[1] whose (k,k) entry is $\langle \mathbf{A}_\mathrm{T}\rangle_{kk} = a_k$. Using the well-established Kronecker model [SFGK00], the end-to-end received signal model can be written as [CO07]

$$\begin{aligned}\mathbf{y} &= \sqrt{P_\mathrm{T}}\underbrace{\mathbf{R}_\mathrm{R}^{1/2}\mathbf{H}_\mathrm{w}\mathbf{R}_\mathrm{T}^{1/2}}_{\mathbf{H}}\,\mathbf{A}_\mathrm{T}^{1/2}\mathbf{v}_\mathrm{s} + \mathbf{n}\\ &= \sqrt{P_\mathrm{I}}\underbrace{\mathbf{R}_\mathrm{R}^{1/2}\mathbf{H}_\mathrm{w}\mathbf{R}_\mathrm{T}^{1/2}}_{\mathbf{H}}\,(\mathbf{\Delta}_\mathrm{T}\mathbf{A}_\mathrm{T})^{1/2}\mathbf{v}_\mathrm{s} + \mathbf{n}\end{aligned} \tag{2.10}$$

such that $\mathbf{R}_\mathrm{R} \in \mathbb{C}^{\mathcal{K}_\mathrm{R}\times\mathcal{K}_\mathrm{R}}$ is the receive covariance matrix and $\mathbf{H} = \mathbf{R}_\mathrm{R}^{1/2}\mathbf{H}_\mathrm{w}\mathbf{R}_\mathrm{T}^{1/2} \in \mathbb{C}^{\mathcal{K}_\mathrm{R}\times\mathcal{K}_\mathrm{T}}$ is the channel transfer matrix. The elements of the matrix $\mathbf{H}_\mathrm{w} \in \mathbb{C}^{\mathcal{K}_\mathrm{R}\times\mathcal{K}_\mathrm{T}}$ are i.i.d. complex Gaussian random variables with zero mean and unit variance, whereas the variance of the zero-mean white Gaussian noise vector $\mathbf{n} \in \mathbb{C}^{\mathcal{K}_\mathrm{R}\times 1}$ is σ_n^2. Unlike the classical approach where the transmit power is constrained, in this work we constrain *the input power* and thus $\mathbf{\Delta}_\mathrm{T}$ becomes part of the optimization criterion, as the adaptive MAMP system is intended for portable radios or sensors with limited storage batteries.

[1] In the literature, $\mathbf{A}_\mathrm{T}$ is known as the signal covariance matrix, which need not be diagonal when applying baseband linear precoding across the transmit active antennas. In this work, $\mathbf{A}_\mathrm{T}$ is only optionally used for further optimizing the power distribution across the active element responses. Notice that baseband linear precoding can be added on top of the proposed non-linear precoder, but requires further channel knowledge and is beyond the scope of this work.

It should be noted that the Kronecker model, though widely used in the literature as it allows analytical tractability and separate transmit and receive optimizations, has been experimentally validated mainly for outdoor channels of up to 8 transmit and receive antennas [BCC04]. However, the Kronecker model underestimates the capacity of relatively large MIMO arrays under indoor NLOS propagation, as explained in [OHW+03] with 8 transmit and receive antennas. Yet, the relative error on the mutual information remains below 10% [CO07]. To summarize, the Kronecker model for indoor channels is mainly valid for arrays with reduced spatial resolution (up to 3 transmit and receive antennas in practice [YBO+01], [KSP+02]).

2.1.2.1 Ergodic Rate Optimization Criterion

Let $m = \min\{\mathcal{K}_{\mathrm{T}}, \mathcal{K}_{\mathrm{R}}\}$. In open-loop operation, the channel is known to the receiver and unknown to the transmitter and the ergodic capacity of a MIMO random channel, denoted by C_{e}, is the ensemble average of the information rate over the distribution of the elements of the end-to-end channel matrix $\overline{\mathbf{H}} = \mathbf{R}_{\mathrm{R}}^{1/2}\mathbf{H}_{\mathrm{w}}\mathbf{R}_{\mathrm{T}}^{1/2}(\mathbf{\Delta}_{\mathrm{T}}\mathbf{A}_{\mathrm{T}})^{1/2} \in \mathbb{C}^{\mathcal{K}_{\mathrm{R}}\times\mathcal{K}_{\mathrm{T}}}$ and is given by [GNP03]

$$C_{\mathrm{e}} = \mathbb{E}_{\mathbf{H}_{\mathrm{w}}}\left[\log_2\det\left(\mathbf{I}_m + \frac{P_{\mathrm{I}}}{\sigma_{\mathrm{n}}^2}\mathbf{\Theta}\right)\right], \tag{2.11}$$

where the random matrix $\mathbf{\Theta} \in \mathbb{C}^{m\times m}$ is defined as $\mathbf{\Theta} = \begin{cases} \overline{\mathbf{H}}\,\overline{\mathbf{H}}^{\mathrm{H}}, & \mathcal{K}_{\mathrm{T}} \geq \mathcal{K}_{\mathrm{R}} \\ \overline{\mathbf{H}}^{\mathrm{H}}\overline{\mathbf{H}}, & \mathcal{K}_{\mathrm{T}} \leq \mathcal{K}_{\mathrm{R}} \end{cases}$. A tight upperbound on (2.11) is written as [aJHL03]

$$C_{\mathrm{e}} \leq \log_2\left[\sum_{\ell=0}^{m}\left\{\left(\frac{P_{\mathrm{I}}}{\sigma_{\mathrm{n}}^2}\right)^{l}\ell!\cdot\sum_{1\leq i_1\leq i_2\leq\ldots\leq i_l\leq\mathcal{K}_{\mathrm{T}}}\det\left[(\mathbf{R}_{\mathrm{T}}\mathbf{\Delta}_{\mathrm{T}}\mathbf{A}_{\mathrm{T}})^{i_1,i_2,\ldots,i_l}_{i_1,i_2,\ldots,i_l}\right]\right.\right.$$
$$\left.\left.\cdot\sum_{1\leq j_1\leq j_2\leq\ldots\leq j_l\leq\mathcal{K}_{\mathrm{R}}}\det\left[(\mathbf{R}_{\mathrm{R}})^{j_1,j_2,\ldots,j_l}_{j_1,j_2,\ldots,j_l}\right]\right\}\right] \tag{2.12}$$

where $\det\left[(\mathbf{R}_{\mathrm{R}})^{j_1,j_2,\ldots,j_l}_{j_1,j_2,\ldots,j_l}\right]$ is a minor determinant of $\mathbf{R}_{\mathrm{R}}$, i.e., a determinant of the $\ell\times\ell$ matrix lying in the $j_1, j_2, \ldots, j_l$ rows and $j_1, j_2, \ldots, j_l$ columns of $\mathbf{R}_{\mathrm{R}}$ (similarly for $\det\left[(\mathbf{R}_{\mathrm{T}}\mathbf{\Delta}_{\mathrm{T}}\mathbf{A}_{\mathrm{T}})^{i_1,i_2,\ldots,i_l}_{i_1,i_2,\ldots,i_l}\right]$) [Bro58]. The 0-rowed principal minor determinant (i.e., $\ell = 0$) is assumed to be 1.

An alternative upperbound on (2.11) for $\mathbf{R}_{\mathrm{R}} = \mathbf{I}_{\mathcal{K}_{\mathrm{R}}}$ (e.g., when the receiver is equipped with $\mathcal{K}_{\mathrm{R}}$ uncorrelated and uncoupled antennas), is the one that comes from the Jensen's inequality and the concavity of $\log_2\det(\cdot)$ [CT06] as

$$C_{\mathrm{e}} \leq \log_2\det\left[\mathbf{I}_{\mathcal{K}_{\mathrm{T}}} + \frac{P_{\mathrm{I}}}{\sigma_{\mathrm{n}}^2}\mathbb{E}_{\mathbf{H}_{\mathrm{w}}}(\mathbf{\Theta})\right] = \log_2\det\left(\mathbf{I}_{\mathcal{K}_{\mathrm{T}}} + \frac{P_{\mathrm{I}}}{\sigma_{\mathrm{n}}^2}\mathbf{R}_{\mathrm{T}}\mathbf{\Delta}_{\mathrm{T}}\mathbf{A}_{\mathrm{T}}\right). \tag{2.13}$$

The tightness of the upper bound in (2.12) against the one in (2.13) will be shown in Section 2.1.3. Consequently, a reliable MIMO ergodic capacity optimization criterion is available in (2.12) and the described adaptive MAMP system, aware of the channel structure expressed by $\mathcal{A}(\varphi)$, can search the realizable range for each kth imaginary load X_k given by $X_{\mathrm{LB}} \leq X_k \leq X_{\mathrm{UB}}$ (where usually $X_{\mathrm{LB}} < 0$, i.e., capacitive and $X_{\mathrm{UB}} > 0$, i.e., inductive) and find the optimal load values that maximize the average throughput upper bound in (2.12).

2.1.2.2 Outage Rate Optimization Criterion

The outage capacity, defined as the maximum rate that can be maintained throughout the transmission with a given outage probability, is another figure of merit when considering flat-fading MIMO channels. In this part we consider simple receiver architectures that use linear operations to decode the substreams and extract the multiplexing gains of MIMO systems. For linear processing with minimum mean square error (MMSE) detection on the receiver side, the transmitted data symbols $\mathbf{v}_s$ are estimated by forming $\hat{\mathbf{v}}_{\mathrm{s}} = \mathbf{G}_{\mathrm{MMSE}}\mathbf{y}$. The matrix $\mathbf{G}_{\mathrm{MMSE}}$ is defined as $\mathbf{G}_{\mathrm{MMSE}} = \sqrt{P_{\mathrm{I}}{}^{-1}}\left(\overline{\mathbf{H}}^{\mathrm{H}}\overline{\mathbf{H}} + \frac{\sigma_{\mathrm{n}}^2}{P_{\mathrm{I}}}\right)^{-1}\overline{\mathbf{H}}^{\mathrm{H}}$ [GNP03] (assuming perfect knowledge of $\mathbf{H}$ at the receiver). Similarly, the linear zero forcing (ZF) detector estimates the transmitted symbols by forming $\hat{\mathbf{v}}_{\mathrm{s}} = \mathbf{G}_{\mathrm{ZF}}\mathbf{y}$ where $\mathbf{G}_{\mathrm{ZF}}$ is given in [GNP03] as $\mathbf{G}_{\mathrm{ZF}} = \sqrt{P_{\mathrm{I}}{}^{-1}}\left(\overline{\mathbf{H}}^{\mathrm{H}}\overline{\mathbf{H}}\right)^{-1}\overline{\mathbf{H}}^{\mathrm{H}}$. The vertical-Bell laboratories layered space time (V-BLAST) receiver employs ordered successive interference cancellation (OSIC) and MMSE projection [Fos96]. Under the assumptions of spatial multiplexing-horizontal encoding (SM-HE), independent decoding at the receiver, $\mathcal{K}_{\mathrm{R}} \geq \mathcal{K}_{\mathrm{T}}$, and by defining γ_{min} as the minimum post-processing substream SNR, the open-loop capacity between the transmitter and the receiver is given by [GNP03]

$$C = \mathcal{K}_{\mathrm{T}} \log(1 + \gamma_{\mathrm{min}}). \tag{2.14}$$

Thus, the outage probability, denoted by $\Pr_{\mathrm{out}}$, is given by

$$\Pr{}_{\mathrm{out}} = 1 - \Pr\left[R \leq C\right], \tag{2.15}$$

where $R \leq C$ is the achievable rate of communication for a given outage probability. In [Nar06], upper and lower bounds on the outage probability are derived from lower and upper bounds on the γ_{min} of linear MMSE or MMSE-OSIC detection based on the γ_{min} of linear ZF. These bounds can be extended so as to encompass the described channel model as

$$\Pr{}_{\mathrm{out}} \leq F_X\left(\frac{\sigma_{\mathrm{n}}^2(2^{R/\mathcal{K}_{\mathrm{T}}} - 1)}{P_{\mathrm{I}}} \cdot \frac{1}{\lambda_{\mathrm{min}}(\mathbf{R}_{\mathrm{R}})\lambda_{\mathrm{min}}(\mathbf{R}_{\mathrm{T}}\boldsymbol{\Delta}_{\mathrm{T}}\mathbf{A}_{\mathrm{T}})}\right), \tag{2.16}$$

$$\Pr_{\text{out}} \geq F_Y\left(\frac{\sigma_{\text{n}}^2\left(2^{R/\mathcal{K}_{\text{T}}}-1\right)}{P_{\text{I}}}\cdot\frac{1}{\left\|\mathbf{R}_{\text{R}}^{1/2}\right\|_F^2\cdot\min\limits_{l=1,\ldots,\mathcal{K}_{\text{T}}}\left\|\left[(\mathbf{R}_{\text{T}}\boldsymbol{\Delta}_{\text{T}}\mathbf{A}_{\text{T}})^{1/2}\right]_{(l)}\right\|_F^2}\right), \quad (2.17)$$

where $\left[(\mathbf{R}_{\text{T}}\boldsymbol{\Delta}_{\text{T}}\mathbf{A}_{\text{T}})^{1/2}\right]_{(l)}$ denotes the lth column of $(\mathbf{R}_{\text{T}}\boldsymbol{\Delta}_{\text{T}}\mathbf{A}_{\text{T}})^{1/2}$, $F_X(\cdot)$ is the cumulative distribution function (cdf) of a gamma random variable X with parameters $(\mathcal{K}_R-\mathcal{K}_{\text{T}}+1, 1/\mathcal{K}_{\text{T}})$, and $F_Y(\cdot)$ is the cdf of a gamma random variable Y with parameters $(\mathcal{K}_{\text{R}}\mathcal{K}_{\text{T}}, 1)$. Normally, a tight upper bound on the outage probability can be used to obtain a tight upper bound on the outage rate. However, the outage rate criterion to be optimized, denoted by C_{out}, combines both the upper and the lower bounds of the expressions in (2.16) and (2.17) via a Pythagorean mean such as the geometric mean [Nar06], since the upper bound in (2.16) is based on linear ZF detection and can be quite loose for more sophisticated receivers like the MMSE-OSIC

$$C_{\text{out}} = \mathcal{K}_{\text{T}}\log_2\left(1+\frac{P_{\text{I}}}{\sigma_{\text{n}}^2}\sqrt{F_X(\Pr_{\text{out}})^{-1}F_Y(\Pr_{\text{out}})^{-1}\lambda_{\min}(\mathbf{R}_{\text{T}}\boldsymbol{\Delta}_{\text{T}}\mathbf{A}_{\text{T}})}\right.$$
$$\left.\cdot\sqrt{\lambda_{\min}(\mathbf{R}_{\text{R}})\left\|\mathbf{R}_{\text{R}}^{1/2}\right\|_{\text{F}}^2\cdot\min_{l=1,\ldots,\mathcal{K}_{\text{T}}}\left\|\left[(\mathbf{R}_{\text{T}}\boldsymbol{\Delta}_{\text{T}}\mathbf{A}_{\text{T}})^{1/2}\right]_{(l)}\right\|_{\text{F}}^2}\right). \quad (2.18)$$

Similarly to Section 2.1.2.1, a MIMO outage rate optimization criterion (whose performance will be also shown in Section 2.1.3) is available in (2.18) and the proposed adaptive MAMP system can directly search the realizable range of each kth passive load X_k and find the optimal load values that maximize the quantity in (2.18). Notice that both (2.12) and (2.18) are independent of the instantaneous channel $\mathbf{H}_{\text{w}}$ and depend only on the channel covariance matrix, the array coupling, and the array efficiency. Thus, the transmit adaptive MAMP system based only on the knowledge of the PAS, given by $\mathcal{A}(\varphi)$, can estimate the channel covariance matrix and adjust the loading conditions so that the transmit correlation, coupling and antenna efficiency maximize the average or the instantaneous communication rate. The PAS can easily be estimated using traditional super-resolution techniques, such as CLEAN, ESPRIT, SAGE, and their variants [TS88], [RK89], [FTH+99], or the efficient and accurate sparse PAS estimation (SPASE) recently proposed in [WJ09].

2.1.3 Simulation Results

2.1.3.1 Tightness of the Bounds

In this part we investigate the tightness of the upper bounds in (2.12), (2.13) over a wide range of the SNR. A system example corresponding to an indoor uplink channel for IEEE 802.11 [Erc04] was established. The base station or the access point is equipped with $\mathcal{K}_{\text{R}} = 2$ distantly spaced antennas and surrounded by many scatterers (hence, the receive correlation matrix is just an identity matrix of size 2). The transmitter has a single cluster of scatterers of a uniform PAS, with a mean AoD of 120° from

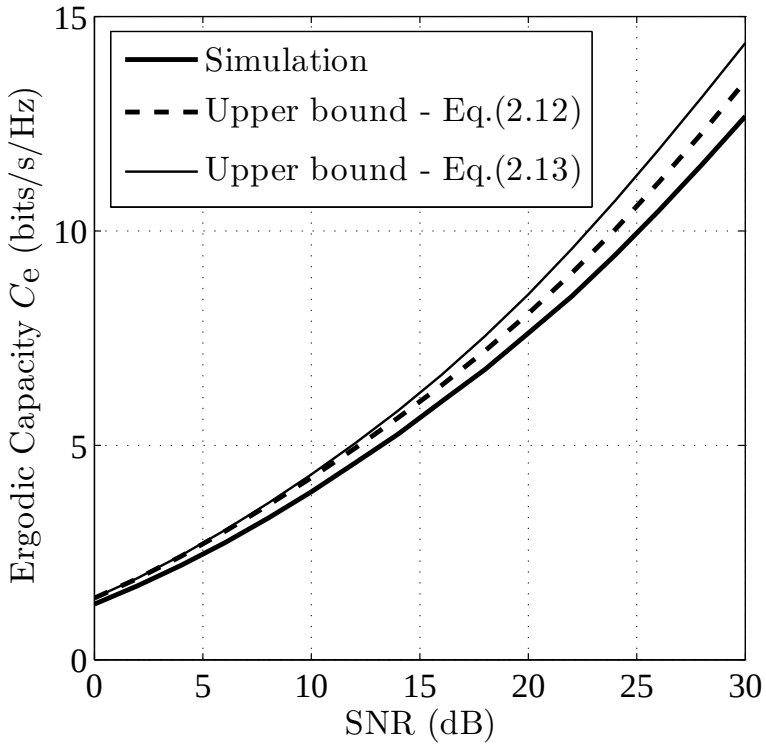

Figure 2.1: Ergodic capacity and the capacity upper bound for a coupled MIMO system example under the IEEE 802.11 clustering RF channel model.

the broadside and an angle spread (AS) of 20°. The transmit antenna system is a conventional (non adaptive) ULA of two half-wavelength thin electrical dipoles with an inter-element spacing of 0.25λ, having a mutual impedance matrix given by

$$\mathbf{Z} = \begin{bmatrix} 62.17 - \mathrm{j}24.09 & -16.56 - \mathrm{j}23.82 \\ -16.56 - \mathrm{j}23.82 & 62.17 - \mathrm{j}24.09 \end{bmatrix},$$

calculated using the analytical formulas shown in the Appendix 6. The transmit covariance matrix which takes into account the mutual coupling when the two dipoles are terminated with $Z_o = 50$ Ohm is

$$\mathbf{R}_T = \begin{bmatrix} 1 & 0.6 \\ 0.6 & 1 \end{bmatrix}.$$

$10,000$ different channel realizations where created in order to evaluate (2.11) via Monte Carlo simulation. Thus, a small simulation error of around 1% is maintained (the error is approximately inversely proportional to the square root of the number of simulation samples [Caf98]).

Figure 2.1 shows that the upper bound from (2.12) is more tight than the upper

bound from (2.13) for the entire range of SNR's as compared to the Monte Carlo simulation of (2.11). Specifically, the upper bound from (2.12) exhibits a maximum difference of only 1 bit/s/Hz at the high SNR regime.[1]

2.1.3.2 Adaptive MAMP System Performance Evaluation

Single-Passive, Two-Active Adaptive MAMP System

To evaluate the performance of the adaptive MAMP system described in Section 2.1.1 and to illustrate the basic concept of the work in a comprehensive manner, we first consider a simple ULA comprising 3 half-wavelength thin electrical dipoles (two active, i.e., elements 1 and 2 in Figure 2.2(a), and one common passive, i.e., element 0 in the same figure) with an inter-element spacing of 0.1 λ, thus $\mathcal{K}_{\mathrm{T}} = 2$. The (3×3) mutual impedance matrix $\mathbf{Z}$ of the 3-port antenna system has entries $\langle \mathbf{Z} \rangle_{00} = 73.1 + \mathrm{j}43$, $\langle \mathbf{Z} \rangle_{01} = 67 + \mathrm{j}7.6$, $\langle \mathbf{Z} \rangle_{12} = 51 - \mathrm{j}19$, and $\langle \mathbf{Z} \rangle_{11} = \langle \mathbf{Z} \rangle_{00}$. A feasible realizable range for the imaginary load is $-200 \leq X \leq 200$ Ohm and uniform power allocation across the two active elements is assumed. Moreover, we assume a receiver equipped with $\mathcal{K}_{\mathrm{R}} = 2$ distantly spaced antennas and surrounded by many scatterers, thus both the receive coupling and correlation are negligible ($\mathbf{R}_{\mathrm{R}} = \mathbf{I}_2$).

We consider a rich scattering environment at the transmitter for which $\mathcal{A}(\varphi)$ is uniform, i.e., $\mathcal{A}(\varphi) = \frac{1}{2\pi}$ and a clustering environment for which $\mathcal{A}(\varphi)$ is Laplacian, i.e., $\mathcal{A}(\varphi) = \frac{c}{\sigma} e^{-|\varphi - \bar{\varphi}|/\sigma}$, with an AS of $\sigma = 30°$ and a mean AoD of $\bar{\varphi} = 60°$ representing an indoor office environment with no line-of-sight [SJJS00] ($c = \frac{\sigma}{\int_0^{2\pi} e^{-|\varphi - \bar{\varphi}|} d\varphi}$ is a normalization factor).

Figure 2.3 shows how the active element response of the first active antenna changes by changing the imaginary load of the passive antenna (as stated before, the active element response is obtained by exciting the first active antenna element with a unit excitation voltage while terminating the other active one with Z_{o} and the tunable radiator with the variable $\mathrm{j}X$). The response of the second active antenna is simply a mirror image of the first element response with respect to the axis $90° - 270°$.

Figure 2.4 shows the magnitude of the correlation coefficients $|\langle \mathbf{R}_{\mathrm{T}} \rangle_{12}|$ in the rich scattering and clustering environments. It also shows the antenna efficiency, which in this case is the same for the two active elements, i.e., $\Delta_1 = \Delta_2 = \Delta_{\mathrm{T}}$. The figure illustrates how the different parameters change as the imaginary load varies over its feasible range.

In order to evaluate the performance of the proposed adaptive MAMP system and the way it adapts to the structure of the surrounding environment, we have calculated the average throughput C_{e} via Monte Carlo simulations at an average input SNR $P_{\mathrm{I}}/\sigma_{\mathrm{n}}^2$ of 10 dB for two system examples. The 1st assumes a transmit adaptive MAMP system with the aforementioned antenna parameters at the transmitter side and the 2nd assumes the same antenna system at the transmitter, however the reactive load

[1] Also, it is easy to see that the upper bound in (2.12) can be used under both transmit and receive correlation / coupling, whereas the upper bound in (2.13) can be used with single-sided (i.e., only transmit or only receive) correlation / coupling.

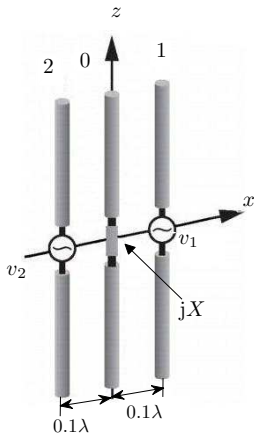

(a)

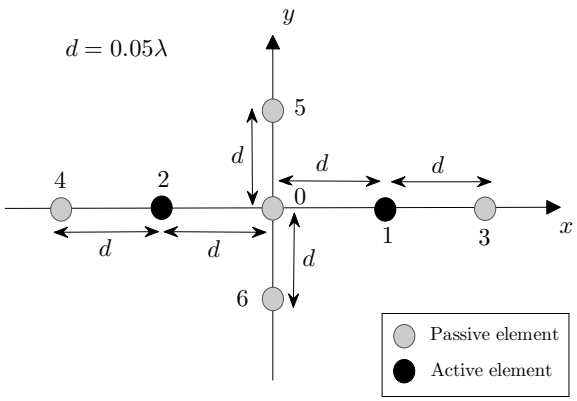

(b)

Figure 2.2: Proposed adaptive MAMP system examples comprising 3 [(a): 3D view] and 7 [(b): top view] half-wavelength thin electrical dipoles spaced by 0.1λ and 0.05λ, respectively.

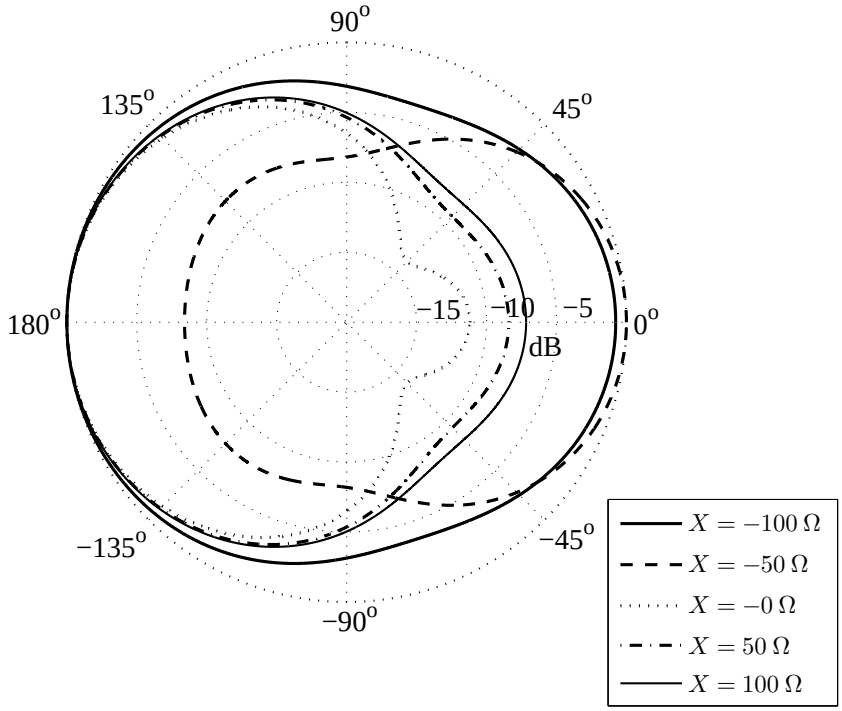

Figure 2.3: Active element response of the proposed adaptive MAMP system in Figure 2.2(a) as a function of the tunable load jX.

is detuned (i.e., set to a very high value so it becomes open-circuited), following the LTE-Advanced [lte] trend of transmitting over two antennas out of the available set of antennas. Therefore, the adaptive MAMP system in Figure 2.2(a) is compared against a conventional 2-element transmit ULA (keeping the spacing between the ULA antennas to 0.2λ for fairness). On the transmitter side there is a single cluster with $\sigma = 20°$ [SJJS00] and $\bar{\varphi}$ that varies from 0° to 180°. The adaptive MAMP system of Figure 2.2(a) consists of a single passive element, i.e., the optimization of the ergodic / outage performance with respect to the passive load is a unidimensional optimization problem which can be efficiently solved with direct search over the realizable reactance range.

Figure 2.5 shows C_{e} for both systems where the performance of the adaptive MAMP system is optimized regarding C_{e} using (2.12) at every $\bar{\varphi}$ ($\bar{\varphi}$ may change in practice when the transmitter changes its location with respect to a reference cluster). It is clear that the performance gains of the proposed adaptive MAMP system are significant whereas the proposed metric in (2.12) is adequate for obtaining the optimal trade-off between correlation, coupling, and antenna efficiency over the different channel structures when optimizing the adaptive MAMP system for the maximum ergodic rate.

Next, the ergodic capacity is plotted in Figure 2.6 versus the average input SNR

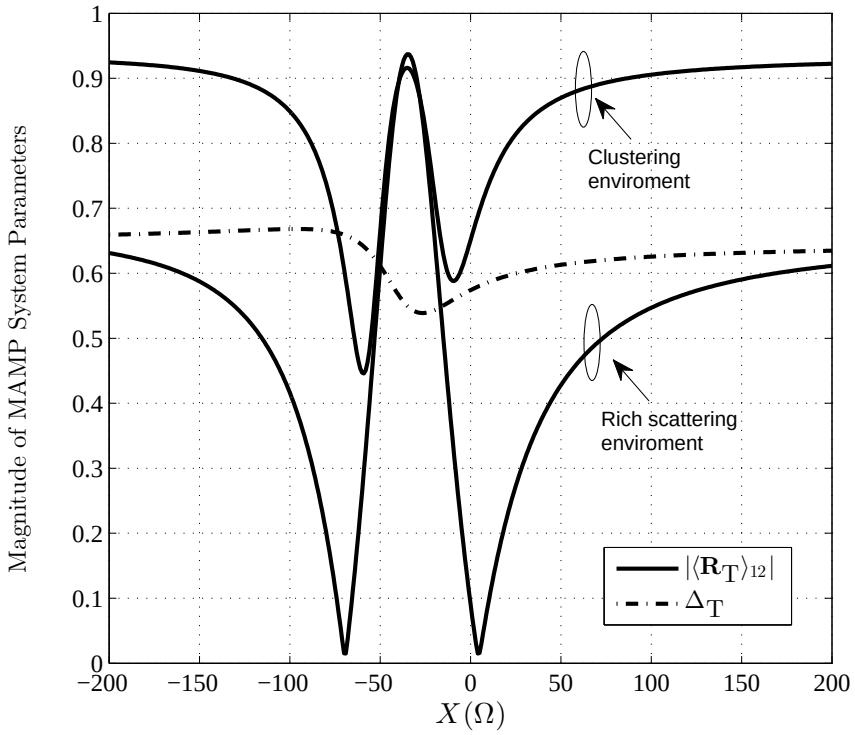

Figure 2.4: Correlation and antenna efficiency as functions of the tunable load jX.

for different propagation environments including an indoor office environment with a cluster AS of 10° accounting for a NLOS scenario [SJJS00] as well as a typical urban environment where the AS is 40° [LPB00] (in both cases $\mathcal{A}(\varphi)$ is Laplacian and $\bar{\varphi} = 60°$). The i.i.d. 2×2 performance of an uncoupled transmit system under independent fading is also shown as a theoretical benchmark. It can be observed that the benefit of the proposed adaptive MAMP system optimized using (2.12) increases as the AS decreases, which is expected as the adaptive MAMP system basically tunes the reactance to the value that decorrelates and decouples the two active antennas. The optimal reactive load in the office environment starts from an inductive reactance of -150 Ohm and increases to -56 Ohm as the SNR increases whereas in the urban environment it starts from an inductive reactance of -117 Ohm and increases to -71 Ohm as the SNR increases.

The performance results are now presented for the adaptive MAMP system aiming at maximizing the outage rate via (2.18) for $\mathrm{Pr}_{\mathrm{out}} = 10\%$, given the input SNR. The results are plotted in Figure 2.7 for MMSE and MMSE-OSIC reception, with the clustered channel of Figure 2.5 with $\bar{\varphi} = 120°$. The optimal reactive load for the MMSE receiver starts from an inductive reactance of -55 Ohm and slightly decreases to -57 Ohm as the SNR increases whereas for MMSE-OSIC reception it starts from an inductive reactance of -61 Ohm and increases to -58 Ohm as the SNR increases. In the

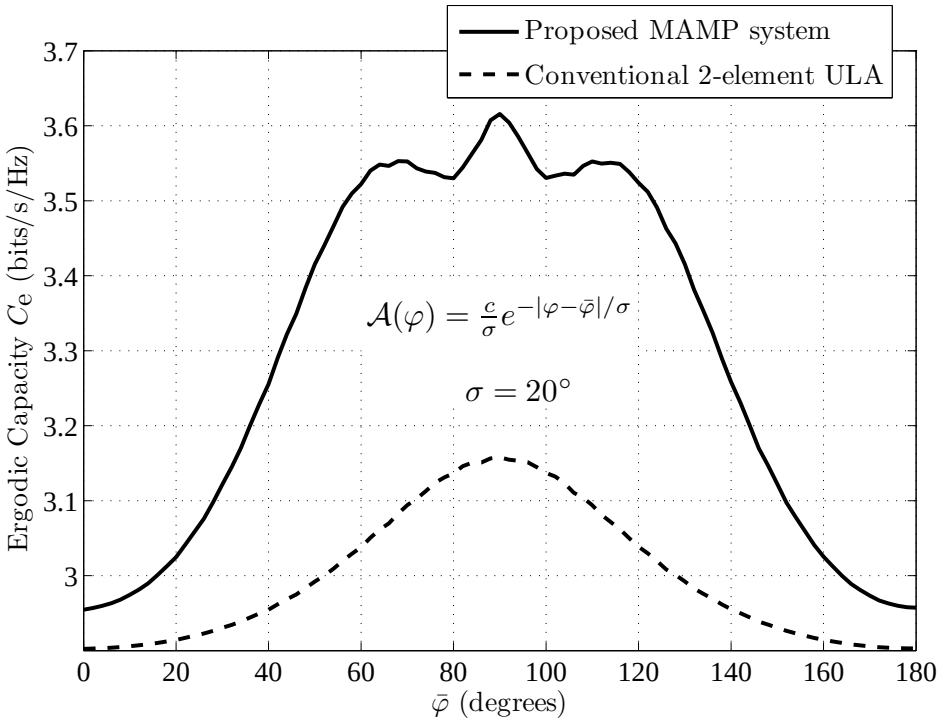

Figure 2.5: Average rate of transmission when the adaptive MAMP system of Figure 2.2(a) adapts to the mean AoD, as compared to the same antenna system when the reactive load is detuned (i.e., two active transmit antennas spaced by 0.2λ)

figure, the maximum outage rates at each SNR among all possible imaginary load values for MMSE and MMSE-OSIC detection are also plotted. It can be observed that, in all cases, the proposed adaptive MAMP system optimized using (2.18) [curves marked with "+"] provides large performance gains against the conventional all-active antenna system, whereas the optimization criterion in (2.18) *provides the maximum outage rate or very close to the maximum outage rate among the possible loads in the realizable range of* $\mathrm{j}X$.

Five-Passive, Two-Active Adaptive MAMP System

In this part, a more involved adaptive MAMP system example of 7 half-wavelength thin electrical dipoles (out of which 5 are passive and 2 are active) with an inter-element spacing of 0.05λ is considered, as shown in Figure 2.2(b). The realizable range for the imaginary loads is $-200 \leq X_k \leq 200$ Ohm, $k \in \{0, 3, 4, 5, 6\}$ and the (7×7) mutual impedance matrix of the 7-port antenna system has $\langle \mathbf{Z} \rangle_{kk} = 73.07 + \mathrm{j}42.49, k \in \{0, 1, \ldots, 6\}$, $\langle \mathbf{Z} \rangle_{01} = (\mathbf{Z})_{02} = \langle \mathbf{Z} \rangle_{13} = \langle \mathbf{Z} \rangle_{24} = 71.60 + \mathrm{j}24.25$, $\langle \mathbf{Z} \rangle_{03} = \mathbf{Z}_{04} = \langle \mathbf{Z} \rangle_{56} = 67.28 + \mathrm{j}7.53$, $\langle \mathbf{Z} \rangle_{45} = \langle \mathbf{Z} \rangle_{46} = \langle \mathbf{Z} \rangle_{35} = \langle \mathbf{Z} \rangle_{36} = 65.87 + \mathrm{j}3.87$ and $\langle \mathbf{Z} \rangle_{15} = \langle \mathbf{Z} \rangle_{25} =$

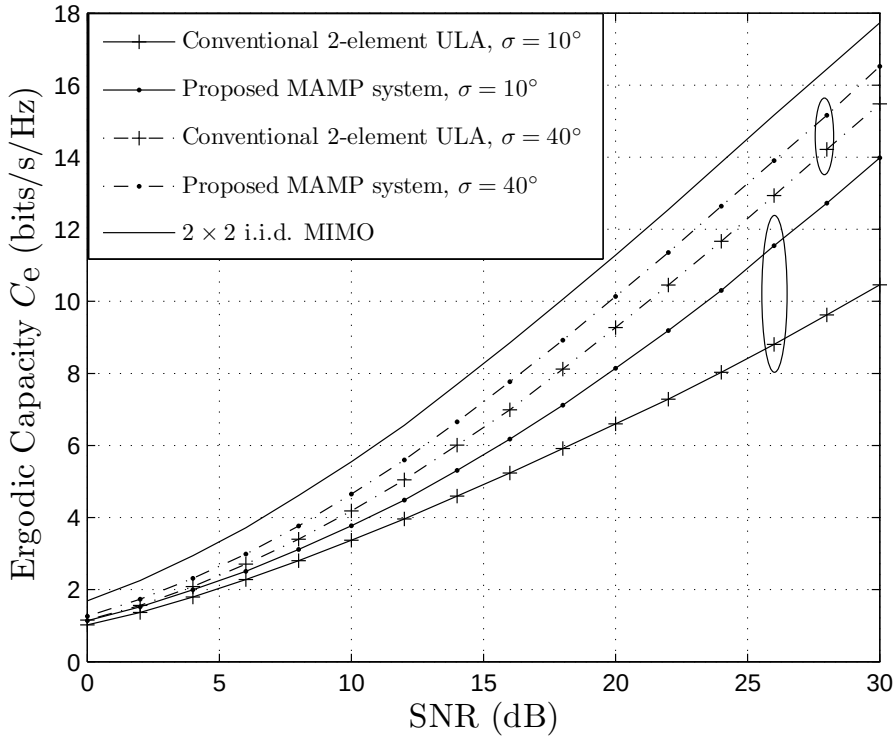

Figure 2.6: Ergodic capacity results in indoor and outdoor environments where the transmitter is either equipped with the proposed adaptive MAMP system of Figure 2.2(a) or with a conventional 2-active element ULA.

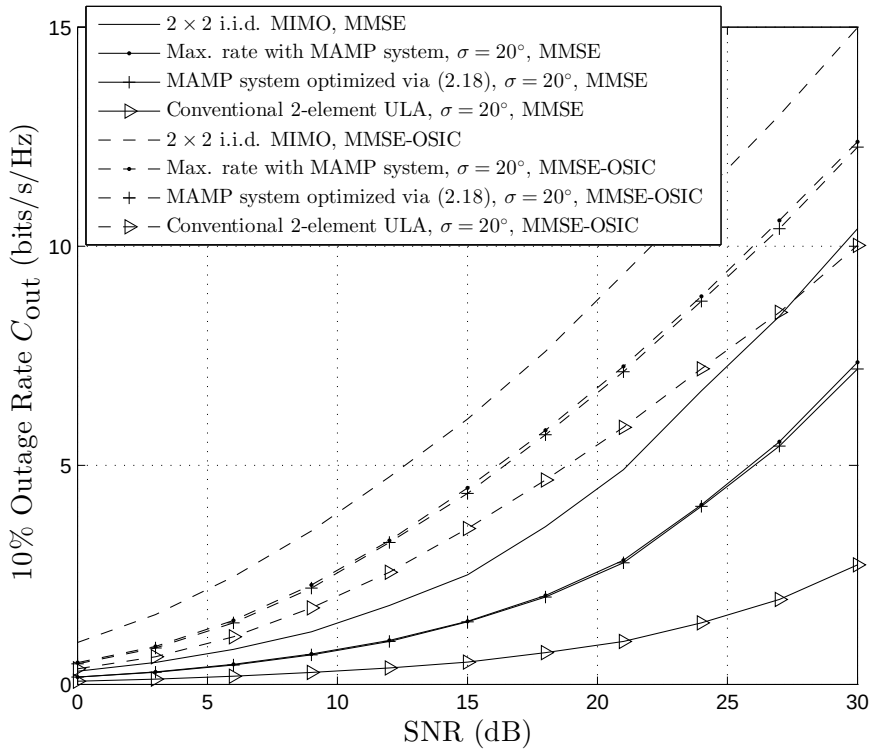

Figure 2.7: Outage rate versus SNR for different channels and reception schemes where the transmitter is either equipped with the proposed adaptive MAMP system of Figure 2.2(a) or with a conventional 2-active element ULA.

$\langle \mathbf{Z} \rangle_{16} = \langle \mathbf{Z} \rangle_{26} = 70.15 + \mathrm{j}17.10$. As the reactance space is large, exhaustive search is not practical in this set-up, thus we resort to an efficient interior point method for non-convex programming [BGN00; WMNO06] available in MATLAB® [mat]. We consider the same indoor and urban propagation environments described for Figure 2.6 with 20 dB SNR. On top of optimizing the set of the reactive loads, the power allocation a_1 is considered as an extra optimization parameter. Thus, the case of adaptive load tuning combined with dynamic power allocation (where the power allocation can be varied according to the CDI expressed by the PAS) is also included.

The optimization algorithm for load tuning with both uniform and dynamic power allocation based on the criterion in (2.12) has found to converge after a reasonable number of iterations. This is indeed practical as the CDI changes quite slowly when compared to the channel fading rate, thus imposing reduced complexity on the proposed adaptive MAMP system. It is noted that dynamic power allocation presented considerable gains in the indoor scenario where the spatial correlation is higher. Specifically, the dynamic power allocation converged in the indoor environment to $a_1 = 1$ and $a_2 = 0$, resulting in a mere beamforming system, and to $a_1 = a_2 = 0.5$ in the urban environment. Table 2.1 summarizes the ergodic capacities attained for the optimal loads

Table 2.1: Ergodic capacity results and optimal loads for SNR=20 dB where the transmitter is equipped with the adaptive MAMP system of Figure 2(b) or with a conventional 2-Element ULA (i.e., two active antennas spaced by 0.1λ)

		Ergodic Capacity C_e (bits/s/Hz)	Optimal Reactance Loads $\{X_0, X_3, X_4, X_5, X_6\}$ (Ohm)
2×2 i.i.d. MIMO		11.10	—
$\sigma = 40°$	Uniform power allocation	9.40	$\{-33.4, 198.2, -192.0, -108.3, 3.8\}$
	Dynamic power allocation	9.41	$\{109.2, 174.2, -121.8, -46.2, 72.5\}$
	Conventional 2-element ULA	7.62	—
$\sigma = 10°$	Uniform power allocation	7.59	$\{30.7, -2.0, -198.9, -43.7, 39.7\}$
	Dynamic power allocation	8.61	$\{-6.9, -4.9, -58.7, -40.5, -24.3\}$
	Conventional 2-element ULA	5.73	—

and the ergodic capacities that would have been obtained when open-circuiting all the reactive loads (i.e., for a conventional all-active 2-element ULA with $2 \times 0.05\,\lambda = 0.1\lambda$ spacing), as well as the i.i.d. 2×2 performance of an uncoupled system under independent fading for comparison reasons. The table shows that the adaptive MAMP system is mostly useful in low spread environments, especially when combined with a dynamic power allocation. The adaptive MAMP system is still useful in high spread environments, where dynamic power allocation exhibits marginal gains.

So far, we have proposed an adaptive MAMP system capable of changing its correlation and matching properties according to the structure of the channel, using tunable passive elements. The adaptive MAMP system adapts to the channel distribution information requiring a low-rate feedback from its receiver. Specific adaptive MAMP systems were evaluated under different channel propagation conditions, showing performance gains over classical all-active antenna systems. Further, the proposed adaptive MAMP system addresses the limitations of portable radios regarding size and cost permitting an efficient usage of the spare transmit antennas according to future wireless standards.

In the next section, we shift from point-to-point MIMO communication to focus on the multiuser cellular downlink providing MAMP antenna arrays that enhance the average cell throughput performance.

2.2 Switched-Beam Parasitic Arrays for Enhanced Receive Selection Combining in Multiuser Diversity Systems

Recent studies have shown that a capacity achieving strategy for the cellular downlink is dirty paper coding (DPC) at the multiple antenna BS [CS03]. A less computationally complex ZF technique is proposed in [YG06a] exhibiting an identical grow rate of the sum-rate with respect to the number of user terminals (UTs). However, both DPC and

ZF require perfect channel state information at the transmitter (CSIT). Since perfect CSIT is practically infeasible, the focus is on low rate feedback techniques exploiting *multiuser diversity* by scheduling opportunistically transmissions to the users when their channel is good. These techniques, termed as opportunistic beamforming (OB), were introduced in [VTL02]. Therein, taking into account fairness, the BS schedules in each time slot data transmission to the UT with the best normalized instantaneous channel condition relative to a random beamforming precoding. This approach achieves the asymptotic average throughput of coherent beamforming with modest SNR feedback. Several extensions to this technique are mentioned in the literature. For example, [ALP04] proposes an OB and scheduling algorithm that enhances the throughput and delay characteristics of the system whereas, in [SH05], multiple orthonormal random beams at the BS serve multiple UTs simultaneously in each time slot.

OB techniques rely on the assumption that, with a large number of UTs, there is a high probability that an arbitrary choice of a BS beamforming vector will be aligned to a user's channel vector [ZJ05]. Thus, the benefits of OB are more evident when the number of users is large. To further improve the data rates of multiuser diversity systems, especially for reasonable user populations, the authors in [ZJ05; BS07; PKP07; CL09] consider multiple antenna UTs with different combining techniques ranging from the simple antenna selection combining (SC) to the more sophisticated equal gain combining (EGC), maximum ratio combining (MRC) and optimum combining (OC). However, complex architectures including multiple receive antennas are often prohibitive in UTs due to implementation complexity and size restrictions. Note that SC is the simplest combining method in terms of hardware complexity keeping the same diversity gain as that for MRC or EGC [CL09]. Moreover, the small spacing of the antenna elements at the UTs often results in significant correlation and coupling degrading the efficiency of the receive antenna system. Therefore, it is desirable to investigate simple to implement solutions ensuring low power consumption and efficient performance in a constrained size device.

In this work, we propose two compact UT antenna architectures accompanied with SC aiming at enhancing the performance of a multiuser system in the downlink. The first antenna architecture consists of a simple switched uniform circular array (S-UCA) of K antenna elements and a central common passive reflector terminated with a passive load (reactance) (Figure 2.8(a)). This is a MAMP array with a single passive element and K potentially active elements. The second antenna architecture comprises a simple switched parasitic array (S-PA) [Thi04; TAPP10b] of a single RF chain circularly surrounded by K passive reflectors terminated with passive loads (Figure 2.8(b)). This is a MAMP array with a single active element and K passive ones. The two proposed architectures (S-UCA and S-PA) satisfy the aforementioned cost, size and power restrictions as they both require a single RF chain and low-cost passive antenna hardware [Vau98]. Moreover, the antenna size is kept small by reducing significantly the radius of the S-UCA and of the S-PA. In this way, the antenna systems retain strong beamforming capabilities due to the intense reactive fields egressed at such small spacing [TAPP10d]. By optimizing the S-UCA and the S-PA loading conditions

a high antenna efficiency is maintained whereas the K beampatterns obtained by the receive architectures remain uncorrelated despite the small inter-element spacing. Consequently, besides multiuser diversity, angular diversity is also made available resulting in significant multiuser performance gains compared not only to conventional single antenna UTs, but also to classical antenna SC with realistic receive antenna systems.

The two proposed antenna architectures preserve the compactness and cost constraints of UT antennas, whereas one can be thought of as the *"dual"* architecture of the other: the central element of the S-UCA is a passive reflector surrounded by potentially active antenna elements (Figure 2.8(a)), whereas in the case of S-PA the central element is an active antenna surrounded by a ring of passive reflectors (Figure 2.8(b)). It should be noted that the S-PA necessitates a more complicated control circuit as compared to the S-UCA which requires a simple conventional antenna switching mechanism, resembling a classical switched UCA topology with the mere modification of inserting a common central passive reflector. On the other hand, the RF switch needed for changing the RF path among the S-UCA antenna elements constitutes a liability in terms of additional insertion losses.

Notice that [BKSK10] proposes a compact single RF antenna system assisted by passive elements extracting a maximum diversity order of 3 (equal to the number of the considered basis beampatterns) in multiuser environments. However, the optimal antenna loading conditions are found according to the *instantaneous* SNR, thus adding extra computational complexity and delay. On the contrary, in our work the optimal loads are found *off-line* within a *single-step design* and remain fixed during communication. More important, tuning the antenna loads at such small spacing degrades the antenna efficiency, unless a dynamic matching circuit is assumed, thus complicating the whole system design. The efficiency degradation is an important issue addressed in this work.

Another relevant previous work on miniaturized antenna systems with desired antenna properties is [HSB+06] which describes a method to design a decoupling and matching network (DMN) for a set of preselected desired beampatterns and for compact antenna arrays. The present work is different from [HSB+06] the following ways

(i) A single active antenna and, thus, a single radio is used in the proposed architectures compared to the all-active antenna system of [HSB+06];

(ii) The DMN with shunt connections between the ports in [HSB+06] results in significant bandwidth reduction, enhanced Ohmic losses and, thus, smaller power gain compared to the type of uncoupled port matching of the proposed antenna systems [MKAL06; Alr11];

(iii) In the proposed work, we are able to express analytically the desired antenna properties in terms of antenna efficiency and diversity as function of the antenna loading conditions; This permits the proposed reduced-complexity radio architectures to be optimized for both antenna efficiency and angular diversity using a single optimization procedure (as described in Section 2.2.2). However, [HSB+06]

follows a different approach according to which two iterative processes are required; The first iterative process aims at designing a DMN fulfilling the power conservation under a hypothetical lossless network assumption and certain desired port pattern properties whereas the second iterative process describes the creation of a realizable lossy DMN.

In the following, Section 2.2.1 presents the system model whereas Section 2.2.2 describes the proposed UT antenna design approaches. Section 2.2.3 encompasses various practical enhanced receive SC antenna design examples as well as their performance evaluation.

2.2.1 System Model

The downlink scenario of a single cell multiuser wireless communication system is considered with one BS serving N UTs. We assume the BS equipped with M uncorrelated antennas whereas each of the UTs has K beams serving as K virtual antenna elements. A narrowband, quasi-static fading channel model is considered so that the channel response remains constant during one time slot and then it abruptly changes to a new independent realization. At the beginning of each time slot, the base station is initialized subject to a random beamforming vector and retains its beamforming configuration constant over the slot. Collecting signals received from K beams at the ℓth UT into one vector $\mathbf{y}_\ell \in \mathbb{C}^{K\times 1}$, we get

$$\mathbf{y}_\ell = \underbrace{(\eta\,\mathbf{R})^{1/2}\mathbf{H}_{\mathrm{w},\ell}}_{\mathbf{H}_\ell}\,\mathbf{w}\,s + \mathbf{n}_\ell, \tag{2.19}$$

where $s \in \mathbb{C}^{1\times 1}$ is the transmitted symbol whereas the transmit power level is fixed at P (i.e., $\mathbb{E}\{|s|^2\} = P$). $\mathbf{w} \in \mathbb{C}^{M\times 1}$ is the transmit beamforming vector applied at the BS in a random fashion with unitary allocated power (i.e., $\|\mathbf{w}\|^2 = 1$). $\mathbf{n}_\ell \in \mathbb{C}^{K\times 1}$ is the noise vector at the ℓth UT having i.i.d. circularly symmetric Gaussian entries with zero mean and variance σ_n^2, i.e., $\mathbf{n}_\ell \sim \mathcal{CN}\left(0, \sigma_\mathrm{n}^2\mathbf{I}_K\right)$. Assuming closely spaced antennas on the receiver side and UTs equipped with identical antenna systems, the spatial correlation and the antenna efficiency are modeled by the receive correlation matrix $\mathbf{R} \in \mathbb{C}^{K\times K}$ and the efficiency of the UT antenna system $\eta \in [0, 1]$, respectively. $\mathbf{H}_\ell \in \mathbb{C}^{K\times M}$ is the total channel matrix, $\langle\mathbf{H}_\ell\rangle_{kj}$ being the complex channel gain from the jth antenna at the BS to the kth antenna at the ℓth UT, given by $\mathbf{H}_\ell = (\eta\,\mathbf{R})^{1/2}\,\mathbf{H}_{\mathrm{w},\ell}$. This equation results by applying the well-established Kronecker model [SFGK00] with singe-sided (i.e., only receive) correlation, incorporating the receive antenna efficiency. $\mathbf{H}_{\mathrm{w},\ell} \in \mathbb{C}^{N\times M}$ has i.i.d. entries distributed as $\langle\mathbf{H}_{\mathrm{w},\ell}\rangle_{kj} \sim \mathcal{CN}(0, 1)$.

The equivalent SIMO channel $\mathbf{h}_\ell \in \mathbb{C}^{K\times 1}$ at the ℓth UT can be written as $\mathbf{h}_\ell = \mathbf{H}_\ell \cdot \mathbf{w}$,where $\langle\mathbf{h}_\ell\rangle_k$ is the equivalent channel seen at the kth antenna. Thus, the SNR perceived by the kth antenna at the ℓth UT is given by $\gamma_{\ell,k} = P\,|\langle\mathbf{h}_\ell\rangle_k|^2\,/\sigma_\mathrm{n}^2$.

2.2.2 Enhanced Selection Combining Antenna Architectures

In this section we describe the two proposed antenna architectures for enhanced SC at the UT, i.e., the S-UCA (Figure 2.8(a)) and the S-PA (Figure 2.8(b)). The S-UCA and the S-PA are smart antenna systems that present a significant advantage over their classical all-active antenna array counterparts: they are able to control their beampatterns as any smart antenna system, while being implemented using a *single RF chain*. The suggested architectures are depicted with wire antenna elements in Figure 2.8. However, it should be noted that the following analysis is general regardless of the specific antenna element deployed and that the proposed designs accept any kind of antenna elements that can be practically integrated into compact UTs, such as printed monopoles, slot antennas, planar inverted-F antennas (PIFAs), fractal antennas, etc.

2.2.2.1 Switched Uniform Circular Array

The first proposed UT antenna architecture is a S-UCA comprising a ring of K antenna elements (elements $1, 2, \ldots, K$ in Figure 2.8(a)) surrounding a central common passive reflector (element 0 in Figure 2.8(a)) at relative local angles of $0, 2\pi/K, \ldots, (K-1)2\pi/K$, respectively. According to the antenna SC, only one antenna out of the K available ones is active at each slot, i.e., connected to the single RF chain via a switch and used for communication. The passive reflector is short-circuited and loaded with a reactance $\mathrm{j}X_{\mathrm{L}}$ rather than being connected to the RF port. The passive reflector is fed inductively by radiated energy coming from the active (driven) element.

The kth (active) antenna, $k \in \{1, 2, \ldots, K\}$ has a corresponding beampattern $\mathcal{B}_k(\varphi)$ given by

$$\mathcal{B}_k(\varphi) = \mathbf{i}^{\mathrm{T}} \boldsymbol{\alpha}_k(\varphi), \tag{2.20}$$

where the azimuth angle φ denotes the angle of arrival (AoA). $\boldsymbol{\alpha}_k(\varphi)$ is the 2×1 response vector given by

$$\boldsymbol{\alpha}_k(\varphi) = \left[1 \quad e^{-\mathrm{j}\kappa r \cos[\varphi - (2\pi/K)(k-1)]}\right]^{\mathrm{T}}, \tag{2.21}$$

where r is the radius of the S-UCA corresponding to the spacing between each ith antenna and the passive reflector. Let I_{A} and I_{P} denote the current on each ith antenna and the current induced on the passive reflector, respectively. $\mathbf{i} \in \mathbb{C}^{2\times 1}$ is the corresponding current vector, given by

$$\mathbf{i} = v_{\mathrm{s}} \left(\mathbf{Z} + \mathbf{X}_{\mathrm{L}}\right)^{-1} \mathbf{u} = \left[I_{\mathrm{A}} \quad I_{\mathrm{P}}\right]^{\mathrm{T}}. \tag{2.22}$$

From (2.20)-(2.22) notice that the beampatterns $\mathcal{B}_k(\varphi)$, $k \in \{1, 2, \ldots, K\}$ are circularly symmetric to each other. In (2.22), v_{s} represents the transmitted voltage signal source with the amplitude and the phase from the driven RF port whereas $\mathbf{u} = [1 \quad 0]^T$.

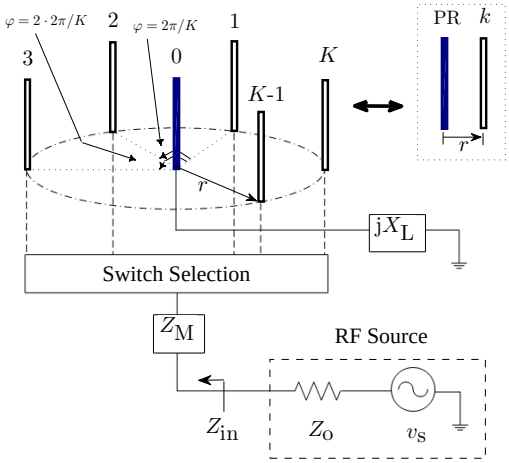

(a)

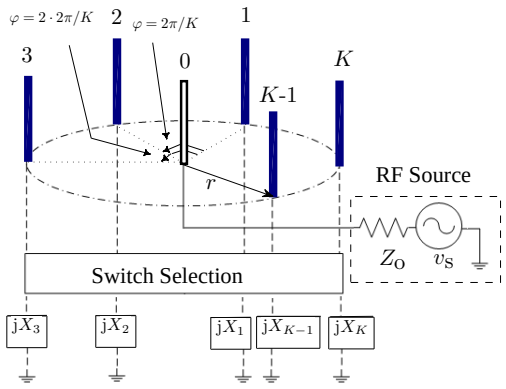

(b)

Figure 2.8: The proposed UT antenna configurations. (a): S-UCA of K antenna elements surrounding a single passive reflector (PR, element 0). (b): S-PA of K passive reflectors surrounding a single active element (element 0).

$\mathbf{Z} \in \mathbb{C}^{2\times 2}$ is the mutual impedance matrix given by

$$\mathbf{Z} = \begin{bmatrix} Z_{\mathrm{AA}} & Z_{\mathrm{AP}} \\ Z_{\mathrm{PA}} & Z_{\mathrm{PP}} \end{bmatrix}, \tag{2.23}$$

where Z_{AA} and Z_{PP} is the self-impedance of each kth antenna and of the passive reflector, respectively. $Z_{\mathrm{AP}} = Z_{\mathrm{PA}}$ is the mutual impedance between each kth antenna and the passive reflector. The loading matrix $\mathbf{X}_{\mathrm{L}} \in \mathbb{C}^{2\times 2}$ can be defined as

$$\mathbf{X}_{\mathrm{L}} := \mathrm{diag}\left([Z_{\mathrm{o}} + Z_{\mathrm{M}} \quad \mathrm{j}X_{\mathrm{L}}]\right), \tag{2.24}$$

where Z_{o} denotes the terminal impedance at the active port (equal to the characteristic impedance of 50 Ohm). $Z_{\mathrm{M}} = R_{\mathrm{M}} + \mathrm{j}X_{\mathrm{M}}$ represents the matching impedance attached to the active element as an additional degree of freedom (besides $\mathrm{j}X_{\mathrm{L}}$) when optimizing the antenna system for efficiency and diversity.

Defining the vector

$$\boldsymbol{\mathcal{B}}(\varphi) := [\mathcal{B}_1(\varphi) \;\; \mathcal{B}_2(\varphi) \;\; \ldots \;\; \mathcal{B}_K(\varphi)]^{\mathrm{T}} \tag{2.25}$$

and assuming a uniform PAS, the correlation matrix $\mathbf{R}$, whose entry $\langle \mathbf{R} \rangle_{kj}$ denotes the correlation between the kth and jth beam, can be written as

$$\mathbf{R} = \frac{1}{2\pi} \int_{-\pi}^{+\pi} \boldsymbol{\mathcal{B}}(\varphi) \boldsymbol{\mathcal{B}}^{\mathrm{H}}(\varphi) \cdot d\varphi, \tag{2.26}$$

where $\frac{1}{2\pi} \int_{-\pi}^{+\pi} \mathcal{B}_k(\varphi) \mathcal{B}_k^*(\varphi) \cdot d\varphi = 1$, $\langle \mathbf{R} \rangle_{kk} = 1$ and $\langle \mathbf{R} \rangle_{kj} = \langle \mathbf{R} \rangle_{jk}$, $k, j \in \{1, 2, \ldots, K\}$ by reciprocity. Notice that $\mathbf{R}$ is real-valued for circularly symmetric beampatterns over a full angular spread [VA87]. Moreover, the structure of $\mathbf{R}$ is characterized by the expression

$$\begin{aligned} &\forall \;\; k \in \{1, 2, \ldots, \lfloor K/2 \rfloor\}, \;\; j \in \{0, 1, \ldots, K-2\} : \\ &\langle \mathbf{R} \rangle_{1+(j \bmod K),[1+(j+k \bmod K)] \bmod K} = \\ &\qquad\qquad \langle \mathbf{R} \rangle_{2+(j \bmod K),[2+(j+k \bmod K)] \bmod K} \end{aligned} \tag{2.27}$$

which comes from the topology symmetry of any UCA and from the fact that pairs of equidistant antenna elements have the same correlation.

The efficiency of the S-UCA is given by

$$\eta = 1 - |\Gamma_{\mathrm{in}}|^2, \tag{2.28}$$

where Γ_{in} is the input reflection coefficient (return loss). Γ_{in} is given by

$$\Gamma_{\mathrm{in}} = (\mathrm{Z}_{\mathrm{in}} + Z_{\mathrm{o}})^{-1} (Z_{\mathrm{in}} - Z_{\mathrm{o}}),$$

where Z_{in} is the driving point impedance seen by any active antenna such that

$$Z_{\text{in}} = Z_{\text{AA}} + Z_{\text{M}} + \frac{I_{\text{P}}}{I_{\text{A}}} Z_{\text{AP}} = Z_{\text{AA}} + Z_{\text{M}} - \frac{Z_{\text{AP}}^2}{Z_{\text{AP}} + \text{j}X_{\text{L}}}. \tag{2.29}$$

Notice that Z_{in} remains constant $\forall k \in \{1, 2, \ldots, K\}$ and thus η is maintained for any active antenna due to topology symmetry.

In order to find the optimal loading conditions that jointly maximize the S-UCA efficiency and minimize the maximum correlation among the available set of antennas, we solve the following optimization problem over the variable loads Z_{M} and X_{L}

$$\begin{aligned} &\underset{(\text{over } R_{\text{M}}, X_{\text{M}}, X_{\text{L}})}{\text{maximize}} \quad \eta \\ &\text{subject to} \quad \max\{\langle \mathbf{R} \rangle_{kj}\} \leq 0.7, \quad k, j \in \{1, 2, \ldots, K\}, \\ &\qquad\qquad 0 \leq R_{\text{M}} \leq R_{\text{UB}}, \\ &\qquad\qquad X_{\text{LB}} \leq X_{\text{M}}, X_{\text{L}} \leq X_{\text{UB}}. \end{aligned} \tag{2.30}$$

We have constrained the magnitude of maximum correlation to be less that 0.7, which is an empirical value at which significant diversity gain is obtained (see the detailed work in [VA87]). The constraints on R_{M}, X_{M} and X_{L} depend on the realizable range of the loads, where R_{UB} is the upper bound on R_{M} whereas X_{LB} and X_{UB} are the lower and the upper bounds on X_{M} or X_{L}, respectively.

2.2.2.2 Switched Parasitic Array

The second proposed UT antenna architecture is a S-PA (see [Thi04] and references therein). The single active element is surrounded by a ring of passive reflectors where every passive reflector is short-circuited and loaded with passive loads via on/off switches, rather than being connected to the RF port. A S-PA has as many possible main beampatterns as the number of passive reflectors (given by K). The characteristics of the beampatterns (e.g., width, gain, nulls) depend on the passive reflectors loading and the array dimensions. The S-PA can switch among the K beam positions by properly controlling the state of the switches. This operation can be performed very fast, e.g. a PIN diode has a transient switching time in the order of nanoseconds [Poz05].

The proposed S-PA comprises K passive reflectors, i.e., elements $1, 2, \ldots, K$ in Figure 2.8(b), surrounding the single active element (element 0 in the same figure) at relative local angles of $0, 2\pi/K, \ldots, (K-1)2\pi/K$. Similarly to the S-UCA, each of the K beampatterns (in the far-field) is denoted by $\mathcal{B}_k(\varphi)$, $k \in \{1, 2, \ldots, K\}$ and is given by

$$\mathcal{B}_k(\varphi) = \mathbf{i}_k^{\text{T}} \boldsymbol{\alpha}(\varphi). \tag{2.31}$$

The jth element of the S-PA $K \times 1$ response vector $\boldsymbol{\alpha}(\varphi)$ is given by $\langle \boldsymbol{\alpha}(\varphi) \rangle_j = e^{-\text{j}\kappa r \cos[\varphi - (2\pi/K)(j-1)]}$. r is the spacing between the active element and the passive

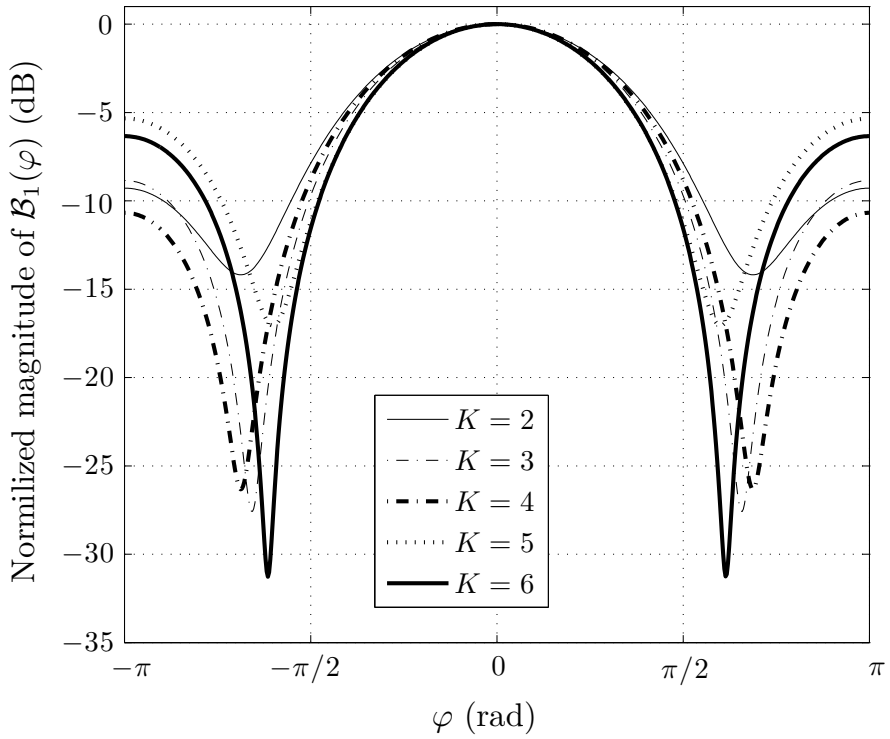

Figure 2.9: The normalized magnitude of the beampattern $\mathcal{B}_1(\varphi)$ for the different K-element S-UCAs.

reflectors and is equal to the radius of the S-PA. The notation $\mathbf{i}_k$ refers to the vector of induced currents on the antenna elements, required for creating the ith beampattern, given by

$$\mathbf{i}_k = v_\mathrm{s} \left(\mathbf{Z} + \mathbf{X}_k\right)^{-1} \mathbf{u} \in \mathbb{C}^{K\times 1}, \tag{2.32}$$

where v_s represents the transmitted voltage signal source. The matrix $\mathbf{Z} \in \mathbb{C}^{(K+1)\times(K+1)}$ is the mutual impedance matrix whose entry $\langle\mathbf{Z}\rangle_{kk}$, $k \in \{0, 1, \ldots, K\}$ is the self-impedance of the kth antenna element and $\langle\mathbf{Z}\rangle_{kj}$, $k \neq j$ is the mutual impedance between the kth and the jth antenna element (where $\langle\mathbf{Z}\rangle_{kj} = \langle\mathbf{Z}\rangle_{jk}$, $k, j \in \{0, 1, \ldots, K\}$ by reciprocity). The vector $\mathbf{u}$ is given by $\mathbf{u} = [1 \underbrace{0 \ \ldots \ 0}_{K}]^\mathrm{T}$.

Let the loading vector $\mathbf{x} = [X_1 \ X_2 \ \ldots \ X_K]$ Ohm denote the set of K loads to be mapped to the K passive reflectors, such that the circular rotation of the loading vector rotates the beampattern to one of the K angular positions (due to symmetry). Then, the matrix $\mathbf{X}_k \in \mathbb{C}^{(K+1)\times(K+1)}$ can be defined as

$$\mathbf{X}_k := \mathrm{diag}([Z_\mathrm{o} \ j\hat{\mathbf{x}}_k]), \tag{2.33}$$

where $\hat{\mathbf{x}}_k$, $k \in \{1, 2, \ldots, K\}$, is a circular permutation of $\mathbf{x}$ at which the ith beampattern is created and Z_o is the terminal impedance at the central active port. The jth element of $\hat{\mathbf{x}}_k$ is simply given by $X_{1+[(k+j-2) \bmod K]}$.

Similar to the S-UCA, defining the vector $\boldsymbol{\mathcal{B}}(\varphi)$ as in (2.25) and assuming a uniform PAS, the $K \times K$ correlation matrix $\mathbf{R}$, whose entry $\langle \mathbf{R} \rangle_{kj}$ denotes the correlation between the kth and jth beampattern, is given by (2.26) whereas the S-PA efficiency η is given by (2.28). However, in the case of the S-PA, the driving point impedance seen by the central active element Z_in is

$$\begin{aligned} Z_\mathrm{in} &= \langle \mathbf{Z} \rangle_{00} + \frac{1}{\langle \mathbf{i}_k \rangle_0} \sum_{j=1}^{K} \langle \mathbf{Z} \rangle_{0j} \langle \mathbf{i}_k \rangle_j \\ &= \frac{\mathbf{u}^\mathrm{T} \mathbf{Z} \left(\mathbf{Z} + \mathbf{X}_k \right)^{-1} \mathbf{u}}{\mathbf{u}^\mathrm{T} \left(\mathbf{Z} + \mathbf{X}_k \right)^{-1} \mathbf{u}}. \end{aligned} \tag{2.34}$$

Z_in remains constant $\forall k \in \{1, 2, \ldots, K\}$ and thus η is maintained for all $\mathcal{B}_k(\varphi)$, due to topology symmetry.

In the S-PA case, the optimization problem yielding the set of optimal reactive loads that jointly maximize the S-PA efficiency and minimize the maximum correlation among the available set of beams over the reactance space $\mathbf{x}$ can be written as

$$\begin{aligned} &\underset{(\text{over } \mathbf{x})}{\text{maximize}} \quad \eta \\ &\text{subject to} \quad \max\{\langle \mathbf{R} \rangle_{kj}\} \leq 0.7, \quad k, j \in \{1, 2, \ldots, K\}, \\ &\qquad\qquad X_\mathrm{LB} \leq X_j \leq X_\mathrm{UB}, \; j \in \{1, 2, \ldots, K\}, \end{aligned} \tag{2.35}$$

where X_LB is the lower bound and X_UB is the upper bound on the realizable range of the reactances X_j.

Comparing the optimization problems (2.30) and (2.35), we observe that the number of (real-valued) control variables is limited to 3 in the case of the S-UCA, whereas the S-PA has $2 \cdot K$ control variables. Thus, depending on the value of K (design parameter), the S-PA may have more degrees of freedom with respect to optimization flexibility compared to the S-UCA.

From the hardware point of view, while the RF path is switched in case of the S-UCA, the RF path remains unchanged in the S-PA as the loads surrounding the central active element are rotated. Mathematically this has been represented by a constant current vector and a permuting steering vector in the S-UCA case, whereas a fixed steering vector and a permuting current vector expresses the S-PA switching mechanism.

2.2.2.3 Average Throughput

Within SC and assuming all UTs equipped with the described optimally loaded S-UCA or S-PA, the antenna element with the highest SNR $\gamma_{\ell,k}$ is selected to receive the signal

Table 2.2: Optimized S-UCA Characteristics ($\eta = 1$)

K	Optimal loads (Ohm) $\{R_{\mathrm{M}}, X_{\mathrm{M}}, X_{\mathrm{L}}\}$	Correlation	FBR (dB)
2	$\{45, -32, -3\}$	$\langle \mathbf{R} \rangle_{12} = 0.0058$	9.2
3	$\{45, -8, -30\}$	$\langle \mathbf{R} \rangle_{12} = 0.4752$	8.8
4	$\{45, -6, -32\}$	$\langle \mathbf{R} \rangle_{12} = 0.6000$	10.6
		$\langle \mathbf{R} \rangle_{13} = 0.2379$	
5	$\{46, -27, -10\}$	$\langle \mathbf{R} \rangle_{12} = 0.6000$	5.3
		$\langle \mathbf{R} \rangle_{13} = 0.0078$	
6	$\{50, -8, -27\}$	$\langle \mathbf{R} \rangle_{12} = 0.5942$	6.3
		$\langle \mathbf{R} \rangle_{13} = 0.2030$	
		$\langle \mathbf{R} \rangle_{14} = 0.5935$	

for the ℓth UT. Once the ℓth UT selects the best beampattern and feeds back the corresponding SNR $\gamma_\ell^* = \max(\gamma_{\ell,1}, \ldots, \gamma_{\ell,K})$, the BS can schedule the user with the strongest γ_ℓ^*. The resulting average throughput can be computed as [PKP07]

$$C = \mathbb{E}\left\{\log_2\left[1 + \max_{\ell=1,\ldots,K}(\gamma_\ell^*)\right]\right\}. \tag{2.36}$$

2.2.3 Enhanced Selection Combining Antenna Design Examples and Performance Evaluation

2.2.3.1 Design Examples using Thin Electrical Dipoles

Throughput Performance

In this part we consider S-UCA set-ups of thin electrical dipoles vertical to the azimuth plane with $r = \lambda/20$ and different number of antenna elements, i.e., $K \in \{2, 3, 4, 5, 6\}$. The $\mathbf{Z}$ matrix is calculated using the analytical formulas shown in the Appendix 6 obtaining $Z_{\mathrm{AA}} = Z_{\mathrm{PP}} = 73.08 + \mathrm{j}42.50$ and $Z_{\mathrm{AP}} = 71.61 + \mathrm{j}24.25$. In order to solve the non-linear optimization problem in (2.30), we utilize an efficient interior point method for non-convex programming [BGN00; WMNO06] available in MATLAB® [mat]. We set $X_{\mathrm{LB}} = -100$ Ohm and $X_{\mathrm{UB}} = 100$ Ohm as a feasible realizable range for X_{M} or X_{L} whereas R_{M} is upper bounded by $R_{\mathrm{UB}} = 100$ Ohm. The efficiency is found maximum ($\eta = 1$) for all S-UCA setups whereas the calculated optimal loads and correlation values are shown in Table 2.2. The normalized magnitude of the obtained beampattern $\mathcal{B}_1(\varphi)$ at the first antenna is illustrated in Figure 2.9 for the different S-UCA set-ups. The front-to-back ratio (FBR) of the beampatterns, defined as $20\log_{10}|\mathcal{B}_1(0)/\mathcal{B}_1(\pi)|$, is also included in Table 2.2 which summarizes the favorable properties of the proposed S-UCA: maximum efficiency, low correlation values and high FBR are available within a compact single radio UT antenna system.

In order to evaluate the SC via the proposed UT architecture, we consider the optimally loaded S-UCA with $K = 6$ antennas. We compare to classical antenna SC

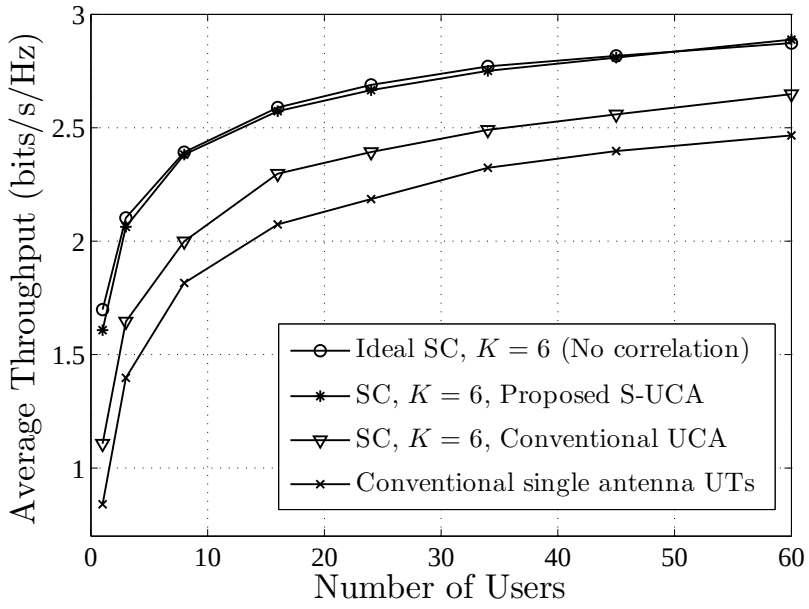

Figure 2.10: Average throughput as a function of the number of users.

with the same number of diversity branches [SA05]. For this reason, we consider a conventional UCA of the same radius r consisting of $K = 6$ dipoles with the same self-impedance $Z_{\text{AA}} = 79.33 - \text{j}19.65$. The UCA structure is similar to the proposed S-UCA structure of Figure 2.8(a), assuming the elements $1, 2, \ldots, 6$ as the available set of antennas and omitting the central dipole (element 0). We assume each dipole matched for maximum efficiency ($\eta = 1$). The correlation is given by a real-valued 6×6 receive correlation matrix $\mathbf{R}$. From [VA87] the correlation between any two antenna elements of the UCA assuming uniform PAS is given by $\langle \mathbf{R} \rangle_{kj} = \frac{1}{2\pi} \int_{-\pi}^{+\pi} e^{\text{j}\kappa d^{(k,j)} \cos\varphi} \cdot d\varphi = J_{\text{o}}(\kappa d^{(k,j)})$, where $d^{(k,j)}$ is the distance between the kth and the jth antenna element, $k, j \in \{1, 2, \ldots, 6\}$. In our case, $d^{(1,2)} = 2r \sin((2\pi/6)/2)$, $d^{(1,3)} = 2r \sin((2\pi/3)/2)$ and $d^{(1,4)} = 2r \sin((2\pi/2)/2)$. Therefore, we get $\langle \mathbf{R} \rangle_{12} = 0.9755$, $\langle \mathbf{R} \rangle_{13} = 0.9273$ and $\langle \mathbf{R} \rangle_{14} = 0.9037$.

As an upper bound on the achieved average throughput, we also consider the ideal case of SC with $\eta = 1$ and $K = 6$ fully uncorrelated diversity branches, i.e., $\langle \mathbf{R} \rangle_{kj} = 0, k \neq j, k, j \in \{1, 2, \ldots, 6\}$.

From Figure 2.10 it is evident that SC with the proposed optimally loaded S-UCA provides a significant increase to the average throughput as compared to the conventional single antenna UTs as well as to classical antenna SC for $M = 2$ and $P/\sigma_{\text{n}}^2 = 0$ dB. The observed gain for 3 users is 54% whereas classical antenna SC achieves only 17% with respect to single antenna UTs, revealing the significance of the proposed technique for small user populations. For 60 users, where the multiuser diversity gain dominates, the gain of SC with the proposed S-UCA decreases to 17%, whereas the gain of antenna SC with conventional UCAs drops to 6.5%. Notice that the

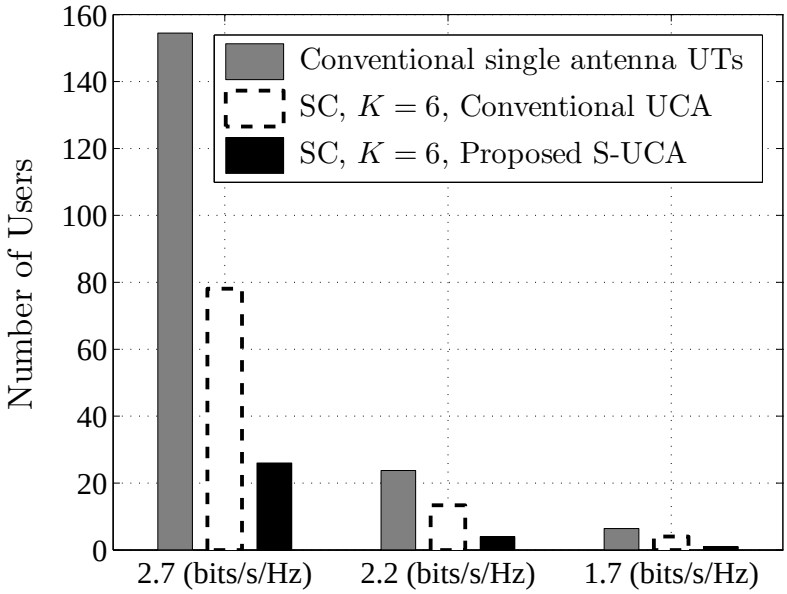

Figure 2.11: Number of users achieving a target average throughput.

performance of SC with the proposed practical antenna architecture almost achieves the throughput of the ideal case of 6 fully uncorrelated diversity branches.

Figure 2.11 shows the number of users required to achieve a target average throughput under different receive techniques ($M = 2$ and $P/\sigma_n^2 = 0$ dB). The figure shows that the SC with the proposed S-UCA requires almost one sixth the user population in order to obtain a certain performance compared to single antenna UTs. This confirms that SC represents an inherent form of multiuser diversity so that the degrees of freedom in the maximum selection increases from N to $N \cdot K$ [BS07]. It should be noted that comparable performance gains of SC using the proposed S-PA compared to the classical antenna SC have been obtained as illustrated in the simulation results of [TAPP10b].

Bandwidth Performance

The previous calculations are solely valid at the resonant frequency. In this part we aim at investigating the frequency response of the proposed antenna system. In general, the array bandwidth decreases as the mutual coupling level increases which is a natural phenomenon when considering closely spaced antenna elements where the strength of the reactive fields increases the quality factor of the antenna system. The problem worsens when decoupling the antennas using a DMN [MKAL06; Alr11]. In this work, however, we perform a type of uncoupled matching (i.e., without any shunt connections between the ports) for maximum efficiency and low correlation. In order to examine the frequency response of the proposed enhanced receive diversity system we establish

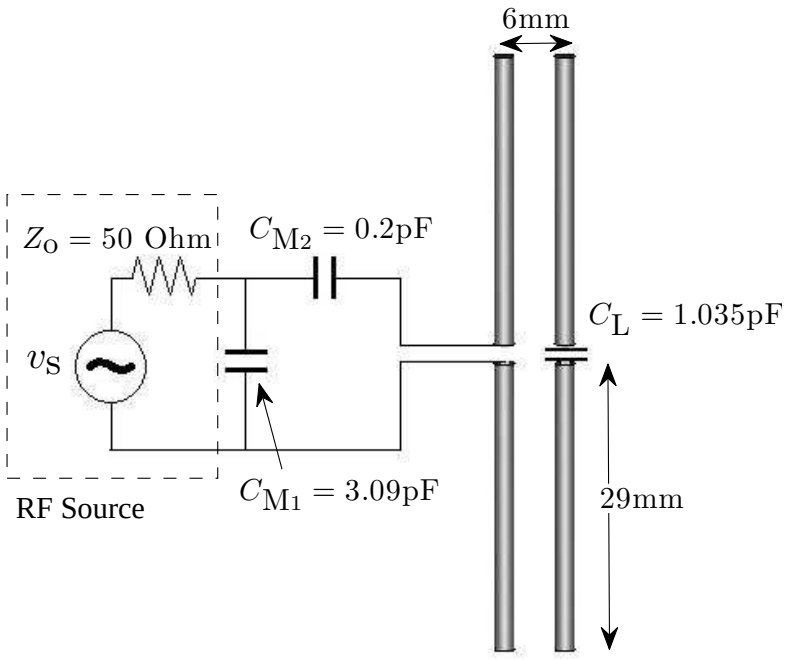

Figure 2.12: A four-element S-UCA design example comprising 60 mm long dipoles of 1 mm radius. At each time instant one dipole (out of the four) is active and closely coupled to the central passive one that is closed on a loading capacitor C_L.

a well-defined design of a four-element S-UCA comprising 60 mm long dipoles, each having a radius of 1 mm. A stand-alone dipole with these characteristics resonates at $f = 2.5$ GHz. A parasitic dipole (passive reflector) with the same dimensions closed on a capacitor C_L is placed at the center of the S-UCA (i.e., $X_L = (2\pi f C_L)^{-1}$). Figure 2.12 shows the proposed S-UCA structure depicting only one out of the four potentially active dipoles in close proximity to the central passive reflector. The RF source has a characteristic impedance $Z_o = 50$ Ohm and is assumed to be frequency independent and attached to the S-UCA through a L-section matching network of two capacitors C_{M1} and C_{M2}, after which a switch selects one of the four dipoles. An ideal RF switch modeled as short and open circuit at the on and off state, respectively, is assumed. The impedance parameters of the antenna system were obtained by full-wave electromagnetic modeling, using the commercially available electromagnetic wave simulator IE3D®. The 2×2 impedance matrix at the operating frequency of 2.5 GHz is

$$\mathbf{Z} = \begin{bmatrix} 113.84 + \text{j}36.01 & 112.27 - \text{j}29.30 \\ 112.27 - \text{j}29.30 & 113.84 + \text{j}36.01 \end{bmatrix}.$$

The values of the matching capacitors and the loading capacitor C_{M1}, C_{M2} and C_L,

respectively, are obtained by solving the optimization formulation in (2.30) (the optimal values are shown in Figure 2.12) leading to a maximum correlation of 0.5983 and efficiency of $\eta = 1$.

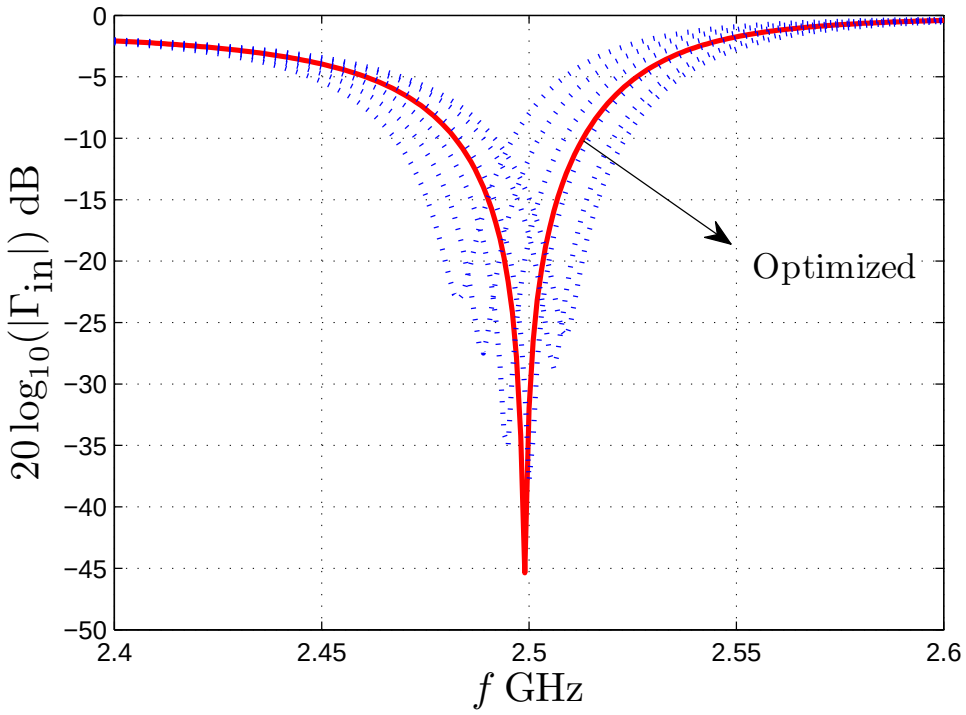

Figure 2.13: Frequency response of the four-dipole S-UCA design of Figure 2.12.

The frequency response of this S-UCA at the optimal component values is shown in the (red) solid curve in Figure 2.13 which depicts the absolute value of the input reflection coefficient (return loss) Γ_{in} in dB. The fractional bandwidth is 1.28% which maps to 32 MHz. It should be noted that an attempt to optimize the bandwidth has not been attained. Moreover, modern wideband systems requiring more bandwidth do not usually claim the whole band at one time, thus, the loading values can be tuned on demand in order to cover other bands as well.

Furthermore, in order to investigate the tolerance of the input return loss on the antenna loading, we varied C_L over a 16 Ohm range in steps of 2 Ohm and obtained the frequency responses corresponding to the (blue) dotted curves in Figure 2.13. It is obvious from Figure 2.13 that the change in the load does not alter the operational bandwidth but it alters the central frequency. This, however, can be recovered by local handset calibration which is already required in practice to compensate for the user proximity effects [MT10].

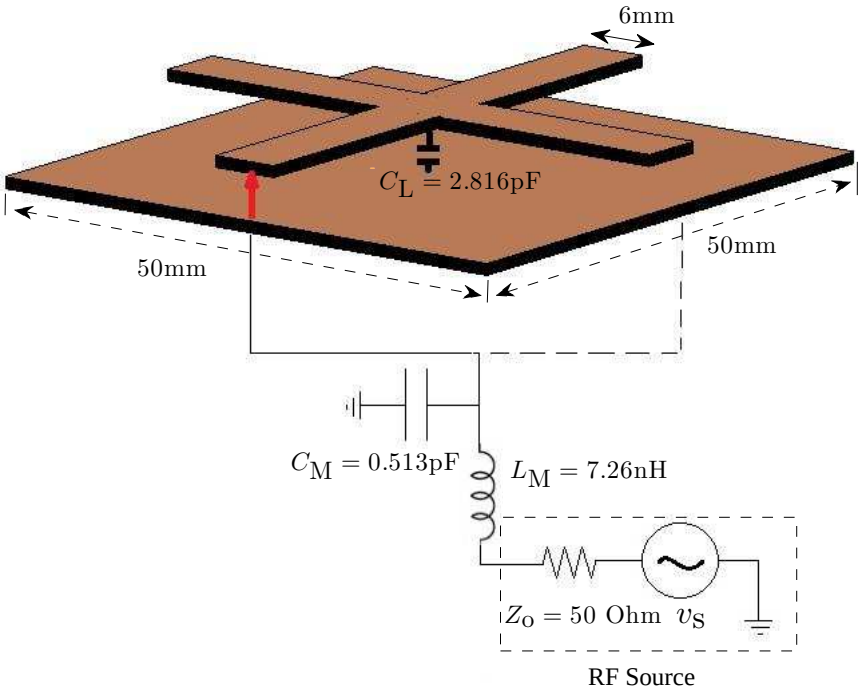

Figure 2.14: Practical S-UCA antenna design of four merged PIFA elements at 2.5 GHz.

2.2.3.2 Design Examples using Practically Integrable Antenna Elements

A design example of a S-UCA with antenna elements that can be practically integrated into compact UTs is the four-modified PIFA antenna system shown in Figure 2.14, which has been designed on a 50 mm $\times$ 50 mm printed circuit board (PCB) (almost half of the PCB area required for a bar-type phone chassis) operating at $f = 2.5$ GHz. The PIFA elements of this antenna system are modified in the sense that the excitation is done at the edge and the shorting is done in the middle of the element, whereas the inverse holds in a conventional PIFA element. The four antennas are merged over their common areas while a common shorting pin is terminated with a loading capacitor C_{L} mounted on the antenna structure itself (i.e., $X_{\mathrm{L}} = (2\pi f C_{\mathrm{L}})^{-1}$). The dimensions of the antenna are given on the same figure.

Figure 2.15 shows how the proposed structure has evolved from two opposite modified PIFAs which are merged together. The operation is repeated on the second and fourth edges of the PCB. The RF source in Figure 2.14 has a characteristic impedance $Z_{\mathrm{o}} = 50$ Ohm and is assumed to be frequency independent and attached to the S-UCA through a L-section matching network of a capacitor C_{M} and an inductor L_{M}, after which a switch selects one of the four ports of the merged PIFA structure (an ideal RF switch model is also assumed here). The red arrow in Figure 2.14 indicates such

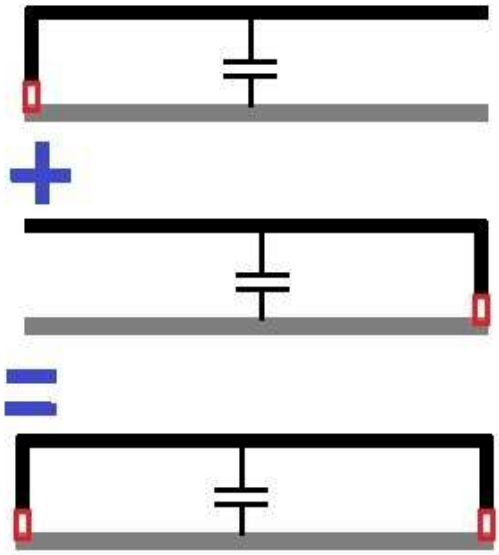

Figure 2.15: Two opposite merged modified PIFA antennas comprising the building block of the proposed S-UCA structure of Figure 2.14.

a potentially active PIFA port. The correlation between the PIFA pairs was obtained by full-wave electromagnetic modeling, using the electromagnetic simulator IE3D®. The reference port patterns (i.e., the radiation pattern of each port when excited by a unit voltage signal and the other ports are terminated with 50 Ohm) at the operating frequency of 2.5 GHz were extracted and exported to a MATLAB routine out of which the correlation between the communication beams is found, in a procedure similar to the one in [APCK12]. The 2×2 impedance matrix at 2.5 GHz is obtained as

$$\mathbf{Z} = \begin{bmatrix} 17.88 + \mathrm{j}382.60 & 1.06 - \mathrm{j}29.71 \\ 1.06 - \mathrm{j}29.71 & 1.13 + \mathrm{j}25.12 \end{bmatrix}.$$

The L-section matching of C_{M} and L_{M} as well as the value of the loading capacitor C_{L} are optimized for low correlation and maximum efficiency according to the optimization formulation in (2.30). The optimal values of the load C_{L} and matching elements C_{M}, L_{M} are given on Figure 2.14. The maximum correlation at the designated values in Figure 2.14 is found equal to 0.63 whereas the efficiency is $\eta = 0.99$. The frequency response of the antenna is given in Figure 2.16.

Another excellent example of extremely compact antennas for mobile terminals are

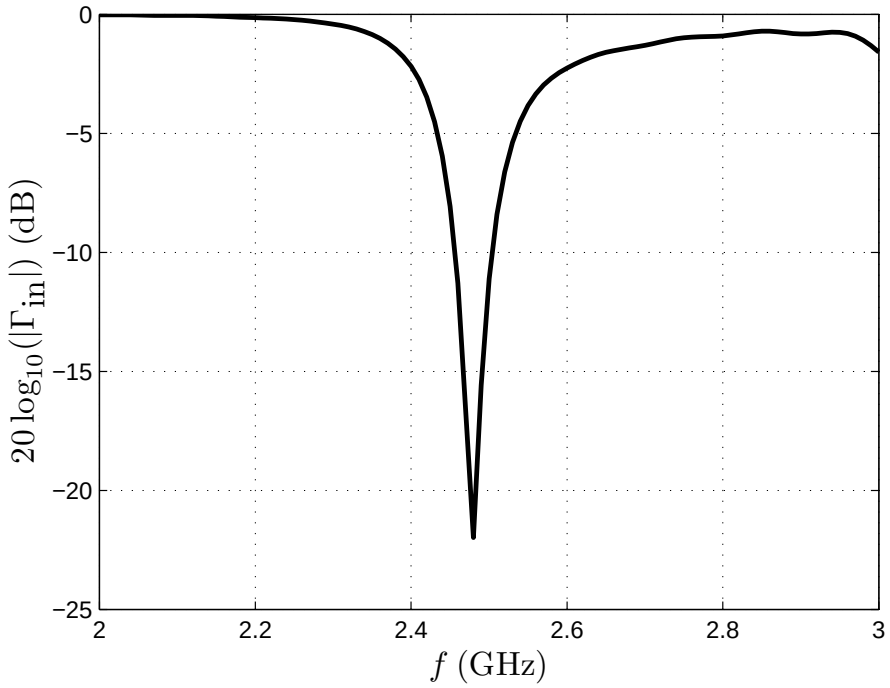

Figure 2.16: Frequency response of the practical receive diversity antenna design of Figure 2.14.

element couplers [SST06] where the antenna is simply a matching component that excites the characteristic modes of the ground plane of the mobile device (i.e., the mobile device chassis modes) [HM71]. This type of antenna, namely the switched-chassis mode system, is capable of exciting different weakly-correlated modes acting as virtual uncorrelated antennas. It should be noted that an analysis similar to the one proposed for the S-UCA or the S-PA system can be also applied to the switched-chassis mode system.

The work in this section has proposed SC via optimized realistic receive antenna architectures for compact low cost UTs in multiuser environments. It has been shown that the proposed compact S-UCA or S-PA antenna systems are able to achieve performance gains in terms of average throughput comparable to widely-spaced antennas, by properly optimizing the antenna loading conditions for both antenna efficiency and diversity.

2.3 Conclusions

In this chapter we have shown how to utilize passive radiators in order to alter the far-field and the near-field properties of an antenna system and, therefore, to alter the propagation channel. Specifically, in Section 2.1, this technique has been exploited in order to enhance the ergodic and outage single-link MIMO performance. On the other hand, in Section 2.2, the passive radiators have been deployed to virtually increase the user population in a multiuser diversity system by equipping the user terminals with reduced-complexity switched-beam systems. By properly optimizing the antenna terminations, we have demonstrated that efficient and weakly correlated beams may provide a performance comparable to distantly spaced (switched) antennas. Finally, these performance gains come at no significant additional cost and hardware complexity.

2. MULTI-ACTIVE MULTI-PASSIVE ANTENNA ARRAYS FOR MIMO AND MULTIUSER DIVERSITY SYSTEMS

3

Parasitic Antenna Systems for Cognitive Radio Applications

The coexistence of multiple mobile and static users with various data rate requirements in current wireless network environments is limited by the finite radio resources, especially the electromagnetic spectrum. The traditional licensing of specific-sized swaths of the radio spectrum for personal communications has led to the conclusion that a high percentage of the spectrum becomes underutilized at a specific time and in a specific geographic location [Com02]. CR is a novel technology paradigm towards efficient radio spectrum usage. It refers to a wireless communication system intended to enable a secondary user (SU) to operate in the same frequency subband originally allocated to a legacy or primary user (PU) [Hay05]. By intelligently utilizing any available side information about activity, channel conditions, codebooks or even messages of the other nodes, the SU adapts its transmission parameters so as to preserve the QoS of the PU while trying to maximize its own throughput. Therefore, mitigating the interference caused to the PU by the secondary transmissions is a predominant issue.

The advent of the CR concept has led to significant scientific research resulting in three main CR modes of operation: *overlay*, *underlay* and *interweave* [GJMS09]. In the first two modes the SU is allowed to simultaneously transmit over the same frequency band with the PU. The theoretical overlay paradigm assumes the SU transmitter is aware of the PU's transmission codebooks and messages and of all the channels in the PU-SU coexisting system. The SU exploits such knowledge to *a*) relay the primary signal with a power large enough to ensure that the SNR at the licensed receiver remains unaffected and *b*) cancel the PU's interference caused at the SU receiver. The underlay model requires knowledge only of the channel between the SU transmitter and the PU receiver and allows the SU to communicate subject to the resulting interference at the PU receiver is not exceeding the imposed interference temperature constraint [GJMS09]. Transmit precoding with power control, known as cognitive beamforming, falls under this category. On the other hand, the interweave system, referred to as *opportunistic spectrum access* (OSA), does not permit concurrent PU-SU transmissions. The SU should be able to perform spectrum sensing and identify vacant frequency sub-

bands, the so-called *spectral white spaces*, in order to communicate with its intended receiver. Since the SU transmitter is not required to have knowledge of the channels and of the PU's messages and due to its theoretical promise to avoid simultaneous communications with the PU system, the OSA is considered more practical and favorable from implementation point of view. For instance, the OSA is the approach adopted in the first standardization effort of the CR technology within the IEEE 802.22 standard [SCL+09]; consequently, spectrum sensing is a key element for the establishment of the CR concept.

Focusing on OSA, the CR transceiver has to monitor the available frequency spectrum and reconfigure to transmit on a different frequency when necessary. Spectrum sensing over various frequency subbands and radio reconfiguration impose certain challenges on the CR hardware and the antenna design [GHH+08]. This chapter addresses the major design challenges of antenna systems intended for cognitive transceivers under compactness constraints by proposing CR sensing and communication techniques using reduced-complexity smart-antenna CR transceiver architectures. The antenna systems proposed henceforth are based on parasitic antenna theory, and specifically, on the ESPAR single-radio parasitic array architecture featuring low-power consumption, low cost and ease of fabrication. This antenna system is firstly presented in Section 3.1. Section 3.2, provides an overview of the design challenges with regards to sensing over different frequencies and angular directions, referred to as *spatial spectrum sensing*. Subsequently, we describe a novel approach based on the ESPAR antenna theory aiming at making spatial spectrum sensing feasible for lightweight terminals. The idea is to replace the wideband antenna required for sensing over a large bandwidth by *a tunable narrowband antenna for both sensing and communication purposes*. The flexibility of the proposed antenna system lies in its capability to scan both the frequency and the spatial resource dimension simultaneously via a single RF chain within a miniaturized antenna system. This is done by properly tuning a set of reactive loads connected to a group of parasitic elements closely coupled to the driven (active) element. By doing so, the operational frequency subband leaps to another subband (frequency tuning). Moreover, at every subband, circular permutations of the reactive loads rotate the narrowband beampattern to different angular positions giving the cognitive transceiver the capability of sensing over various segments of the space.

Exploiting the spatial spectrum sensing concept, Section 3.3 describes spectrum sensing using single-radio switched-beam arrays with reactance-loaded parasitic elements based on the ESPAR architecture. As in Section 3.2, circular permutations of the reactive loads at a given frequency rotate the narrowband beampattern to different angular positions dividing the whole space around the cognitive receiver into several angular subspaces. The beampattern directionality leverages the performance of spectrum sensing algorithms like energy detection by enhancing the receive SNR. Moreover, the selection combining across the weakly correlated beampatterns gives rise to a diversity action further boosting the probability of detection.

Finally, Section 3.4 presents the concept of analogue orthogonal precoding allowing to null the interference toward a number of K PUs. Orthogonal transmission toward K

undesired receivers via conventional digital beamforming techniques requires at minimum $K+1$ active transmit antennas. As the RF complexity increases linearly with the number of active antennas, orthogonal transmit precoding becomes impractical for simple user terminals. We propose an alternative solution utilizing the ESPAR antenna system. The presented orthogonal precoding technique emulates classical digital orthogonal precoding for suppressing the interference toward a number of users, but with a highly reduced RF complexity.

3.1 ESPAR Antenna Theory

A parasitic antenna consists of one or more parasitic elements, i.e., antenna elements terminated with passive loads rather than being connected to the RF port. The parasitic element is fed inductively by radiated energy coming from the driven element (i.e., the element connected to the RF port of the transceiver). If the parasitic element radiates away from the driven element, it is called a director which is usually the case when loading the parasitic element with an inductive load (positive reactance). If the parasitic element radiates toward the driven element, it is called a reflector which is usually the case when loading the parasitic element with a capacitive load (negative reactance).

Parasitic antenna systems have been widely used over many years for military and later for commercial analogue TV reception via the well-known Yagi-Uda antenna (the ladder antenna), usually seen on buildings' rooftops. This directive antenna system is mechanically steered toward the angular direction that maximizes the quality of the received signal. In 2000, the ATR labs in Japan developed a smart antenna system referred to as the ESPAR (electronically steerable parasitic array radiator) antenna [OI04; OG00]. A $(K+1)$-element ESPAR antenna has a central active element surrounded circularly by K parasitic elements. Every parasitic element is closed on (i.e., terminated with) a variable reactive load which is usually a variable reactor (varactor) diode or an arrangement of varactor diodes. The ESPAR beampattern is controlled in the analogue domain via DC control signals that properly reverse bias the varactor diodes within a given range of values. The K parasitic elements are kept at quarter of a wavelength away from the central active element so that the tuning of the parasitic elements' loads does not affect the input (driving point) impedance (and hence the efficiency) of the antenna system.

The ESPAR was mainly intended as an adaptive antenna that maximizes the signal to SINR by properly steering the beam gain and null [SHOK04]. Parasitic antenna systems with compact dimensions have been proposed in [AKPP09b] for analogue MIMO where the different datastreams are smartly encoded onto the set of the reactive loads, i.e., the information is embedded within the angular variations of the beampatterns.

The ESPAR antenna is a smart antenna system that presents a significant advantage over its predecessors: it is able to control its beampatterns as any smart antenna system, while being implemented using a *single active element* and K parasitic elements placed around the active one.

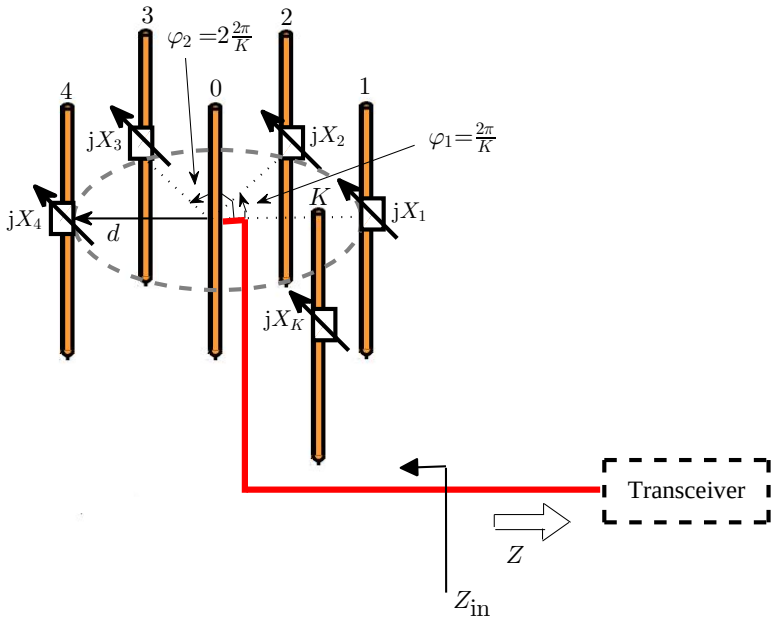

Figure 3.1: The $(K+1)$-element ESPAR antenna system.

To form a beam in space, several parasitic elements are installed near the main radiating elements and are electromagnetically coupled (e.g., Fig 3.1 with half-wavelength thin electrical dipoles dipoles). The parasitic elements are short-circuited and loaded with varactors that control the imaginary part of the parasitic elements' input impedances. By adjusting the varactors' response, the beampattern of the ESPAR antenna system can be controlled to direct its gain and null toward certain directions in an adaptive or predefined fashion. It should be noted that the S-PA presented in Section 2.2 is a specific application of an ESPAR antenna system with a fixed number of different possible beampatterns, equal to the number of parasitic elements.

The currents on the ESPAR antenna elements are induced by mutual coupling with the current on the central active element according to the following equation [OG00]

$$\mathbf{i} = v_{\mathrm{oc}} \underbrace{(\mathbf{Z} + \mathbf{X})^{-1}}_{\mathbf{w}_{\mathrm{eq}}} \mathbf{u}, \tag{3.1}$$

where $\mathbf{i} \in \mathbb{C}^{(K+1)\times 1}$ is the current vector In (3.1), v_{oc} is the open-circuit voltage of the exciting signal source at the central feeding element with the amplitude and the phase from the driving RF port (during transmission) or the open-circuit voltage induced at the central active element during reception. The vector $\mathbf{w}_{\mathrm{eq}} = [\mathbf{Z} + \mathbf{X}]^{-1}\,\mathbf{u}$ is termed as

the "*equivalent weight vector*" [SHOK04]. The matrix $\mathbf{Z} \in \mathbb{C}^{(K+1)\times(K+1)}$ is the mutual impedance matrix whose entry $\langle \mathbf{Z} \rangle_{kk}$ is the self-impedance of the kth antenna element and $\langle \mathbf{Z} \rangle_{kj}$, $k \neq j$ is the mutual impedance between the kth and the jth antenna element, where $\langle \mathbf{Z} \rangle_{kj} = \langle \mathbf{Z} \rangle_{jk}$, $k, j \in \{0, 1, \ldots, K\}$ due to reciprocity. $\mathbf{u}$ is a selective vector

$$\mathbf{u} = [1 \quad \underbrace{0 \quad \ldots \quad 0}_{K}]^{\mathrm{T}}. \tag{3.2}$$

Let the loading vector $\mathbf{x} = [X_1 \; X_2 \ldots X_K]^{\mathrm{T}}$ Ohm denote the set of K loads to be mapped to the K parasitic elements. Then, the matrix $\mathbf{X} \in \mathbb{C}^{(K+1)\times(K+1)}$ can be defined as

$$\mathbf{X} := \mathrm{diag}([Z \; \mathrm{j}\mathbf{x}]). \tag{3.3}$$

In (3.3), $Z = Z_{\mathrm{o}}$ is the terminal impedance at the central active port (at transmission) or $Z = Z_{\mathrm{L}}$ is the load impedance of the receiver, i.e., the output impedance of the LNA (at reception). It is usually assumed $Z = 50$, i.e., that Z is equal to the characteristic impedance of 50 Ohm for matching purposes.

The beampattern of the ESPAR antenna in the far-field is obtained generally as

$$\mathcal{B}(\Omega) = \mathbf{i}^{\mathrm{T}} \boldsymbol{\alpha}(\Omega) = v_{\mathrm{oc}} \mathbf{w}_{\mathrm{eq}}^{\mathrm{T}} \boldsymbol{\alpha}(\Omega) \tag{3.4}$$

where the solid angle Ω (in steradians) represents the AoD (at transmission) or the AoA (at reception). $\boldsymbol{\alpha}(\Omega)$ is a column vector of the isolated patterns of the ESPAR antenna elements corresponding to the response vector (at reception) or the array steering vector (at transmission) and is given by the antenna geometry. In the azimuth plane, the kth parasitic element is placed at a relative local angle of $\varphi_k = (k-1)\frac{2\pi}{K}$, $k \in \{1, \ldots, K\}$, thus we obtain

$$\boldsymbol{\alpha}(\varphi) = \left[1 \; e^{-\mathrm{j}\kappa d \cos(\varphi)} \; \ldots \; e^{-\mathrm{j}\kappa d \cos(\varphi-(K-1)(2\pi/K))}\right]^{\mathrm{T}}, \tag{3.5}$$

where d is the radius of the ESPAR, equal to the spacing between the central active element and the parasitic elements.

Assuming negligible ohmic losses, any losses in the ESPAR system may result from the mismatch between the source impedance and the input impedance seen by the central active antenna. The input impedance Z_{in} of the active element and the corresponding reflection efficiency because of impedance mismatch can be respectively written as

$$Z_{\mathrm{in}} = \langle \mathbf{Z} \rangle_{00} + \frac{1}{\langle \mathbf{i} \rangle_0} \sum_{k=1}^{K} \langle \mathbf{Z} \rangle_{0k} \langle \mathbf{i} \rangle_k = \frac{\mathbf{u}^{\mathrm{T}} \mathbf{Z} \left(\mathbf{Z} + \mathbf{X}\right)^{-1} \mathbf{u}}{\mathbf{u}^{\mathrm{T}} \left(\mathbf{Z} + \mathbf{X}\right)^{-1} \mathbf{u}}, \tag{3.6}$$

$$\eta = 1 - |\Gamma_{\mathrm{in}}|^2, \tag{3.7}$$

where the input reflection coefficient Γ_{in} is given by

$$\Gamma_{\mathrm{in}} = (Z_{\mathrm{in}} + Z)^{-1}(Z_{\mathrm{in}} - Z^*). \tag{3.8}$$

The 7-element ESPAR [OG00] is a concrete application of the ESPAR theory over which a fast beamforming algorithm, described in [SHOK04], is employed.

3.2 Spatial Spectrum Sensing for Small Cognitive Radio Transceivers

Spectrum sensing is an essential component of an OSA CR system aiming to obtain awareness regarding the spectrum occupancy and the PU activity in a specific region. The key role of spectrum sensing is to identify transmission opportunities for the SUs by detecting unoccupied spectrum segments with as much accuracy and low latency as possible. Apart from the frequency dimension, spectral white spaces can be observed across other dimensions such as the *angle* (referred to as *space* herein), rendering the spectrum sensing a multi-dimensional CR functionality [YA09]. The spatial dimension can reveal additional transmission opportunities through sensing along different directions over different beampatterns. The so-called *spatial spectrum sensing* is conventionally implemented using multiple RF chains connected to antenna elements spaced typically by half the carrier wavelength, making the scheme practical for base stations and access points where size, cost and complexity are affordable [TZNZ09]. However, spatial spectrum sensing has not attracted much attention when considering compact lightweight CR terminals. It is the subject of this section to address the major design challenges of cognitive antenna systems intented for size and cost constrained terminals supporting spatial spectrum sensing. Our approach is influenced by the breakthrough work in [SHOK04] and [AKPP09b] where single RF chain transceivers incorporating low-cost passive or parasitic elements have been proposed for analogue beamforming and compact analogue MIMO systems, respectively.

In this section, we first provide an overview of the antenna design challenges and hardware constraints faced in CR systems employing OSA. A concise description of the spatial spectrum sensing approach and its implementation requirements is also provided. To this end, we propose an enhanced cognitive antenna system that is cabable of spatial spectrum sensing comprising a low-cost narrowband antenna tunable over a wide spectrum (frequency-agile antenna).

3.2.1 Design Challenges and the Role of the Spatial Dimension

Spectrum sensing is an essential component of a CR system aiming at obtaining awareness regarding the spectrum occupancy and the PU activity in a specific area. Various approaches, enabling algorithms and aspects of spectrum sensing for CR applications can be found in [YA09]. In this section, we describe in brief the hardware and antenna challenges associated with spectrum sensing. Moreover, we introduce the spatial spectrum sensing concept exploiting the space resource for CRs.

3.2.1.1 Design and Hardware Requirements of Spectrum Sensing

In order to protect the legacy users from interference, a versatile radio is required to monitor the spectrum, sense the existence of PUs and vacate the frequency channel whenever PU activity is detected resuming operation on another spectral white space. The aforementioned actions should be performed fast enough to ensure interference-free communication for the PUs as well as a virtually seamless SU transmission. This imposes certain requirements on the CR front-end declared by the need for high speed processing units (DSPs, FPGAs) to perform computationally demanding signal processing tasks with relatively low delay. Moreover, spectrum sensing demands high sampling rates and high resolution ADCs with small power dissipation ensuring good battery lifetime for portable devices [YA09]. The large dynamic range of the ADCs is an important issue especially with regards to the detection of weak PU signals such as the low-power wireless microphone emissions over the TV spectrum [SCL+09]. In [BRJ08] the ADC parameters which restrict the implementation of current ADCs in CR terminals supporting spectrum sensing are outlined and the main ADC architectures are presented.

In order to utilize all the available spectral opportunities, sensing should be performed over a wide bandwidth, often spanning a frequency range greater than 1.4 GHz [GHH+08]. However, wideband antennas generally have higher complexity and bigger size invoking significant problems for handheld devices and necessitating actions toward size economies [YA09]. Specifically, a wideband antenna with small dimensions compared to the carrier wavelength has low efficiency, denoted by the ratio of the radiated power to the power fed into the antenna [GHH+08]. This, in turn, creates problems in designing wideband antennas for compact CR terminals operating at low frequency bands. Furthermore, narrowband antennas inherently provide a level of bandpass filtering alleviating the need of complicated RF filter circuits. In addition, the selectivity circuit of the RF filter should be tunable so that the CR transceiver can operate over multiple subbands. [Tan06] describes two tunable bandpass filters using varactors for CR implementations in the VHF and UHF bands, respectively. It should be also noted that the large operating bandwidths impose additional requirements to the power amplifiers [YA09].

While the spectrum sensing is a wideband operation, the SUs often communicate over a narrower channel bandwidth (e.g., as in GSM, UMTS, WiMAX, ATSC / NTSC). For this reason, it is conjectured that there is a need for a wideband antenna for sensing while a narrowband antenna with a reconfigurable frequency would handle communication [GHH+08]. For example, the IEEE 802.22 customer premise equipments (CPEs) are equipped with a wideband omni-directional antenna for spectrum sensing whereas a narrowband directional antenna communicates with the base station [SCL+09]. The approach of using two different antennas for sensing and communication is often combined with a dual-radio architecture allowing the spectrum sensing and communication processes to run in parallel over two distinct radio chains [GHH+08]. This has the advantage of continuous, thus, more accurate spectrum monitoring at the expense of increased DC power consumption and extra RF hardware cost and complexity [YA09].

It should be noted here that a single wideband antenna could be sufficient for both chains [YA09] [GHH+08]. On the other hand, in [KEH+08] the authors present two architectures of integrated wideband and narrowband antennas into the same volume for parallel and switched operations, respectively. This integration is an implementation choice of great importance in handheld devices with limited physical area. In the second architecture presented in [KEH+08], the switching between narrowband / wideband operations usually implies a single-radio architecture supporting spectrum sensing and communication on different time slots. As a result of the non-continuous sensing over limited time intervals, only a certain accuracy can be guaranteed for the spectrum sensing results [YA09]. However, due to its simplicity and lower cost, the single-radio architecture is a strong candidate for compact CR devices [GHH+08].

The switching between the narrowband and the wideband operations in [KEH+08] is performed via a reconfigurable antenna by selectively switching in and out parts of the antenna structure. Antenna reconfiguration can be also achieved by changing the antenna geometry via mechanical movement or by adjusting the loading or matching of the antenna using an external circuit [GHH+08]. The proposed spatial spectrum sensing approach described later in this section falls within the last category; however, the dynamic matching of the driven or active element (i.e., the antenna element connected to the RF port of the transceiver) in our work will be implemented without any direct connection to the RF path, thus avoiding possible insertion losses.

3.2.1.2 Spatial Spectrum Sensing for Cognitive Radios

Conventional sensing methodologies identify transmission opportunities across three main dimensions [YA09]:

- frequency: at a particular time instant, certain frequency subbands may be occupied and others may be empty
- time: a certain frequency subband may be occupied in one time instant and might be vacant in another time
- geographic area: radios located at different geo-positions could detect different spectral white spaces due to their physical separation

However, it has been suggested (see [YA09] [GHH+08] and references therein) that orthogonal PU-SU transmissions can also be achieved by exploiting the angular or spatial dimension. For example, knowing the AoA of the PU signal, a transmission opportunity can be created by communicating on another direction without causing interference to the PU. Alternatively, a SU equipped with a directive steerable antenna can monitor the frequency spectrum in all directions supporting spatial spectrum sensing. In this manner, the SU is able to identify angular directions vacant of PU activity in a given frequency, referred to as *spatial-spectral white spaces*. Thus, spatial spectrum sensing unveils new opportunities for transmission enhancing the secondary system capacity.

Increasing significantly the spatial resolution by creating very narrow steerable beams would theoretically increase the transmission opportunities. However, this would

also result in a higher sensing time in order to scan the whole space as well as in a larger computation and storage task. For this reason, the spatial discrimination should be selected in accordance with the aforementioned limitations, a design aspect that is considered in the proposed spatial spectrum sensing approach described in the next section.

Furthermore, the authors in [TZNZ09] propose a space-time frequency sensing technique assuming the SUs equipped with antenna arrays that create a number of orthogonal concurrent beampatterns. Nevertheless, such systems, as well as the conventional steerable directive antennas, incorporate an array of active elements, and thus, extra RF hardware amplifying the cost, complexity and DC power consumption requirements. Moreover, the spacing of the multiple antenna elements is usually set to half the carrier wavelength, leading to large array implementations, especially at low frequencies. For example, regarding the TV bands, the antenna spacing will be in the order of a few meters, making the implementation practical only at the base stations. The size limitations of compact CR front-ends are also taken into account within the proposed sensing approach, as explained in the following.

3.2.2 A Novel Spatial Spectrum Sensing Approach Based on Parasitic Antenna Theory

In this work, we shift the paradigm of the parasitic antenna design from analogue beamforming and analogue MIMO into an analogue cognitive antenna system that is tunable over the frequency dimension and steerable over the spatial dimension. We propose a novel antenna system, similar to the ESPAR antenna in principle, but designed specifically as a space-spectrum sensing antenna system for compactness-constrained transceivers.

3.2.2.1 Electronic Spatial Spectrum Sensing Passive Array Receptor (*E3SPAR*)

The proposed ESPAR antenna paradigm described in the following is referred to as *E3SPAR*. The classical ESPAR antenna has the objective of maximizing the SINR, usually at a given narrowband frequency. However, the main objective in a cognitive front-end is to jump to different parts of the spectrum in a dynamic manner aiming at detecting spectal holes as well as exploiting the precious spatial resource (thus extracting extra degrees of freedom). The main idea we propose in this work is to shift the operational (resonant) subband of the ESPAR antenna by properly controlling the set of varactors, i.e., to perform reactive frequency tuning. This is done by first reducing significantly the distance between the parasitic elements and the central driven element, resulting in a super-directive [OY06] but sensitive array structure due to the strong reactive fields at quite small spacing. The sensitivity of the array structure to any loading conditions is exploited in a way that the set of the parasitic elements are used as a dynamic matching circuit at a given desired frequency subband. Therefore, now we can express the impedance matrix as a function of frequency $\mathbf{Z}(f)$ and we can

explicitly write the loading vector as a function of frequency

$$\mathbf{x}(f) = [X_1(f)\ X_2(f) \dots X_K(f)]^{\mathrm{T}}. \tag{3.9}$$

This means that the parasitic elements can be properly controlled so that the antenna system resonates at the desired frequency subband by minimizing the input reflection coefficient $\Gamma_{\mathrm{in}}(f)$. Moreover, having found the set of the optimal reactive loads at a given frequency, the circular permutation of the reactive loads over the parasitic elements (in a given symmetric antenna topology) shifts the narrow beampattern to one of the K angular positions due to symmetry without affecting $\Gamma_{\mathrm{in}}(f)$. Thus, the circular rotation of the loading vector $\mathbf{x}(f)$ rotates the beampattern to one of the K angular positions (due to symmetry). Hence, we write the equivalent weight vector at which the kth beampattern is created as

$$\mathbf{w}_{\mathrm{eq},k}(f) = [\mathbf{Z}(f) + \mathbf{X}_k(f)]^{-1}\,\mathbf{u}, \tag{3.10}$$

where $\mathbf{X}_k(f)$ is defined as

$$\mathbf{X}_k(f) = \mathrm{diag}([Z\ \mathrm{j}\hat{\mathbf{x}}_k(f)]) \tag{3.11}$$

and $\hat{\mathbf{x}}_k(f) \in \{1, \dots, K\}$ is a circular permutation of $\mathbf{x}(f)$ at which the kth beampattern is created so that the jth element of $\hat{\mathbf{x}}_k(f)$ is given by $\langle \hat{\mathbf{x}}_k(f) \rangle_j = X_{1+[(k+j-2) \mod K]}(f)$. Finally, the free-space beampattern at the kth angular position is

$$\mathcal{B}_k(\Omega, f) = v_{\mathrm{oc}}(f)\mathbf{w}_{\mathrm{eq},k}^{\mathrm{T}} x(f)\boldsymbol{\alpha}(\Omega, f). \tag{3.12}$$

In order to find the set of the optimal reactive loads that allow the E3SPAR antenna system to operate at a given subband, we solve the following optimization problem for the set of reactive loads $\mathbf{x}(f)$

$$\begin{aligned} &\underset{\mathbf{x}(f)}{\text{minimize}} \quad |\Gamma_{\mathrm{in}}(f)| \\ &\text{subject to} \quad X_{\min} \le X_k(f) \le X_{\max},\ k \in \{1, \dots, K\}, \end{aligned}$$

where

$$\Gamma_{\mathrm{in}}(f) = (Z_{\mathrm{in}}(f) + Z)^{-1}(Z_{\mathrm{in}}(f) - Z^*) \tag{3.13}$$

and the input impedance is rewritten as a function of frequency as

$$Z_{\mathrm{in}}(f) = \langle \mathbf{Z}(f) \rangle_{00} + \frac{1}{\langle \mathbf{i}(f) \rangle_0} \sum_{k=1}^{K} \langle \mathbf{Z}(f) \rangle_{0k} \langle \mathbf{i}(f) \rangle_k. \tag{3.14}$$

The constraint on $X_k(f)$ depends on the tunable range of the varactor diodes, where we usually have $X_{\min} \le 0$, i.e., capacitive whereas $X_{\max} \ge 0$, i.e., inductive. Notice that for a specific frequency f, $Z_{\mathrm{in}}(f)$ remains constant $\forall k$ and thus $\Gamma_{\mathrm{in}}(f)$ is maintained

$\forall\ \mathcal{B}_k(\Omega, f)$, $k \in \{1, \ldots, K\}$, due to topology symmetry.

The set of optimal loads for a given subband is found *off-line*. The cognitive transceiver can simply store the sets of the optimal loads in a look-up table, thus reducing the time required for changing the loading conditions.

The main advantages of the proposed antenna system and its novel aspects over the state-of-the-art are:

1. The antenna system has a single RF chain, thus it meets the cost constraints of small terminals, where the cost scales with the complexity of the RF hardware.

2. The antenna system requires the parasitic elements to be very close to the central active element; hence the antenna system meets the compactness constraints of the small terminals where the physical area is limited.

3. The tuning of the varactor diodes is done in the reverse bias state, and hence the DC power consumption is quite negligible. On the other hand, the varactor diodes have no insertion loss unlike PIN diodes and other kinds of RF switches already proposed for reconfigurable cognitive antennas.

4. The strong mutual coupling decreases the antenna bandwidth, and hence the narrowband antenna system is suitable for cognitive transceivers that try to avoid any out-of-band radiation when transmitting. Another consequence is that the cognitive transceiver need not have a sharp (expensive) RF filter as the antenna systems is a filter by itself.

5. The circular permutation of the reactive loads rotates the narrowband beampattern to one of the K angular positions while keeping the input impedance unchanged due to symmetry. Consequently, the antenna system is capable of exploiting the spatial dimension by sensing over one of the K narrowband beampatterns.

6. The strong reactive field at such small spacing results in super-gain arrays [OY06]. The directive beampattern, not only spatially filters out the PU signal, but also enhances the quality of reception due to the high beamforming gain.

On the other hand, the main caveats of the proposed antenna system are:

1. The beampatterns are weakly mutually correlated rather than fully orthogonal to each other[1].

2. The beampatterns are directive at some of the subbands but not at all of them due to the fundamental limitation of electrically small-sized antennas (the gain-bandwidth product of an arbitrary antenna system is constrained by its size [Whe47]).

[1]Notice, however, that this is a desirable property in compressed sensing applications where a non-orthogonal basis is needed.

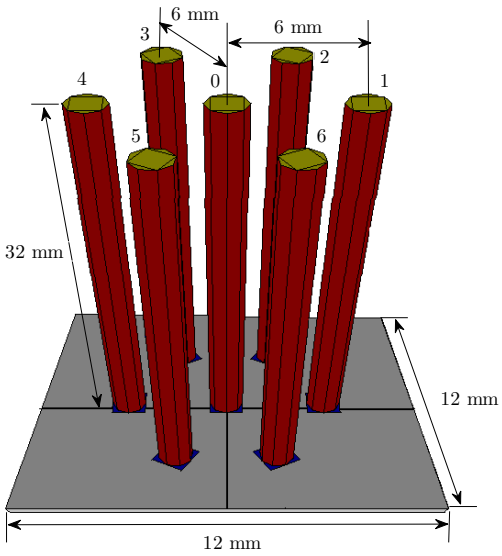

(a)

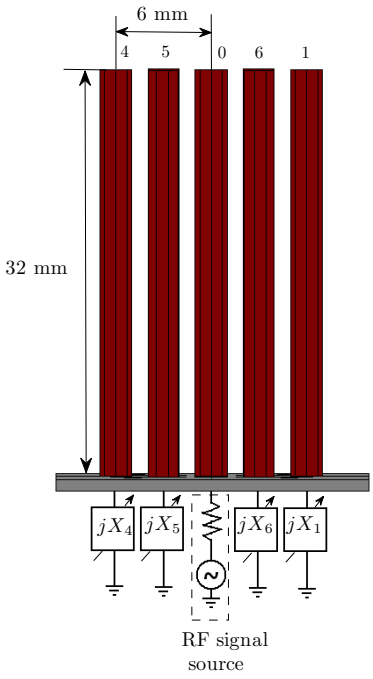

(b)

Figure 3.2: (a) The 7-element E3SPAR antenna consisting of seven monopoles over a small rectangular ground. (b) Side view of the antenna showing the feeding of the driven monopole (element 0) and the termination of the parasitic monopoles.

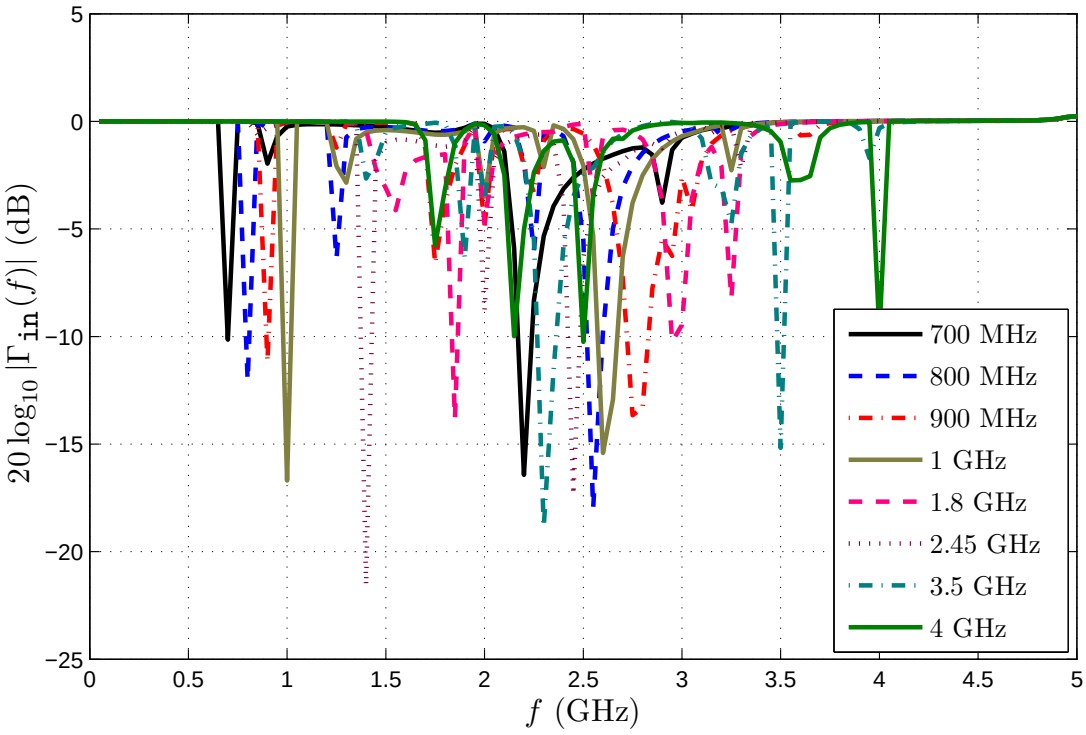

Figure 3.3: Return loss for the 7-element E3SPAR antenna of Figure 3.1 intended for spatial spectrum sensing.

3.2.2.2 E3SPAR Antenna Examples

In this part we propose different E3SPAR topologies with different radiation and frequency characteristics. Figure 3.1 shows an example of a 7-element E3SPAR which has the same topology as the conventional 7-element ESPAR ($K = 6$); however, the radius of the antenna system is 6mm corresponding to one twentieth the carrier wavelength at an operating frequency of 2.5 GHz (rather than quarter a wavelength as in the classical 7-element ESPAR antennas). Figure 3.2(b) shows the side view of the antenna where the driven monopole (element 0) is fed with an RF signal source whereas the parasitic monopoles are terminated with passive loads. Notice that the planar structure, as in the 7-element ESPAR, is quite useful for creating beampatterns over the full azimuth range. The $\mathbf{Z}(f)$ matrix at every desired frequency subband is obtained by the method of moments (MoM) using the electromagnetic simulator IE3D®.

Figure 3.3 depicts the absolute input reflection coefficient of the antenna system in dB, optimized for different frequency subbands, ranging from the TV bands ($700 - 800$ MHz), to the GSM bands (0.9 and 1.8 GHz), up to the ISM bands and beyond. A total

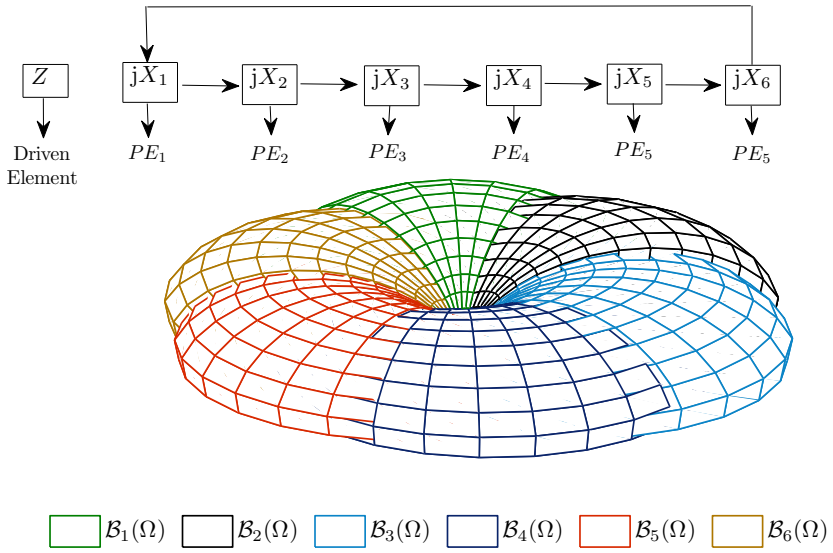

Figure 3.4: Rotated versions of the narrowband beampatterns of the 7-element E3SPAR antenna of Figure 3.1 at the resonant frequency of $f = 2.45$ GHz with 6.5 dBi gain. PE_k refers to the kth parasitic element.

bandwidth of $5:1$[1] could be obtained using the compact 7-element E3SPAR. (The bandwidth is defined as the frequency range where $|\Gamma_{\text{in}}|$ is less than -10 dB, i.e., where the antenna efficiency is above 90%.) Moreover, Figure 3.3 shows that at every set of loads two or three operational subbands may exist simultaneously; hence the antenna system need not change its loading condition once a primary activity is detected over a given subband, but simply needs to change the stop and pass bands of the RF filter to match another operational subband keeping the same loading conditions.

The proposed antenna system is capable of exploiting the spatial dimension via rotating the narrowband beampattern by permuting the optimal set of loads circularly over the parasitic monopoles as shown in Figure 3.4 (where PE_k refers to the kth parasitic element). Accordingly, the narrowband beampattern shifts to one of the K angular positions due to symmetry. Every beampattern samples a different part of the space, hence the probability of detecting a spectrum hole at a given subband increases almost linearly with the number of the beampatterns. It should be noted however that, as mentioned in the drawbacks of the E3SPAR system (Section 3.2.2.1), this property does not hold for the low frequency bands where the beampatterns are not directive.

Last but not least, Figure 3.5 shows how a PU signal impinging onto the cogni-

[1] In general, a frequency range of $\Lambda:1$ denotes that the highest frequency is Λ times the lowest frequency in the range.

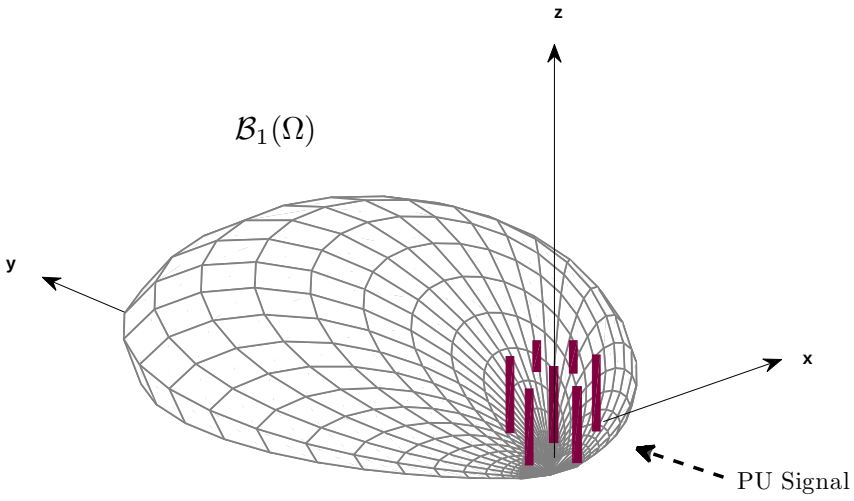

Figure 3.5: Sensing over the directive narrowband beampattern $\mathcal{B}_1(\Omega)$ of 6.5 dBi gain at $f = 2.45$ GHz using the 7-element E3SPAR antenna of Figure 3.1 (the ground plane is not shown in this Figure).

tive antenna system from the designated AoA is filtered out and hence the cognitive transceiver detects no primary activity over the designated narrowband (at $f = 2.45$ GHz) beampattern $\mathcal{B}(\Omega)$ (spatial-spectral white space). Consequently, the SU can proceed to communicate at the same frequency as the PU over the depicted beampattern $\mathcal{B}_1(\Omega)$.

As a second example, we propose the 3-element E3SPAR ($K = 2$) which is constrained to the two dimensions rather than being a planar structure. In this case, $Z_{\text{in}}(f)$ is given by

$$Z_{\text{in}}(f) = \langle \mathbf{Z}(f) \rangle_{00} + \alpha_{10}(f) \langle \mathbf{Z}(f) \rangle_{01} + \alpha_{20}(f) \langle \mathbf{Z}(f) \rangle_{01} ,$$

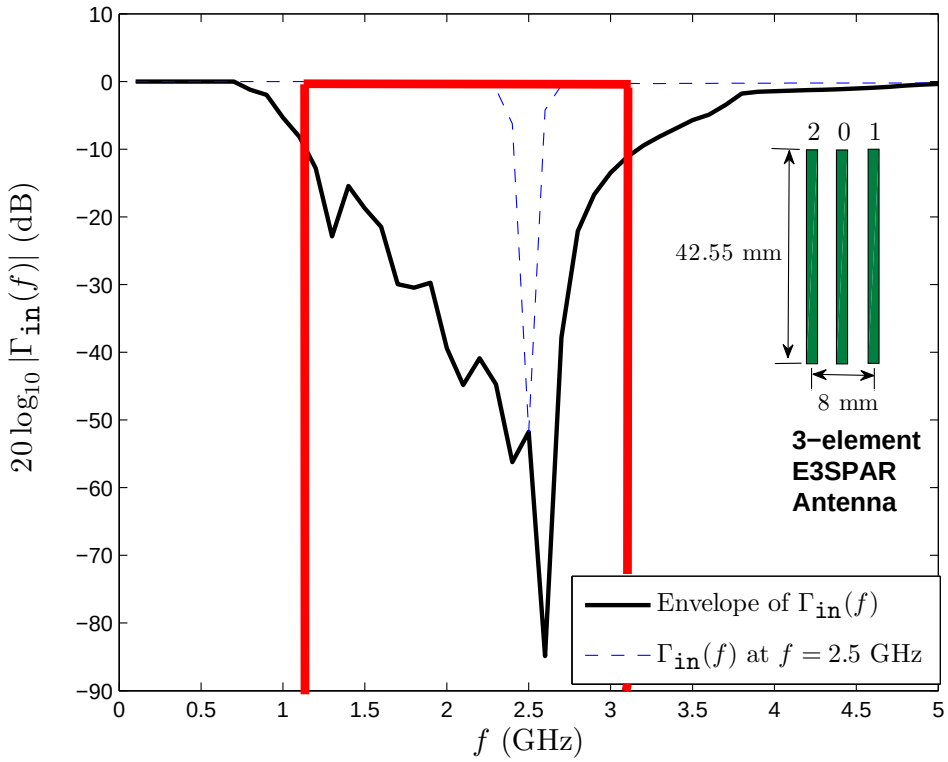

Figure 3.6: Return loss for the 3-element E3SPAR antenna of flat dipoles intended for spatial spectrum sensing.

where the coefficients $\alpha_{10}(f)$ and $\alpha_{20}(f)$ are calculated as [PDL06]

$$\begin{aligned}\alpha_{10}(f) &= \frac{\langle \mathbf{i}(f)\rangle_1}{\langle \mathbf{i}(f)\rangle_0} \\ &= \frac{\langle \mathbf{Z}(f)\rangle_{12}\langle \mathbf{Z}(f)\rangle_{01} - \langle \mathbf{Z}(f)\rangle_{01}\left(\langle \mathbf{Z}(f)\rangle_{11} + \mathrm{j}X_2\right)}{\left[\langle \mathbf{Z}(f)\rangle_{11} + \mathrm{j}X_1\right]\left[\langle \mathbf{Z}(f)\rangle_{11} + \mathrm{j}X_2\right] - \left\langle \mathbf{Z}^2(f)\right\rangle_{12}}, \qquad (3.15a)\\ \alpha_{20}(f) &= \frac{\langle \mathbf{i}(f)\rangle_2}{\langle \mathbf{i}(f)\rangle_0} \\ &= \frac{\langle \mathbf{Z}(f)\rangle_{12}\langle \mathbf{Z}(f)\rangle_{01} - \langle \mathbf{Z}(f)\rangle_{01}\left(\langle \mathbf{Z}(f)\rangle_{11} + \mathrm{j}X_1\right)}{\left[\langle \mathbf{Z}(f)\rangle_{11} + \mathrm{j}X_1\right]\left[\langle \mathbf{Z}(f)\rangle_{11} + \mathrm{j}X_2\right] - \left\langle \mathbf{Z}^2(f)\right\rangle_{12}}. \qquad (3.15b)\end{aligned}$$

The antenna system illustrated in Figure 3.6 is implemented using flat-dipoles and hence can be easily integrated in size-constrained terminals. The antenna system is composed of three flat dipoles (dipole 0 is the driven one, Figure 3.6) with an inter-element spacing of 4 mm corresponding to one thirtieth the carrier wavelength at an

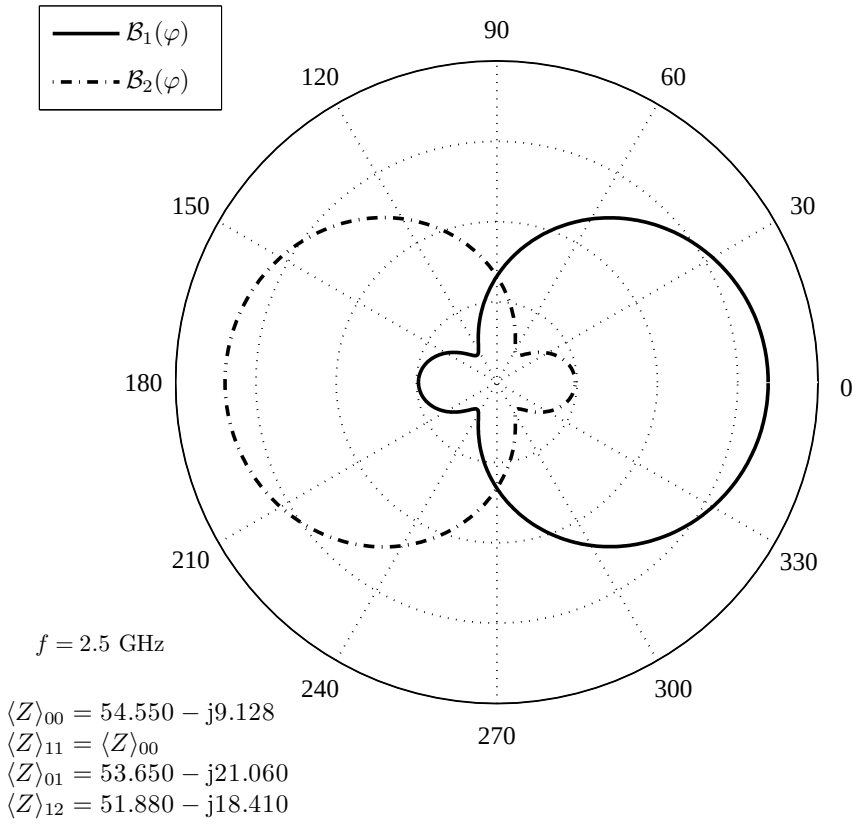

Figure 3.7: The two narrowband beam patterns of the 3-element E3SPAR antenna of Figure 3.6 at the resonant frequency of $f = 2.5$ GHz with 5.0 dBi gain.

operating frequency of $f = 2.5$ GHz [so as to better control $\Gamma_{\text{in}}(f)$], and integrated onto a substrate of a dielectric constant of $\epsilon_r = 4.2$ and a thickness of 0.813 mm. Figure 3.6 shows the envelope of $|\Gamma_{\text{in}}(f)|$ [i.e., the $\min |\Gamma_{\text{in}}(f)|$] in dB, where $|\Gamma_{\text{in}}(f)|$ is optimized for the corresponding frequency bin (the x-axis), as well as $|\Gamma_{\text{in}}(f)|$ optimized at 2.5 GHz as an example. The optimal sets of reactances are found by direct exhaustive search as the dimension of the reactance space is limited to two. Figure 3.6 shows that the antenna system can have a dynamic tunable bandwidth of 2.6 : 1 indicated by the red rectangle, but can exploit the spatial dimension mostly over $K = 2$ narrowband beampatterns (Figure 3.7) rather than $K = 6$ as in the 7-element E3SPAR. It should be noted that in both E3SPAR examples the spatial resolution is limited to a small number of distinct beampatterns (6 and 2, respectively) in order not to increase prohibitively the time for scanning the space as well as to avoid complicated antenna designs.

So far, we have provided an overview of the spatial spectrum sensing design chal-

lenges for CRs employing OSA. Furthermore, we have proposed novel low-profile frequency agile antennas for compact-sized terminals. The E3SPAR antenna, unlike the classical ESPAR, exploits the mutual coupling between the parasitic elements and the central active one for tuning the operational subband rather than for maximizing the SINR. The resonant frequency is varied in a predetermined fashion by properly controlling the varactor diodes, a task not intended by the classical approach of using the ESPAR antennas with relatively larger inter-element spacing merely for beam-steering. Moreover, the narrowband beampatterns are controlled in the analogue domain allowing the tunable cognitive antenna system to exploit the precious spatial resource. In the next section, we will evaluate the performance of spectrum sensing using the proposed single-radio reactance-loaded switched-beam array architecture.

3.3 Spectrum Sensing via Switched-Beam Antenna Systems

Several approaches and enabling algorithms of spectrum sensing for CR applications have been proposed, each having different operational requirements, advantages and disadvantages [YA09]. For example, matched filter (MF) detection [Kay98] needs to know the waveforms and the channels of the PUs whereas cyclostationary detection [Gar91] requires knowledge of the cyclic frequencies of the PUs being sensitive to timing and frequency mismatch. Blind algorithms such as energy detection-based methods [Kos02]-[DAS07] are susceptible to noise power uncertainty but require no a priori knowledge of the PU signals and are quite popular due to their low complexity and simplicity. Techniques like cooperative eigenvalue-based sensing [ZLPH09] or multiantenna-based detection [ZLLZ10] are more immune to noise uncertainty but increase the sensing complexity.

The use of smart antennas and beamforming systems in CR has also be used in other directions toward increasing the spectral reuse and improving the sensing performance. A directional beampattern is able to focus the energy in specific angles limiting the interference to unwanted directions and enabling a denser network deployment. In this context, [SHMM11] studies the maximum number of users that can be allocated in the same frequency in a CR network using transmit and receive beamforming. In [HDL07], the SU transmitter is equipped with a smart antenna having multiple active elements so as to construct a transmission beampattern that is non-intrusive to the PU link. Further, [DM10] studies the improvement to the cyclostationary-based detector performance exploiting smart-antenna radio receivers using certain beamforming algorithms.

Although most of the existing smart-antenna CR techniques rely on systems with multiple active antenna elements where each element is connected to a separate RF chain, in the previous Section 3.2 and [TAPP10d; TAPP10c] we proposed "spatial-spectrum sensing" for scanning both frequency and spatial (angular) resource dimensions via *a single-RF frontend*. The CR antenna designs proposed therein are based on the ESPAR antenna which constitutes a low-hardware complexity smart-antenna

system consisting of one feed radiating element and parasitic radiating elements placed in the near field of the active radiator.

In this section we aim at studying the spectrum sensing performance using smart switched-beam antenna systems. The study considers the single-radio ESPAR antenna structure for the CR receiver whereas the simple energy detection is the deployed sensing algorithm. The purpose is to detect the existence of a PU signal in the vicinity of the SU receiver as shown in Figure 3.8. A statistical analytical clustered channel model is assumed in which the multiple signal paths are organized into wave clusters so that the PU signal impinges on the SU receiver through a set of P clusters each of a certain mean AoA and AS. The reactive loads and the load impedance of the ESPAR receive antenna system are optimized for maximum efficiency and directivity in the beampattern look direction. At a given frequency, circular permutations of the optimal reactive loads of the ESPAR antenna rotate the beampattern to different angular positions dividing the whole space around the cognitive receiver into several *angular subspaces*. At each position, PU signal detection is performed over the directional array diagram. It is shown that beampattern directionality leverages the performance of energy detection by enhancing the receive SNR. The detection performance is evaluated under different propagation conditions. The work also considers the case where, after a full space scan with energy detection being deployed sequentially on every pattern, beam selection combining takes place by choosing the beam with the highest receive signal energy. The performance of the scheme is evaluated in a practical clustering environment showing that the selection combining across the weakly correlated beampatterns gives rise to a diversity action further boosting the probability of detection.

In the following, we first give the signal model and describe the radio environment. Then, spectrum sensing over the ESPAR directional beam response is presented and evaluated under various propagation conditions. Finally, we describe and evaluate the beampattern selection combining method.

3.3.1 Signal Model and Antenna System

We focus on two-dimensional propagation in the horizontal (azimuth) plane. The antenna system can switch among K directional beampatterns. The look direction and the free-space response of the kth complex beampattern is $\varphi_k = (k-1)\frac{2\pi}{K}$ and $\mathcal{B}_k(\varphi)$, $k = 1, \ldots, K$, respectively, where the azimuth angle φ expresses the AoA of the PU signal. The probability density function (pdf) of the angular distribution of impinging PU waves (rays) within a cluster, i.e., the PAS, is denoted by $\mathcal{A}(\varphi)$. The PAS of a wave cluster is parameterized by a mean AoA $\bar{\varphi}$ and AS σ (e.g., in case of a Laplacian PAS $\mathcal{A}(\varphi) = \frac{c}{\sigma} e^{-|\varphi-\bar{\varphi}|/\sigma}$, where $c = \frac{\sigma}{\int_0^{2\pi} e^{-|\varphi-\bar{\varphi}|} d\varphi}$ is a normalization factor). Analyzing the directivity gain in the presence of angular distribution of the impinging waves invokes calculating the distributed directivity gain (DDG) (average beamforming gain) at the

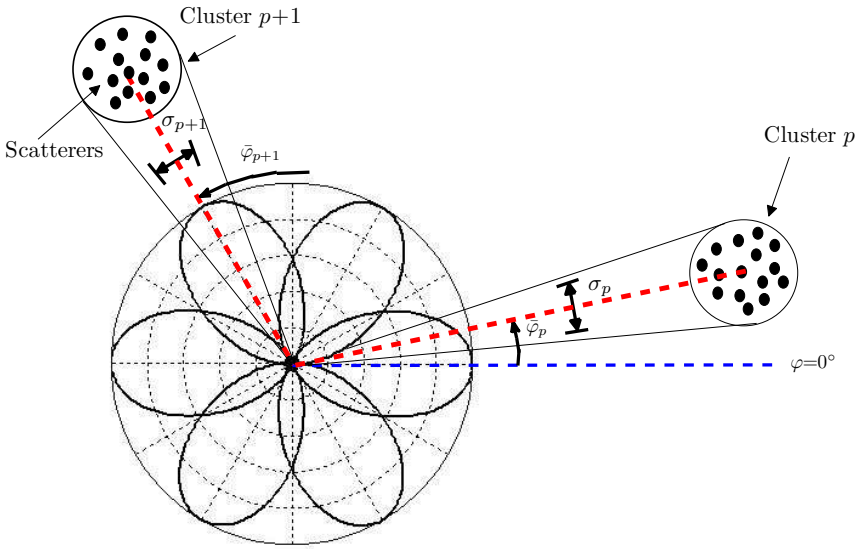

Figure 3.8: A clustered propagation scenario over which sensing a PU signal using a switched-beam receive antenna system can be deployed.

kth beampattern as [VA03]

$$G_k(\varphi) = \eta \underbrace{\frac{\int_0^{2\pi} \mathcal{B}_k(\phi)\mathcal{B}_k^*(\phi)\mathcal{A}(\phi-\varphi)d\phi}{\frac{1}{2\pi}\int_0^{2\pi} \mathcal{B}_k(\phi)\mathcal{B}_k^*(\phi)d\phi}}_{D_k(\varphi)}, \tag{3.16}$$

where $D_k(\varphi)$ is the directivity and $\eta \in [0,1]$ is the efficiency of the antenna system.

The received passband signal waveform at the kth beampattern in the presence of a primary user signal is

$$y_k(t) = \Re\left\{[\tilde{y}_k(t) + n_k(t)]\, e^{\mathrm{j}2\pi f t}\right\}, \tag{3.17}$$

where f is the carrier frequency and $\tilde{y}_k(t) \in \mathbb{C}$ is the PU signal received at the kth beampattern including the effects of fading where the multipath reflections and/or the scatterers are grouped into clusters and modeled as a single path with an associated AS. Let N_0 denote the one-sided flat noise power spectral density (PSD) and W the signal bandwidth. $n_k(t) \in \mathbb{C}$ is the 0-mean Gaussian noise process with variance $\sigma_{\mathrm{n}}^2 = N_0 W$ and is assumed to be white both temporally and spatially (i.e., across the different antenna patterns). The noise and the signal are assumed uncorrelated.

In (3.17), $\tilde{y}_k(t)$ is the superposition of rays arriving from P power-balanced wave

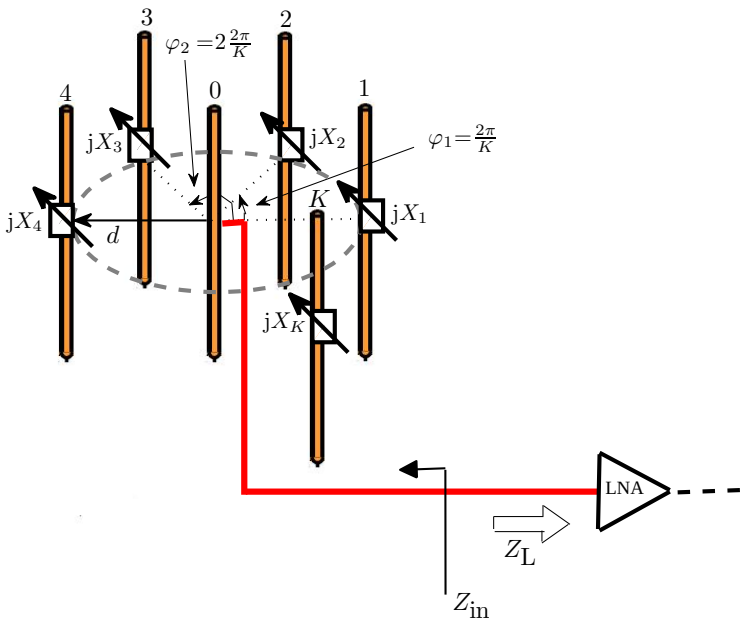

Figure 3.9: Configuration of $(K+1)$-element ESPAR receive antenna.

clusters. Specifically, it is assumed that the unit energy PU signal $s(t)$ impinges on P clusters, where the pth cluster has a Laplacian PAS $\mathcal{A}_p(\varphi)$, mean AoA $\bar{\varphi}_p$ and AS σ_p, $p \in \{1, \ldots, P\}$ (Figure 3.8). Thus, the PU signal received at the kth beampattern can be written as

$$\tilde{y}_k(t) = \sqrt{\frac{P_\mathrm{T}}{P}} \sum_{p=1}^{P} \sqrt{G_k(\bar{\varphi}_p)} h_{k,p} s(t), \tag{3.18}$$

where P_T is the PU transmit power and $h_{k,p} \in \mathbb{C}$ is the slow-fading channel coefficient for the pth PU signal received at the kth beampattern. The receive SNR and the total average DDG at the kth beampattern are respectively given by

$$\gamma_k = \frac{P_\mathrm{T}}{P} \left[\sum_{p=1}^{P} G_k(\bar{\varphi}_p) |h_{k,p}|^2 \right] / \sigma_\mathrm{n}^2, \tag{3.19}$$

$$G_k = \sum_{p=1}^{P} G_k(\bar{\varphi}_p)/P. \tag{3.20}$$

For $\sigma_p = 0°$ and for deterministic $h_{k,p}$ the signal model in (3.18) accounts for the

simple case of additive white Gaussian noise (AWGN) channel or, equivalently, free-space propagation.

We consider directional sensing using a single-radio $(K+1)$-element ESPAR receive antenna (Figure 3.9). The kth parasitic element is placed at a relative local angle of $\varphi_k = (k-1)\frac{2\pi}{K}$, $k \in \{1, \ldots, K\}$ and terminated with a varactor X_k controlling the imaginary part of its input impedance. Considering a specific narrow band, the equations for the free-space beampattern $\mathcal{B}_k(\varphi)$, the equivalent weight vector $\mathbf{w}_{\text{eq},k}$, the matrix $\mathbf{X}_k$, the input impedance Z_{in}, the return loss Γ_{in} and the antenna efficiency η, are taken from Section 3.1 or 3.2.2.1 dropping the frequency dependence. Notice that here $Z = Z_{\text{L}}$ is the load impedance of the receiver, i.e., the output impedance of the LNA.

3.3.2 Spectrum Sensing over Directional Beam Response

In order to analyze the sensing performance using directional CR receiver, the low-complexity energy detection is used for spectrum sensing. The goal of spectrum sensing is to decide between the two hypotheses over the kth beampattern

$$y_k(t) = \begin{cases} \Re\left\{n(t)e^{\mathrm{j}2\pi ft}\right\}, & \mathcal{H}_0 \\ \Re\left\{\left[\tilde{y}_k(t) + n_k(t)\right]e^{\mathrm{j}2\pi ft}\right\}, & \mathcal{H}_1. \end{cases} \tag{3.21}$$

The test or decision statistic is equal to the receive energy over the observation time interval $(0, T)$ over the kth beampattern and can be approximated as [DAS03]

$$\mathcal{T}_k = \int_0^T y_k^2(t) \approx \frac{1}{2W} \sum_{i=1}^{2WT} y_k^2\left(\frac{i}{2W}\right), \tag{3.22}$$

where $y_k\left(\frac{i}{2W}\right)$ is the ith sample of $y_k(t)$ and $N_{\text{sa}} = 2WT$ is the number of samples[1]. When the PU signal is not present (under hypothesis $\mathcal{H}_0$), the decision statistic is the sum of the squares of $2WT$ 0-mean Gaussian distributed random variables with variance σ_{n}^2, thus $\mathcal{T}_k$ will follow a central chi-square distribution. Based on the CDF of $\mathcal{T}_k$, the probability of false alarm is given by [DAS07]

$$P_{\text{f}} = \Pr(\mathcal{T}_k > \delta|\mathcal{H}_0) = \Gamma\left(WT, \delta/2\sigma_{\text{n}}^2\right)/\Gamma(WT), \tag{3.23}$$

where δ is the detection threshold, $\Gamma(a)$ is the Gamma function and $\Gamma(a, b)$ is the unregularized upper incomplete Gamma function [GR00].

Similarly, when the PU signal is present (under hypothesis $\mathcal{H}_1$) and for AWGN channels, the decision statistic $\mathcal{T}_k$ has a chi-square distribution with a non centrality parameter $2WT\gamma_k$ [DAS03]. Based on the statistics of $\mathcal{T}_k$, the probability of detection over the kth beampattern is given by

$$P_{\text{d},k} = \Pr(\mathcal{T}_k > \delta|\mathcal{H}_1) = Q_{WT}(\sqrt{2WT\gamma_k}, \sqrt{\delta/\sigma_{\text{n}}^2}), \tag{3.24}$$

[1] It is assumed that the that the first sample position starts at $t = 0$.

where $Q_z(a,b)$ is the generalized Marcum Q-function [GR00]. Under Rayleigh fading, the receive SNR follows an exponential PDF $f(\gamma_k) = (1/\bar{\gamma}_k)e^{(-\gamma_k/\bar{\gamma}_k)}$, where $\bar{\gamma}_k$ is the average receive SNR. Thus, the average $P_{\mathrm{d},k}$ is given by [Kos02]

$$\bar{P}_{\mathrm{d},k} = 1 - \Gamma'\left(WT, \frac{\delta}{2}\right) + \left(\frac{\bar{\gamma}_k^2+1}{\bar{\gamma}_k^2}\right)^{WT} e^{\frac{\delta}{2(\bar{\gamma}_k^2+1)}} \Gamma'\left(WT, \frac{\delta\bar{\gamma}_k^2}{2(\bar{\gamma}_k^2+1)}\right), \quad (3.25)$$

where $\Gamma'(a,b) = \Gamma(a,b)/\Gamma(a)$ is the regularized upper incomplete Gamma function.

Although the probability of false alarm in (3.23) is not related to the receive SNR (and the receiving beampattern) as there is no signal, the probability of detection is a function of γ_k given in (3.19). Thus, the performance of sensing in terms of probability of detection can be improved by the DDG of the directional beampattern enhancing the receive SNR. To illustrate, we evaluate the sensing performance over a beampattern of specific ESPAR configurations with respect to a standard isotropic receiver ($G(\varphi) = 0$ dBi). In these examples, we take into account sensing over the 1st ($k = 1$) beampattern (the analysis for other beampatterns is similar). We consider ESPAR set-ups of $K+1 = 3$ and $K+1 = 7$ identical half-wavelength thin electrical dipoles with $d = \lambda/4$. The mutual impedance matrix $\mathbf{Z}$ of the 3-port receive antenna system has $\langle\mathbf{Z}\rangle_{00} = 73.07 + \mathrm{j}42.50$, $\langle\mathbf{Z}\rangle_{01} = 40.75 - \mathrm{j}28.32$, and $\langle\mathbf{Z}\rangle_{12} = -12.52 - \mathrm{j}29.90$, calculated using the analytical formulas shown in the Appendix 6. Similarly, the 7-element ESPAR has $\langle\mathbf{Z}\rangle_{00} = 73.07 + \mathrm{j}42.50$, $\langle\mathbf{Z}\rangle_{01} = 40.75 - \mathrm{j}28.32$, $\langle\mathbf{Z}\rangle_{13} = -0.66 - \mathrm{j}35.93$ and $\langle\mathbf{Z}\rangle_{14} = -12.52 - \mathrm{j}29.90$ [1]. The ESPAR systems are optimized with respect to Z_{L} and $\mathbf{x}$ for maximum DDG in the look direction of the array diagram, i.e., for maximum $G_1(0°)$, via the simplex method of [LRWW98] (which is a direct search method available in MATLAB®) yielding the optimized antenna parameters in Table 3.1. The 1st array pattern $\mathcal{B}_1(\varphi)$ of the optimized 7-element ESPAR is shown in Figure 3.11(a). It should be noted that the remaining optimal beampatterns $\mathcal{B}_k(\varphi)$, $k = \{2,\ldots,K\}$ (i.e., with maximum DDG in their look direction) are simply obtained by appropriately rotating the reactive loads.

Table 3.1: Optimized ESPAR Parameters

$(K+1)$	Optimal load impedance Z_{L} (Ohm)	Optimal reactive loads $\mathbf{x}$ (Ohm)	$G_1(0°)$ (dBi)
3	$90.2 - \mathrm{j}97.6$	$[92.4 \quad 6.7]^{\mathrm{T}}$	4.0
7	$52.3 - \mathrm{j}82.3$	$[-33.4 \quad -160.7 \quad 80.7$ $-160.1 \quad -33.2 \quad -71.9]^{\mathrm{T}}$	7.0

It is considered that a single PU signal ($P = 1$) is arriving over an AWGN channel and that the direction of arrival is aligned with the look direction of the beam ($\bar{\varphi}_1 = 0°$). The probability of detection averaged over 10,000 random channel drops (Monte-Carlo simulations) versus the input SNR for $WT = 10$ and $P_{\mathrm{f}} = 0.1$ is shown in Figure 3.10. It can be observed that sensing with the directional optimized ESPAR

[1] The other entries of the $\mathbf{Z}$ matrices can be easily obtained from the antenna topology symmetry.

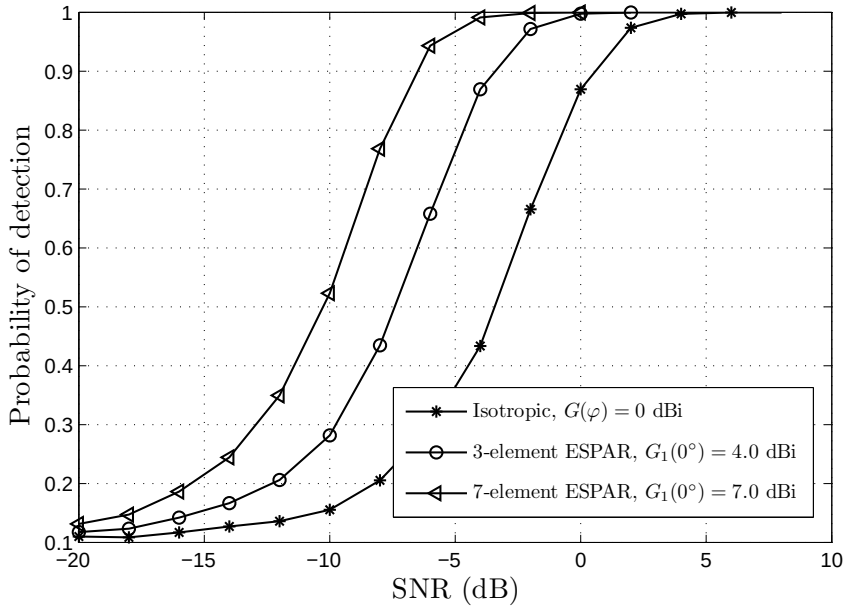

Figure 3.10: Probability of detection versus SNR for spectrum sensing over the directional ESPAR beam response ($P_\mathrm{f} = 0.1$, $WT = 10$).

systems significantly improves the detection performance, resulting in SNR gain of up to 4 and 8 dB with the 3-element ESPAR and the 7-element ESPAR, respectively.

In practice, the ideal assumption that the PU mean AoA is aligned with the beam look direction may not be fulfilled. From (3.19) and (3.24) or (3.25), it can be seen that the probability of detection depends on the mean AoA of the received PU signal(s). Moreover, it is realistic to account for more severe channel impairments to the signal reception than simple AWGN, such as the multipath Rayleigh fading. Thus, in this part a single PU signal is assumed arriving from various possible mean AoAs (Figure 3.11(a)) on the aforementioned optimized 7-element ESPAR receive antenna under Rayleigh fading and for $\sigma_p = 0°$. The calculated DDG $G(\bar{\varphi}_1)$ decreases from 7.0 dBi to -0.2 dBi for $\bar{\varphi}_1$ varying from 0° to 50°. The receiver operating characteristic (ROC) ($P_{\mathrm{d},1}$ versus P_f), or equivalently, the complementary ROC (probability of miss detection $P_{\mathrm{m},1} = 1 - P_{\mathrm{d},1}$ versus P_f) for the different situations is shown in Figure 3.11(b). The input SNR is -7 dB. It can be observed, that as the mean AoA deviates from the value $\bar{\varphi}_1 = 0°$ at which the beampattern has bean optimized, the attained DDG decreases, with a direct impact on the sensing performance.

Furthermore, a non-zero AS can also affect the sensing performance. Here it is assumed that the mean AoA of the PU signal is kept at $\bar{\varphi} = 0°$ whereas the AS σ_1 varies from 0° to 50°. As the AS increases (Figure 3.12(a)), the beampatern diffuses and the lobes start to smear, whereas the DDG at the look direction decreases. At high values of AS (e.g., for $\sigma_1 = 50°$ with $G_1(0°) = 4.0$ dBi) the array diagram tends to flatten and tends to approach an omnidirectional diagram, indicating that beamforming

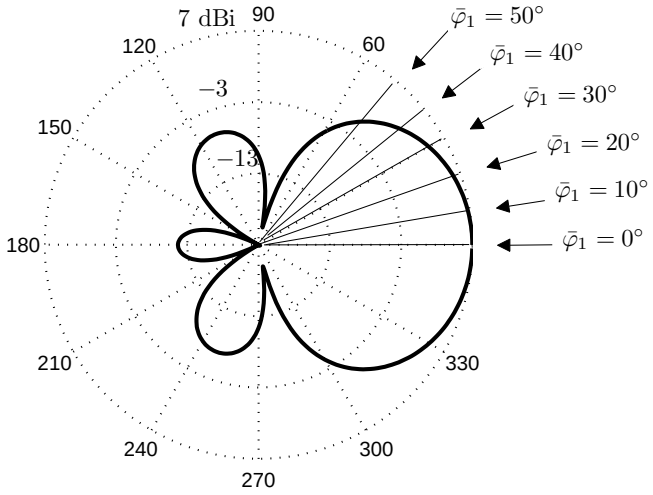

(a)

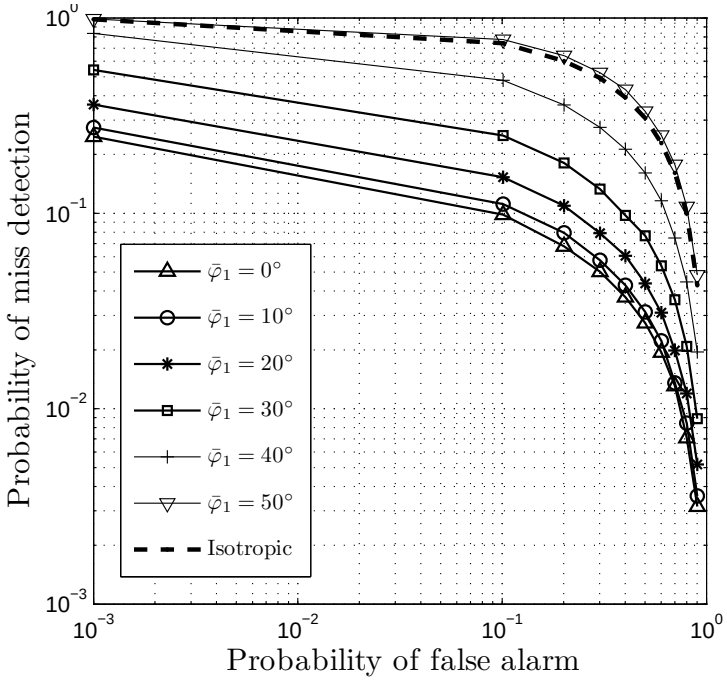

(b)

Figure 3.11: Performance of directional sensing for different values of mean AoA $\bar{\varphi}$. (a): Array diagram $\mathcal{B}_1(\varphi)$ of the optimized 7-element ESPAR and an impinging PU signal with various mean AoA. (b): Complementary ROC curve under Rayleigh fading (-7 dB SNR, $WT = 10$).

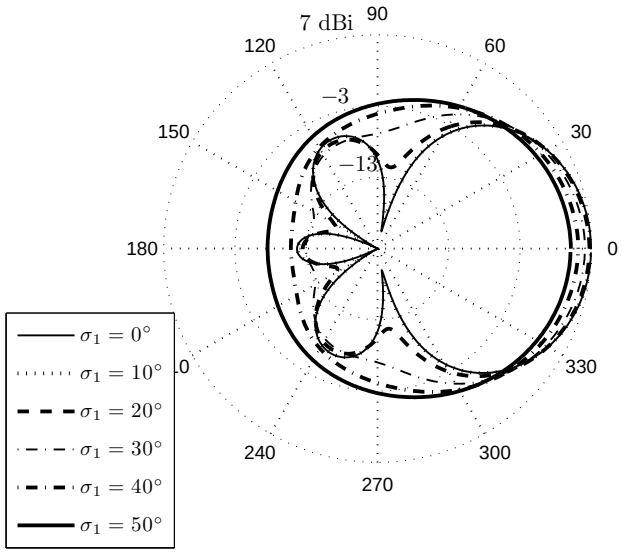

(a)

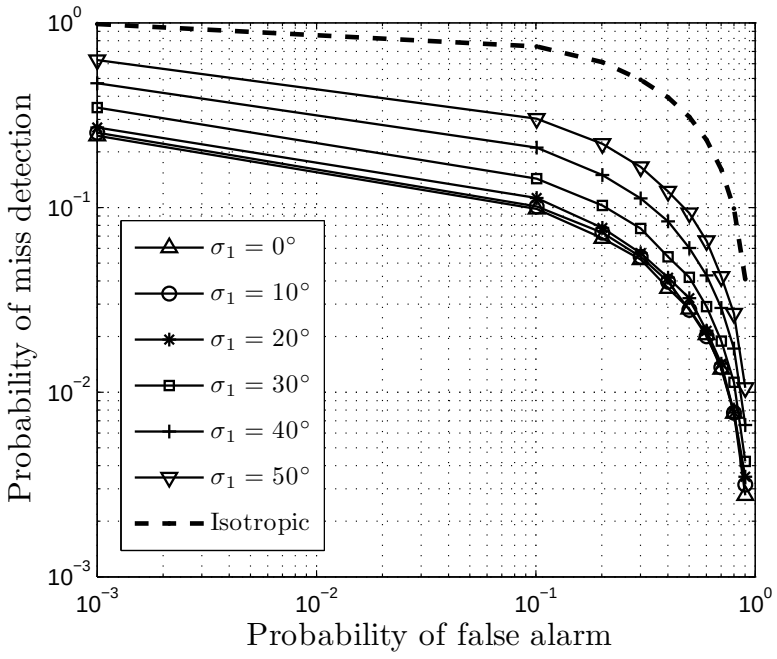

(b)

Figure 3.12: Performance of directional sensing for different values of AS σ. (a): Array diagram $\mathcal{B}_1(\varphi)$ of the optimized 7-element ESPAR for various values of AS of the impinging PU signal. (b): Complementary ROC curve under Rayleigh fading (-7 dB SNR, $WT = 10$).

gains under rich scattering environments are not so significant. Figure 3.12(b) shows that the sensing performance is affected in a way similar to the case of mean AoA misalignment with the beam look direction.

Table 3.2: DDG of the Optimized 7-Element ESPAR Array

	$\bar{\varphi}_1 = 5°$	$\bar{\varphi}_2 = 130°$
$G_1(\bar{\varphi}_p)$ (dBi)	7.0	−8.6
$G_2(\bar{\varphi}_p)$ (dBi)	−2.5	−11.4
$G_3(\bar{\varphi}_p)$ (dBi)	−7.0	6.7
$G_4(\bar{\varphi}_p)$ (dBi)	−11.8	−0.5
$G_5(\bar{\varphi}_p)$ (dBi)	−7.4	−6.8
$G_6(\bar{\varphi}_p)$ (dBi)	−7.3	−12.6

3.3.3 Spectrum Sensing via Beam Scanning with Beam Selection Combining

We assume that spectrum sensing is run sequentially on each one of the K ESPAR optimized beampatterns using energy detection as described in the previous section under Rayleigh fading. It is assumed that the channel fading coefficient remains unchanged during each full angular space scan whereas it changes to another independent realization in a succeeding scan. This assumption is valid for slow fading channels while assuming that beam scanning and detection over each array diagram happens fast enough. After a full space scan, the receiver performs beam selection based on the gathered K test statistics $\mathcal{T}_k$, $k \in \{1, \ldots, K\}$. Specifically, the maximum $\mathcal{T}_k$, $k \in \{1, \ldots, K\}$ is chosen and compared with the detection threshold δ to perform the sensing test and the combined probability of detection $\bar{P}_{\mathrm{d,SC}}$ is thus given by

$$\bar{P}_{\mathrm{d,SC}} = \Pr\left(\max_{k \in \{1,\ldots,K\}} \mathcal{T}_k > \delta | \mathcal{H}_1 \right). \tag{3.26}$$

Optimizing the beampatterns for the maximum DDG at the look direction has the additional advantage of resulting in a sufficiently weak correlation across the K array patterns. In the general case, assuming Kronecker separability and correlation only at the receiver side [SFGK00] (*see* also Section 2.2.1), the signal model accounting for beampattern cross-correlation (under hypothesis $\mathcal{H}_1$) can be written as

$$\mathbf{y}(t) = \sqrt{P_{\mathrm{T}}} \, (\mathbf{R}_{\mathrm{R}})^{1/2} \, \mathbf{h} s(t) + \mathbf{n}(t), \tag{3.27}$$

where $\mathbf{y}(t) \in \mathbb{C}^{K \times 1}$ is the vector of the K collected received signals upon a beam scan. $\mathbf{h} \in \mathbb{C}^{K \times 1}$ is the vector of slow fading channel coefficients with $\langle \mathbf{h} \rangle_k = \sum_{p=1}^{P} h_{k,p}$ and $\mathbf{n}(t) \in \mathbb{C}^{K \times 1}$ is the temporally and spatially white noise vector with $\langle \mathbf{n}(t) \rangle_k = n_k(t)$. $\mathbf{R}_{\mathrm{R}} \in \mathbb{C}^{K \times K}$ is the receive covariance matrix that incorporates both the power

imbalance and the cross-correlation of the beampatterns

$$\mathbf{R}_{\mathrm{R}} = \mathbf{G}^{1/2}\tilde{\mathbf{R}}\mathbf{G}^{1/2}, \tag{3.28}$$

where $\mathbf{G} = \mathrm{diag}[G_1 \quad \dots \quad G_K]$ and the normalised correlation matrix $\tilde{\mathbf{R}} \in \mathbb{C}^{K\times K}$ has entries

$$\begin{aligned}\langle\tilde{\mathbf{R}}\rangle_{kj} &= \frac{\langle\mathbf{R}_{\mathrm{R}}\rangle_{kj}}{\sqrt{\langle\mathbf{R}_{\mathrm{R}}\rangle_{kk}\langle\mathbf{R}_{\mathrm{R}}\rangle_{jj}}} \\ &= \frac{\int_0^{2\pi}\mathcal{B}_k(\varphi)\mathcal{B}_j^*(\varphi)\mathcal{A}_\Sigma(\varphi)d\varphi}{\sqrt{\int_0^{2\pi}\mathcal{B}_k(\varphi)\mathcal{B}_k^*(\varphi)\mathcal{A}_\Sigma(\varphi)d\varphi\int_0^{2\pi}\mathcal{B}_j(\varphi)\mathcal{B}_j^*(\varphi)\mathcal{A}_\Sigma(\varphi)d\varphi}}.\end{aligned} \tag{3.29}$$

In (3.29), $\mathcal{A}_\Sigma(\varphi) = \sum_{p=1}^{P}\mathcal{A}_p(\varphi)/P$ is the total PAS.

To illustrate, we consider the 7-element ESPAR antenna system described in the previous part (Section 3.3.2) optimized for maximum DDG at the look direction (Table 3.1) under Rayleigh fading. It is assumed that $P = 2$ PU signals arrive on the array through two different clusters with Laplacian PAS $\mathcal{A}_1(\varphi)$ and $\mathcal{A}_2(\varphi)$ with $\bar{\varphi}_1 = 5°$ and $\bar{\varphi}_2 = 130°$, respectively, whereas $\sigma_1 = \sigma_2 = 10°$. These parameters describe a typical indoor clustered propagation scenario and are similar to those used in the IEEE 802.11 wireless local area network Task Group N [Erc04]. The attained DDGs at every beampattern at the mean AoA of the PU clusters are summarized in Table 3.2. The probability of detection versus the input SNR of spectrum sensing with beam selection via the 7-element ESPAR for $P_{\mathrm{f}} = 0.1$ is shown in Figure 3.13. The resulting maximum absolute cross-correlation coefficient is $\max|\langle\mathbf{R}\rangle_{kj}| = 0.7$. The figure also shows sensing only over the 1st beampattern $\mathcal{B}_1(\varphi)$ and over a standard isotropic antenna. It can be observed that sensing over $\mathcal{B}_1(\varphi)$ improves the probability of detection due to receive SNR gain as discussed in Section 3.3.2. However, beam scanning with beam selection combining, along with receive SNR improvement due to the beampattern directionality, can enable a diversity action that further boosts the probability of detection. Moreover, the performance approaches the ideal beam selection with uncorrelated beampatterns (i.e., for $\mathbf{R} = \mathbf{I}_K$), indicating that indeed the designed beampatterns are approximately orthogonal.

In this section, we have described directional spectrum sensing using the single-radio switched-beam ESPAR antenna where PU signal detection is performed on each antenna pattern. The antenna's loading conditions have been optimized for maximum average beamforming gain in the beampattern look direction. The simulation results showed that the average beamforming gain of the beam response can improve the probability of detection of the energy detector by enhancing the SNR at the receiver side. Moreover, by selectively combining the sensing results from the K weakly correlated beampatterns diversity gains can be added to the cognitive radio system performance.

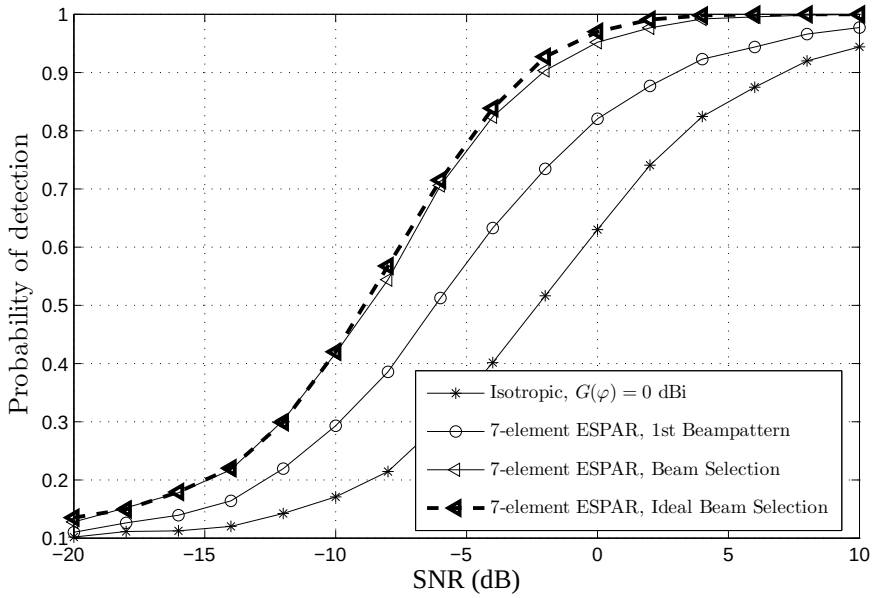

Figure 3.13: Probability of detection versus SNR for beam scanning with beam selection combining under Rayleigh fading ($P_{\mathrm{f}} = 0.1$, $WT = 10$).

3.4 Analogue Orthogonal Precoding

Although hitherto Chapter 3 has focused mainly on spectrum sensing, in this part we present a reduced-complexity communication technique allowing the CR to cancel the interference caused to K PUs. Analogue transceiver techniques where part of the signal processing is handled by low-complexity reactance-assisted antenna systems have been proposed in [AKPP09b; TAPP10d; SHOK04]. In [AKPP09b], the authors describe analogue spatial multiplexing which is made possible using a single-radio 3-element ESPAR antenna [OG00]. In Section 3.2 and [TAPP10d; TAPP10c; TWdCR12], we described a modified ESPAR antenna system utilized as a cognitive transceiver detecting spectrum holes over both the space and the frequency resource dimensions simultaneously via a single RF chain within a miniaturized antenna system. In [SHOK04], analogue beamforming has been proposed using a 7-element ESPAR antenna. The 7-element ESPAR antenna is a three-dimensional structure that is too large to fit in small RF units besides having a complicated DC control circuitry. In this section, we describe how even simple ESPAR antenna structures (for example a two-dimensional 3-element ESPAR) are able to suppress the interference toward a number of users by emulating conventional digital precoding. In order to overcome the limitations of such antenna systems which are constrained in the number of parasitic antennas as well as in the sense that their tunable passive loads can only take imaginary values over a restrained realizable range, our analysis introduces an arbitrary vector $\mathbf{v} \in \mathbb{C}^{(K+1)\times 1}$ increasing the system flexibility for obtaining the desired ESPAR beampattern. The

idea proposed herein assumes that the responses of a set of basis beampatterns (predetermined by the ESPAR system) to the users toward which interference should be nulled (i.e., the geometrical interference directions) are perfectly known. The ESPAR then synthesizes a linear combination of the basis beampatterns using a precoding vector obtained by zero-forcing over the geometrical interference directions. The arbitrary vector $\mathbf{v}$ is embedded within the precoding vector calculation for obtaining arbitrarily many theoretical solutions. The realizable solution is the one that the ESPAR can finally synthesize by searching over the set of the considered reactive loads.

3.4.1 Analogue Orthogonal Precoding

In conventional digital beamforming systems, a transceiver equipped with $(K+1)$ antennas can suppress a maximum of K interfering signals, or alternatively, interference toward up to K single-antenna users can be suppressed. On the other hand, a $(K+1)$-element ESPAR transceiver is able to create a set of $(K+1)$ linearly independent beampatterns (basis) $\boldsymbol{\mathcal{B}}(\Omega) = [\mathcal{B}_1(\Omega) \quad \dots \quad \mathcal{B}_{K+1}(\Omega)]^{\mathrm{T}}$ serving as $(K+1)$ "virtual antennas" [AKPP09a]. Thus, interference toward $N \leq K$ single-antenna users can be also nulled via the single-radio ESPAR system. Assume a transceiver equipped with an $(K+1)$-element ESPAR communicating over a fading channel such that the interference toward $N \leq K$ single-antenna users should be suppressed. Let $\mathbf{h}_j \in \mathbb{C}^{(K+1)\times 1}$, where $\mathbf{h}_j^{\mathrm{T}}$ denotes the fading channel vector from the basis $\boldsymbol{\mathcal{B}}$ toward user j, where $j \in \{1, ..., N\}$, $N \leq K$.

Proposition 1: For an arbitrary vector $\mathbf{v} \in \mathbb{C}^{(K+1)\times 1}$ the precoding vector

$$\mathbf{w} = \left(\mathbf{C}^{\mathrm{H}}\mathbf{C}\right)^{-1}\mathbf{C}^{\mathrm{H}}\mathbf{f} \tag{3.30}$$

is orthogonal to $\mathbf{h}_j^{\mathrm{T}}$, $k \in \{1, ..., N\}$, $N \leq K$, where $\mathbf{f} = [1 \quad \underbrace{0 \quad \dots \quad 0}_{N}]^{\mathrm{T}}$ and

$$\mathbf{C} = [\mathbf{v} \quad \mathbf{h}_1 \quad \dots \quad \mathbf{h}_N]^{\mathrm{T}} \in \mathbb{C}^{(N+1)\times(K+1)}.$$

This can be easily proved by solving $\mathbf{Cw} = \mathbf{f}$, where the entry $\langle \mathbf{f} \rangle_{j+1}$ expresses the desired response toward the jth user, $j \in \{1, ..., N\}$, $N \leq K$, as in zero-forcing beamforming [YG06b] [LB03].

Corollary 1: The beampattern

$$\mathcal{B}_{\mathrm{t}}(\Omega) = \boldsymbol{\mathcal{B}}^{\mathrm{T}}(\Omega)\mathbf{w} \tag{3.31}$$

has a null response in the geometrical direction of any jth user, $j \in \{1, ..., N\}$, $N \leq K$.

In order to prove that $\mathcal{B}_{\mathrm{t}}(\Omega)$ creates zero interference at any jth user, we assume that the fading channel between the ESPAR transceiver and the jth user comprises L multi-paths. The ℓth path has complex gain $g_{j,\ell}$ and angle of departure $\Omega_{j,\ell}$ with respect to the jth user. The interference signal received at the jth (omni-directional)

user can be written as

$$y_j = \sum_{\ell=1}^{L} g_{j,\ell}\mathcal{B}_{\mathrm{t}}(\Omega_{j,l}) = \sum_{\ell=1}^{L} g_{j,\ell}\boldsymbol{\mathcal{B}}^{\mathrm{T}}(\Omega_{j,\ell})\mathbf{w} = \mathbf{h}_j^{\mathrm{T}}\mathbf{w} = 0,$$

by Proposition 1.

Notice that the existence of $\mathbf{v}$ in (3.30), (3.31) provides arbitrarily many desired solutions, i.e., *it creates arbitrarily many desired theoretical beampatterns* $\mathcal{B}_{\mathrm{t}}(\Omega)$. We have seen that the beampattern of the ESPAR antenna in the far-field is obtained generally as (*see* also Section 3.1)

$$\mathcal{B}_{\mathrm{r}}(\Omega) = \mathbf{i}^{\mathrm{T}}\boldsymbol{\alpha}(\Omega). \tag{3.32}$$

The objective is to synthesize a realizable beampattern $\mathcal{B}_{\mathrm{r}}(\Omega)$ using the ESPAR that resembles one of the possible theoretical beampatterns given by (3.31), i.e., to minimize the objective function

$$d^2 = 1 - |\varrho|^2 \tag{3.33}$$

over $\mathbf{v}$ and $\mathbf{x}$, where

$$\varrho = \frac{1}{\sqrt{P_{\mathrm{r}}P_{\mathrm{t}}}}\int_{\Omega}\mathcal{B}_{\mathrm{r}}(\Omega)\mathcal{B}_{\mathrm{t}}^{*}(\Omega)\cdot d\Omega \tag{3.34}$$

is the cross correlation coefficient between the theoretical and the realizable beampatterns, such that

$$\begin{aligned} P_{\mathrm{r}} &= \int_{\Omega}\mathcal{B}_{\mathrm{r}}(\Omega)\mathcal{B}_{\mathrm{r}}^{*}(\Omega)\cdot d\Omega, \\ P_{\mathrm{t}} &= \int_{\Omega}\mathcal{B}_{\mathrm{t}}(\Omega)\mathcal{B}_{\mathrm{t}}^{*}(\Omega)\cdot d\Omega. \end{aligned} \tag{3.35}$$

Although the ESPAR is constrained in the sense that its tunable loads can only take imaginary values on a restrained realizable range, the optimization variable $\mathbf{v}$ increases the space of possible solutions.

3.4.2 Simulation Results

We deploy our proposed technique over a simple 3-element ESPAR ($K = 2$) which is constrained to two dimensions and hence can be easily integrated in size-constrained terminals, rather than being a three-dimensional structure as in [SHOK04]. The antenna system illustrated in Figure 3.14 is implemented using thin half-wavelength electrical dipoles spaced by $\lambda/4$. The two passive dipoles are attached to imaginary loads $\mathrm{j}X_1$ and $\mathrm{j}X_2$ limited to a realizable range of $[-\mathrm{j}250, \mathrm{j}250]$ Ohms. The mutual impedance matrix of the system is calculated using the analytical formulas shown in the Appendix

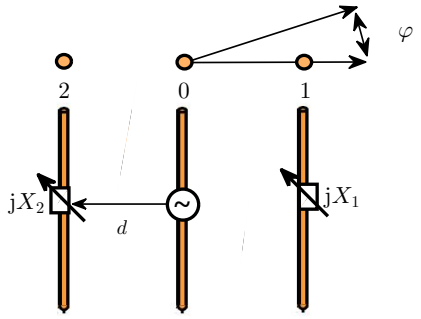

Figure 3.14: The 3-element ESPAR antenna intended for analogue precoding.

6 as

$$\mathbf{Z} = \begin{bmatrix} 73.0 + \mathrm{j}42.5 & 40.7 - \mathrm{j}28.3 & 40.7 - \mathrm{j}28.3 \\ 40.7 - \mathrm{j}28.3 & 73.0 + \mathrm{j}42.5 & -12.5 - \mathrm{j}29.9 \\ 40.7 - \mathrm{j}28.3 & -12.5 - \mathrm{j}29.9 & 73.0 + \mathrm{j}42.5 \end{bmatrix}.$$

For illustration, free space propagation over the azimuth plane is assumed, although we note that unlike typical constrained beampattern designs, the free space assumption is not a requirement of analogue precoding. A choice on the basis $\boldsymbol{\mathcal{B}}(\varphi) = [\mathcal{B}_1(\varphi) \;\; \mathcal{B}_2(\varphi) \;\; \mathcal{B}_3(\varphi)]^{\mathrm{T}}$ is initially made such that a low cross-correlation factor across the basis is maintained. The basis is shown in Figure 3.15 in dB scale and can be obtained from (3.32) using $X_1 = -50$ and $X_2 = -50$ for $\mathcal{B}_1(\varphi)$, $X_1 = 250$ and $X_2 = -40$ for $\mathcal{B}_2(\varphi)$ and $X_1 = 250$ and $X_2 = -40$ for $\mathcal{B}_3(\varphi)$.

Next, we consider the case where interference should be suppressed toward a single user ($N = 1$) located at $\varphi_1 = 120°$. In this case, $\mathbf{h}_1 = \boldsymbol{\alpha}(\varphi_1)$, $\mathbf{C} = [\mathbf{v} \;\; \mathbf{h}_1]$ and $\mathbf{f} = [1 \;\; 0]^{\mathrm{T}}$. A number of theoretical beampatterns that can be obtained by arbitrarily varying $\mathbf{v}$ using (3.31) is plotted in Figure 3.16. As it can be observed, a common characteristic of all beampatterns is that a null toward the direction of 120° (indicated by the black dashed arrow) is attained. In order to synthesize one of the desired theoretical beampatterns we minimize d^2 in (3.33) over $\mathbf{v}$, X_1 and X_2 across the realizable reactance range, utilizing the simplex method of [LRWW98] which is a direct search method available in MATLAB® [mat]. The resulting realizable beampattern is depicted in Figure 3.17 and is given by $X_1 = -140$ and $X_2 = -20$ corresponding to the theoretical one at $\mathbf{v} = \begin{bmatrix} -0.86 - \mathrm{j}0.77 & 1.84 - \mathrm{j}0.57 & -1.01 + \mathrm{j}0.79 \end{bmatrix}^{\mathrm{T}}$.

Another scenario is considered where interference should be suppressed toward

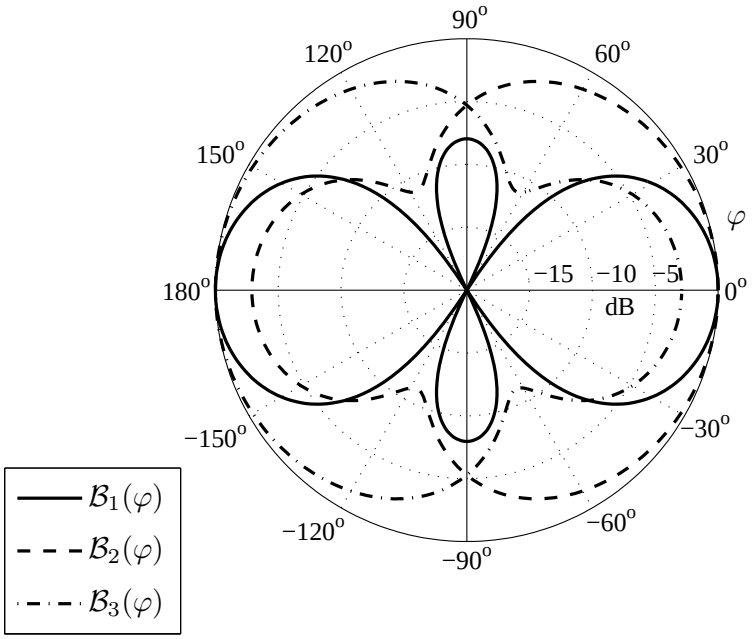

Figure 3.15: The 3 beampatterns that form the basis $\boldsymbol{\mathcal{B}}(\varphi)$.

two users ($N = 2$) located at $\varphi_1 = 55°$ and $\varphi_2 = 120°$, respectively. In this case, $\mathbf{h}_1 = \boldsymbol{\alpha}(\varphi_1)$, $\mathbf{h}_2 = \boldsymbol{\alpha}(\varphi_2)$, $\mathbf{C} = [\mathbf{v} \quad \mathbf{h}_1 \quad \mathbf{h}_2]$ and $\mathbf{f} = [1 \quad 0 \quad 0]^{\mathrm{T}}$. Similarly, by minimizing (3.33), the resulting realizable beampattern is depicted in Figure 3.18 and is given by $X_1 = -40$ and $X_2 = -60$ corresponding to the theoretical one at $\mathbf{v} = \begin{bmatrix} 0.89 - \mathrm{j}0.58 & 1.30 - \mathrm{j}1.28 & -0.04 + \mathrm{j}0.28 \end{bmatrix}^{\mathrm{T}}$.

To summarize, in the last part of this chapter we have enabled orthogonal precoding for suppressing the interference toward a maximum of K single-antenna users using a reduced-complexity wireless $(K+1)$-element ESPAR system. The proposed technique requires a single-radio antenna, whereas the parasitic elements require no extra RF hardware making it a viable option for small terminals where size, cost, and DC power consumption are major limitations.

3.5 Conclusions

In the CR context, we have shown that a space-steerable, frequency-agile, narrowband cognitive antenna system is made possible by exploiting the strong mutual coupling in a compact parasitic array (Section 3.2). The beam directionality and diversity can be directly employed to enhance the probability of detecting primary activity (Section 3.3). Furthermore, it is possible to emulate a baseband ZF filter using a single active

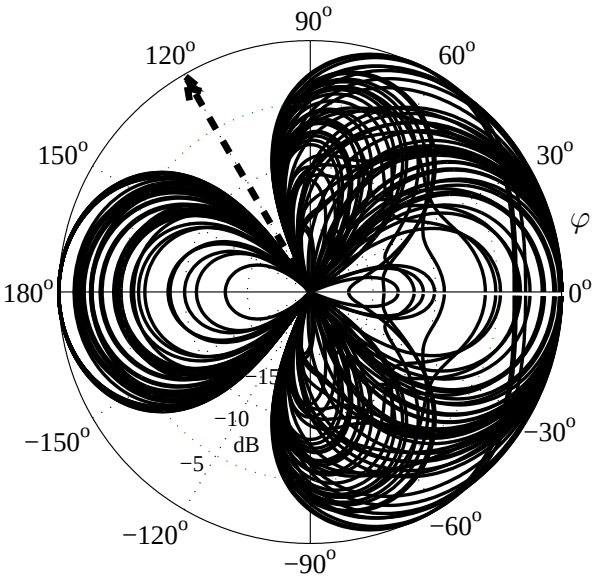

Figure 3.16: Possible theoretical beampatterns $\mathcal{B}_{\mathrm{t}}(\varphi)$ forming a null toward 120°, obtained by arbitrarily varying $\mathbf{v}$ using (3.31).

antenna coupled to passive radiators for canceling the interference toward a set of legacy users (Section 3.4).

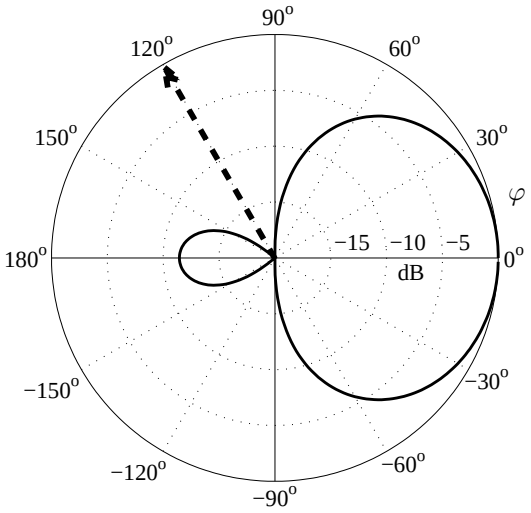

Figure 3.17: The realizable 3-element ESPAR beampattern obtained by minimizing (3.33), forming a null toward 120°.

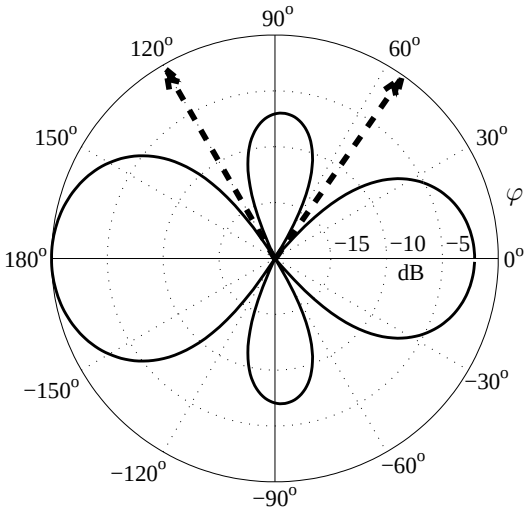

Figure 3.18: The realizable 3-element ESPAR beampattern obtained by minimizing (3.33), forming nulls toward 120° and 55°.

3. PARASITIC ANTENNA SYSTEMS FOR COGNITIVE RADIO APPLICATIONS

4

Non-Cooperative Space-Time Communication for Energy Efficiency in Sensor Networks

Space-time coded cooperative transmission has been proposed as a means to prolong the battery lifetime of conventional single-antenna energy-constrained wireless sensor nodes. However, newly proposed smart-antenna sensor prototypes enable the existence of more than one antenna within a *single-radio transceiver architecture*. Exploiting such a capability, this chapter proposes simple non-cooperative space-time techniques for single-RF switched-antenna systems that reduce significantly both the transmission and the circuit energy consumption. The energy savings of the suggested schemes will be shown not only against conventional SISO systems, but also against cooperative diversity schemes in Rayleigh and log-normal shadowed Rayleigh fading channels with distance-based path loss.

Energy efficiency is a critical issue in energy-constrained WSNs system design. Motivated by the theoretical potential of MIMO systems to provide the same throughput or bit error rate (BER) performance as a SISO system in fading channels with a smaller transmit power requirement [GNP03], MIMO techniques have attracted significant attention toward energy-efficient communications in WSNs. Among the MIMO techniques considered for WSNs, space-time block codes (STBCs) are attractive because of their linear complexity and simple encoding and decoding requirements [VY03]. However, due to the physical constraints regarding size, cost, and circuit energy consumption of most conventional sensor nodes, the direct application of STBCs in WSNs is not feasible. This has led to the cooperative diversity solution allowing single-antenna-single-radio nodes to cooperate on information transmission so as to form a virtual multi-antenna array, as described in [CGB04; LCL05; Jay06]. However, scheduling joint transmissions comes at the cost of increased energy overhead for local information flow among the sensors. Moreover, although the transmission energy can be reduced, node cooperation involves more circuit energy compared to a SISO system. These fun-

damental energy trade-offs are well expressed via the *break-even distance* indicating that cooperative MIMO may beat SISO with respect to the total energy consumption per bit when the communication distance exceeds a threshold value [CGB04; LCL05; Jay06]. Last but not least, *applying cooperative STBC requires accurate synchronization among the sensors in terms of carrier frequency, carrier phase, symbol timing, and timing phase*[LCL05].

On the other hand, recent advances in cost-effective wireless node architectures in millimeter levels have lead to novel designs of smart antennas for WSNs [LK04; KKOC10]. The designs are modular and inexpensive, comprising a 2−element switched-antenna array using a single RF frontend. Unlike prior art where space-time techniques have been considered for WSNs only in a cooperative multi-radio architecture, herein we exploit these new smart-antenna capabilities in order to introduce simple *non-cooperative* diversity techniques for reducing the total energy per bit required for achieving a target error performance. This is done by first proposing a novel approach for emulating the Alamouti code [Ala98] via a single-radio switched-antenna system under fixed-rate BPSK transmission. Further, we evaluate the energy saving capability of TS STC [VY03] under variable-rate MQAM (M-ary quadrature amplitude modulation) communication. At the receiving node, the switched-antenna design permits antenna selection for extracting the receive diversity. The proposed non-cooperative schemes are compared not only against SISO systems, but also against cooperative STBC, in terms of the total circuit and transmission energy consumption under various channel conditions. Specifically, the energy efficiency comparisons are performed under Rayleigh fading or under composite Rayleigh fading with log-normal shadowing, whereas the path loss exponent takes different values in its typical range. We also present an example of the latest single-radio switched-antenna designs onto which the non-cooperative space-time techniques can be practically deployed.

The rest of the chapter is organized as follows. Section 4.1 presents a set of reduced complexity space-time codes and demonstrates an example of a switched-antenna prototype for WSNs. The energy expenditure analysis follows in Section 4.2 which is a modification of previously proposed energy consumption models that differentiates between the RF frontends and the transmit / receive antennas and considers the circuitry of switched-antenna systems. Finally, Section 4.3 evaluates the performance of the different space-time techniques under various system configurations and channel conditions.

4.1 Reduced Complexity Space-Time Codes and Transceiver Designs

Several recent lines of research have addressed the multifaceted challenge of constructing space-time codes with reduced RF hardware from different dimensions. For example, the authors in [GRJF05] proposed an antenna system of two RF ports exciting two orthogonal polarizations of the radiated electric field. The proposed antenna system is capable of changing its polarization state (at the symbol rate via a switching mecha-

nism) and is used in [FGJF08] for transmitting a 4×4 STBC. However, having two radios per transceiver is still considered costly for wireless sensor nodes. On the other hand, a transmit diversity technique that emulates the Alamouti code has been proposed in [AKPP09b], using a single radio and two tunable radiators, closely coupled to the single driven antenna. However, the approach in [AKPP09b] requires a complex DC control circuitry as compared to the one proposed herein. Moreover, the mutual coupling of such closely coupled antennas degrades the antenna system efficiency (thus draining the sensor's battery) and distorts the desirable omnidirectional coverage. It should be noted that the omnidirectional coverage is desired as the sensor may need to broadcast and / or receive from all directions. An example where broadcasting and eavesdropping are essential functions in a WSN demanding uniform radiation capabilities is the environmental monitoring application in [DCBV07], where sensor nodes exchange broadcast packets according to a certain communication protocol for organizing themselves in a clustered network architecture.

In this section, we propose simple STBCs that can be deployed on reduced RF hardware transceivers. The first technique emulates the Alamouti code for BPSK signaling via a single RF chain. By this way, a full rate, full diversity, and a delay optimal code can be constructed with a single radio. The second scheme is a simple space-time switched-antenna code which can be directly constructed using switched-antenna systems. The code is full diversity and delay optimal but half-rate (when using two transmit antennas). Finally, we describe an example of a novel smart-antenna sensor node transceiver that is capable of constructing the proposed codes while having a single RF frontend.

4.1.1 Modified Alamouti Code

In this part we describe a modification of the Alamouti code (originally proposed with two active transmit antennas) that allows it to be constructed with a single radio and a switched-antenna system, i.e., a single antenna active at a time. The modification of the code is fully equivalent to the original, thus leading to similar performance gains. Consider two BPSK symbols x_1 and x_2, transmitted over two antennas according to the Alamouti code, and received using N_R antennas after propagating through the channel $\mathbf{H}$. The narrowband received signal model can be written as

$$\mathbf{Y} = \mathbf{H}\mathbf{X} + \mathbf{n}, \tag{4.1}$$

where $\mathbf{Y} \in \mathbb{C}^{N_\mathrm{R} \times 2}$, $\mathbf{X} \in \mathbb{R}^{2\times 2}$ defined as $\mathbf{X} := \begin{bmatrix} x_1 & -x_2 \\ x_2 & x_1 \end{bmatrix}$, and $\mathbf{n} \in \mathbb{C}^{N_\mathrm{R} \times 2}$ is a vector representing the AWGN. The noise is assumed spatially white across the N_R receive antennas, with zero mean and variance σ_n^2. By introducing an orthonormal 2×2 matrix $\mathbf{U}$ such that $\mathbf{U}\mathbf{U}^\mathrm{T} = \mathbf{U}^\mathrm{T}\mathbf{U} = \mathbf{I}$, the received signal model can be rewritten as

$$\begin{aligned} \mathbf{Y} &= \mathbf{H}\mathbf{U}\mathbf{U}^\mathrm{T}\mathbf{X} + \mathbf{n} \\ &= \widetilde{\mathbf{H}}\widetilde{\mathbf{X}} + \mathbf{n}, \end{aligned} \tag{4.2}$$

where $\widetilde{\mathbf{H}} = \mathbf{HU}$ and $\widetilde{\mathbf{X}} = \mathbf{U}^{\mathrm{T}}\mathbf{X}$ are unitary transformations of $\mathbf{H}$ and $\mathbf{X}$, respectively. Notice that (4.2) is equivalent to (4.1), since $\widetilde{\mathbf{H}}$ and $\widetilde{\mathbf{X}}$ are just rotations of $\mathbf{H}$ and $\mathbf{X}$, respectively. However, by setting

$$\mathbf{U} = \frac{1}{\sqrt{2}} \begin{bmatrix} 1 & 1 \\ 1 & -1 \end{bmatrix},$$

and considering that in BPSK signaling, x_2 is at one of the two possible states: $+x_1$ or $-x_1$, the block $\widetilde{\mathbf{X}}$ becomes

- either diagonal, i.e.,

$$\widetilde{\mathbf{X}} = \mathbf{U}^{\mathrm{T}}\mathbf{X} = \begin{bmatrix} x_1 & 0 \\ 0 & -x_1 \end{bmatrix},$$

  when $x_2 = x_1$

- or anti-diagonal, i.e.,

$$\widetilde{\mathbf{X}} = \mathbf{U}^{\mathrm{T}}\mathbf{X} = \begin{bmatrix} 0 & -x_1 \\ -x_1 & 0 \end{bmatrix},$$

  when $x_2 = -x_1$.

The result is quite remarkable in the sense that a transmitter with a single RF frontend and two transmit antennas will be capable of transmitting the Alamouti code of two BPSK signals via antenna switching. For example, an RF switch can be used as we describe later to swap the driven antenna (the RF excitation port) according to the location of the non-zero entries of $\widetilde{\mathbf{X}}$, at the modulation rate. On the other hand, the receiver recovers the received signal exactly as in classical Alamouti decoders, by constructing the equivalent matrix of $\mathbf{H}$ over the two symbol periods. The matrix $\mathbf{H}$ is obtained from $\widetilde{\mathbf{H}}$ (i.e., $\mathbf{H} = \widetilde{\mathbf{H}}\mathbf{U}^{\mathrm{T}}$) which can be estimated by training the receiver using $\widetilde{\mathbf{X}}$.

Finally, the difficulty of finding a unitary matrix $\mathbf{U}$ (whether being real or complex) that collapses the space-time block code into a matrix of column vectors each with a single non-zero entry increases as the signaling dimension increases, a drawback that is addressed in the next part.

4.1.2 Time-Switched Space-Time Code

In [VY03], the TS STC

$$\mathbf{X} = \begin{bmatrix} x_t & 0 \\ 0 & x_t \end{bmatrix}$$

is presented, where 0 means erasure and x_t is the symbol of *any modulation format*. The associated received signal model is given in (4.1). In this simple scheme, only one antenna is active at each time slot. Thus, the code lends itself nicely to single-RF switched-antenna prototypes, transmitting x_t from antenna one and two at times $2t$

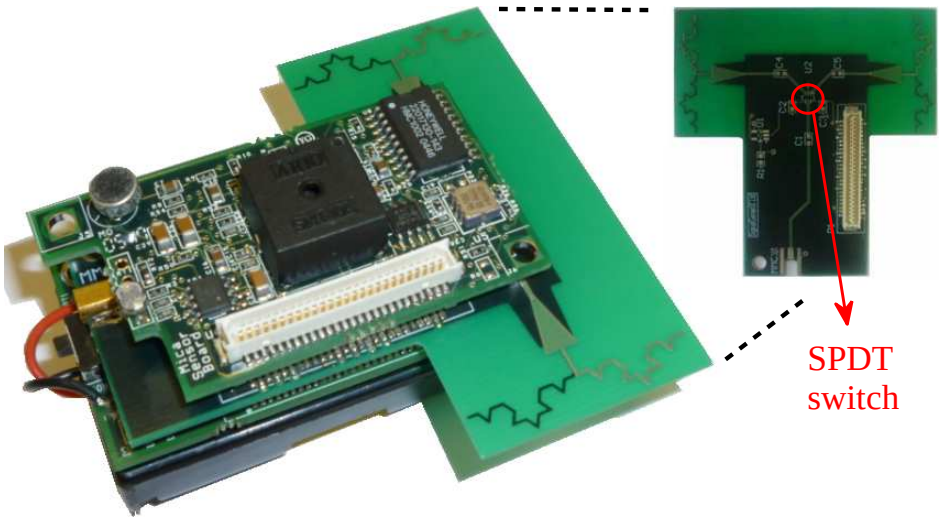

Figure 4.1: Example of an integrated add-on solution with a switched-antenna printed fractal structure for single-radio sensor nodes.

and $2t + 1$, respectively. Although the TS STC extracts the full transmit diversity (transmit diversity of order 2 in this case), the code is of half rate as each modulated symbol is transmitted in two time slots. The advantages of this code are

- Being modulation independent as compared to the unitary rotation (transformation) approach described earlier.
- Switching the antennas can be done at every encoded data-packet $\mathbf{p}_t$ rather than at every encoded data-symbol x_t, i.e.,

$$\mathbf{X} = \begin{bmatrix} \mathbf{p}_t & 0 \\ 0 & \mathbf{p}_t \end{bmatrix},$$

  thus further simplifying the switching circuitry[1].

4.1.3 A Switched-Antenna Example for Single-Radio Sensor Nodes

Although current implementations of sensor nodes use a single omnidirectional antenna to achieve coverage, [LK04; KKOC10] introduced the innovative concept of utilizing smart antennas on wireless sensor nodes. This approach was motivated by the advantages of smart antennas already witnessed in wireless ad-hoc networks, such as

[1]For this to work, the channel fading rate should be equal to or smaller than half of the packet rate.

range increase, power consumption decrease, and interference cancellation at the network level [KD05]. These benefits are quite attractive for WSNs where range, node power consumption, and interference largely dictate the overall network lifetime. Here we demonstrate an example of a newly developed switched-antenna prototype (Figure 4.1), which is an add-on board built for a type of widely-used motes [xbo]. The design includes a SPDT switch capable of switching the RF path to two different connectors, thus supporting two efficient fractal antennas at opposite edges of the module. Each antenna is a 30.94 mm $\times$ 5.07 mm standard Koch fractal dipole (indentation angle equal to 60°) of 2 iterations [PBRP+98] with bipolar feed. The antenna structure lays on a PCB, where one leg of the dipole is placed on the component layer and the second leg is connected to the intermediate ground layer of the PCB. The fact that the second leg is placed within the dielectric structure (0.3 mm from component layer) has the advantage that the antenna structure is easier to match, with modest impact on the antenna efficiency[1] which is in the order of 90%, producing a gain of 4.2 dBi with a maximum toward the antenna side. The distance between the two fractal elements is $\sim$ 5.6 cm, i.e., the two antennas are almost $\lambda/2$ spaced at the operating frequency of 2.5 GHz. According to the measured antenna diagrams, the spacing is quite sufficient for having the two antennas decorrelated in environments with moderate angular spreads. The add-on board can be transparently connected between the sensing board and the node, this connection being unrelated to the use of the switched-antenna running on the node's board. The modular design increases its overall expandability allowing for building more advanced hardware platforms without requiring total system redesign. Further, the existence of more than one antenna *enables the application of multi-antenna techniques on low-power sensor nodes*, a concept that seems quite unachievable with conventional wireless node architectures.

4.2 Energy Efficiency Analysis

In this section, we provide energy efficiency analysis for different system configurations including the cases where at least one of the two communicating sensor nodes is equipped with a switched-antenna system, thus encoding the signals in space and time at the transmitter side, according to the aforementioned reduced complexity codes, and / or performing receive antenna selection (assuming perfect channel knowledge) at the receiver side.

4.2.1 Energy Consumption Model

We consider a general communication link connecting two wireless nodes with $N_{\mathrm{RF}}^{\mathrm{Tx}}$ RF frontends at the transmitter and $N_{\mathrm{RF}}^{\mathrm{Rx}}$ RF frontends at the receiver. The receiver can be thought as the relay node in multi-hop based routing, where intermediate sensor nodes forward collected data toward the central processing unit. We use a similar uncoded

[1] The antenna efficiency accounts for the ohmic and dielectric losses within the antenna structure as well as for the reflection efficiency due to impedance mismatch.

system to the one in [CGB04], where the transmit and receive analog circuit blocks are given in [3, Figure 1-2], the baseband signal processing blocks are intentionally omitted, and the frequency synthesizer is assumed shared among all the RF paths. In addition, our model accounts for the RF switch insertion loss, in case switched antennas are used. The total power consumption can be categorized into two main parts, namely, the power consumption of all the power amplifiers P_{A}, which is a function of the transmission power P_{T}, and the power consumption of all other circuit blocks P_{c}.

The power consumption of the power amplifiers can be approximated as

$$P_{\mathrm{A}} = P_{\mathrm{T}}\,\xi/(\eta_{\mathrm{drain}}\,\eta_{\mathrm{switch}}^{\mathrm{Tx}}\,\eta_{\mathrm{switch}}^{\mathrm{Rx}}), \tag{4.3}$$

with η_{drain} being the drain efficiency of the RF power amplifier and ξ being the peak-to-average ratio (PAR) which is dependent on the modulation scheme and the associated constellation size [CGB05]. $\eta_{\mathrm{switch}}^{\mathrm{Tx}}$ and $\eta_{\mathrm{switch}}^{\mathrm{Rx}}$ are defined as $\eta_{\mathrm{switch}}^{\mathrm{Tx}} = 10^{-\mathcal{L}_{\mathrm{switch}}^{\mathrm{Tx}}/10}$ and $\eta_{\mathrm{switch}}^{\mathrm{Rx}} = 10^{-\mathcal{L}_{\mathrm{switch}}^{\mathrm{Rx}}/10}$, where $\mathcal{L}_{\mathrm{switch}}^{\mathrm{Tx}}$ and $\mathcal{L}_{\mathrm{switch}}^{\mathrm{Rx}}$ are the transmit and receive RF switch insertion losses in dB (in case of having an RF switch in the RF signal path), respectively.

When the channel experiences a β-law path loss (typically, $2 \leq \beta \leq 5$, with $\beta = 2$ representing free-space propagation), P_{T} can be calculated according to the link budget relationship [Jay06; CCV01]

$$P_{\mathrm{T}} = \bar{E}_{\mathrm{b}} R_{\mathrm{b}} \frac{(4\pi)^2 d^{\beta}}{G_{\mathrm{T}} G_{\mathrm{R}} \lambda^2} M_{\mathrm{l}} N_{\mathrm{f}}, \tag{4.4}$$

where $\bar{E}_{\mathrm{b}}$ is the required average energy per bit at the receiver for a given BER specification, R_{b} is the bit rate, d is the transmission distance, G_{T} and G_{R} are the transmit and receive antenna gains respectively (assuming matched antenna systems), λ is the carrier wavelength, M_{l} is the link margin compensating the hardware process variations and other additive background noise or interference, $N_{\mathrm{f}} = (N_{\mathrm{r}}/N_0)$ is the receiver noise figure, with N_{r} being the PSD of the total effective noise at the receiver input and N_0 the single-sided thermal noise PSD at room temperature ($N_0 = -171$ dBm/Hz). The circuit consumption P_{c} is estimated as [CGB05]

$$P_{\mathrm{c}} \approx N_{\mathrm{RF}}^{\mathrm{Tx}}(P_{\mathrm{DAC}} + P_{\mathrm{mix}} + P_{\mathrm{filt}}^{\mathrm{TX}}) + 2P_{\mathrm{syn}} + N_{\mathrm{RF}}^{\mathrm{Rx}}(P_{\mathrm{LNA}} + P_{\mathrm{mix}} + P_{\mathrm{IFA}} + P_{\mathrm{filt}}^{\mathrm{Rx}} + P_{\mathrm{ADC}}) \tag{4.5}$$

In (4.5), P_{DAC}, P_{mix}, $P_{\mathrm{filt}}^{\mathrm{Tx}}$, P_{syn}, P_{LNA}, P_{IFA}, $P_{\mathrm{filt}}^{\mathrm{Rx}}$, and P_{ADC} stand, respectively, for the power consumption of the DAC, the mixer, the active filters at the transmitter, the frequency synthesizer, the low noise amplifier, the intermediate frequency amplifier, the active filters, and the ADC at the receiver. The total energy consumption per bit $E_{\mathrm{b,t}}$ is given by

$$E_{\mathrm{b,t}} = \frac{P_{\mathrm{A}} + P_{\mathrm{c}}}{R_{\mathrm{b}}} \overset{(4.3),(4.4)}{=} \bar{E}_{\mathrm{b}} \frac{\xi(4\pi)^2 d^{\beta}}{\eta_{\mathrm{drain}}\,\eta_{\mathrm{switch}}^{\mathrm{Tx}}\,\eta_{\mathrm{switch}}^{\mathrm{Rx}}\,G_{\mathrm{T}} G_{\mathrm{R}} \lambda^2} M_{\mathrm{l}} N_{\mathrm{f}} + \frac{P_{\mathrm{c}}}{R_{\mathrm{b}}}. \tag{4.6}$$

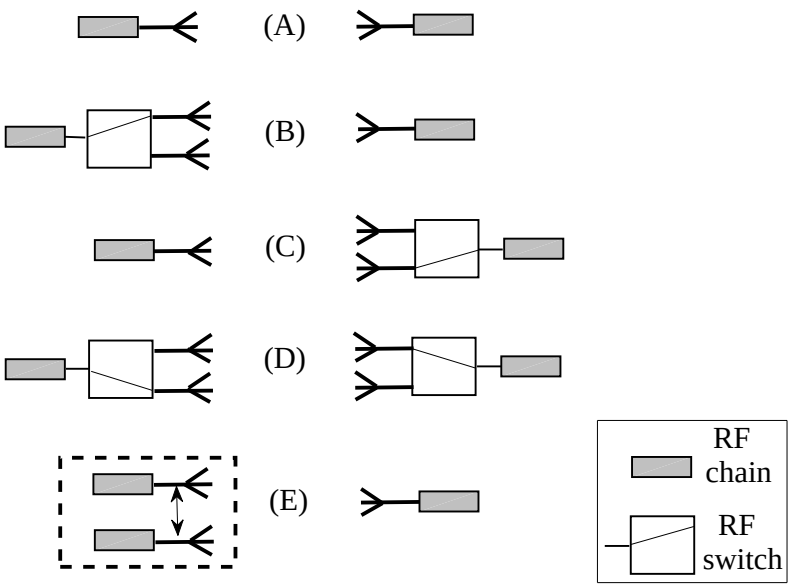

Figure 4.2: Configurations A-D: Non cooperative cases, Configuration E: Cooperative 2×1 Alamouti.

It should be noted that in certain cases where certain digital signal processing is performed on the received data at the node level (e.g., data compression[DCBV07]), it is important to also account for the energy per bit for data processing. In this development, such processing on the received data is not performed.

Suppose that on top of the β-law path loss in (4.4), the signal is further attenuated by a flat-fading Rayleigh channel with log-normal shadowing (simply referred to as the *shadowed Rayleigh* channel). Thus, according to the stochastic Suzuki process [AKH05], each entry of $\mathbf{H}$ is given by the product of a) a zero-mean circulant symmetric random variable with unit variance modeling the short-time channel variations and b) a log-normal random variable, with standard deviation of the associated Gaussian random variable equal to σ (dB) and mean equal to 0 dB, accounting for the long-term fading (shadowing). It should be noted that by setting $\sigma = 0$ dB the model collapses to pure Rayleigh fading. The fading is assumed constant during the transmission of a STBC codeword (quasi-static fading model). In the following, we assume that a total of L bits need to be transmitted.

4.2.2 Non Cooperative Systems

We assume the transmit and / or the receive sensor node equipped with a switched-antenna system. The possible considered configurations are shown in Figure 4.2 (Configurations A-D). With the switched antenna at the transmitter (Figure 4.2, Configurations B, D), the STBCs proposed in Section 4.1 can be applied. At the switched-antenna receiver (Figure 4.2, Configurations C, D) antenna selection can be employed.

Notice that in these non cooperative schemes, the number of RF chains in (4.5) is $N_{\mathrm{RF}}^{\mathrm{Tx}} = N_{\mathrm{RF}}^{\mathrm{Rx}} = 1$.

4.2.2.1 Fixed-Rate BPSK

We consider BPSK modulation and a fixed data rate R_{b}. The reference SISO system (Figure 4.2, Configuration A) has $\mathbf{H} = [h]$ and instantaneous received SNR $\gamma_{\mathrm{b}} = |h|^2 \frac{\bar{E}_{\mathrm{b}}}{N_0}$. In Configuration B, the proposed modified 2×1 Alamouti scheme is considered, where $\mathbf{H} = [h_1 \ h_2]$ and $\gamma_{\mathrm{b}} = \frac{|h_1|^2+|h_2|^2}{2} \frac{\bar{E}_{\mathrm{b}}}{N_0}$ [GNP03]. In Configuration C, with single-antenna transmission and receive antenna selection, we have $\mathbf{H} = [h_1 \ h_2]^T$ and $\gamma_{\mathrm{b}} = \max\{|h_1|^2, |h_2|^2\} \frac{\bar{E}_{\mathrm{b}}}{N_0}$. The proposed Alamouti is combined with receive antenna selection in Configuration D, where $\mathbf{H} = \begin{bmatrix} h_{11} & h_{12} \\ h_{21} & h_{22} \end{bmatrix}$ and $\gamma_{\mathrm{b}} = \frac{\max\{|h_{11}|^2+|h_{12}|^2, |h_{21}|^2+|h_{22}|^2\}}{2} \frac{\bar{E}_{\mathrm{b}}}{N_0}$.

The average BER for BPSK is given by [GNP03]

$$\bar{P}_{\mathrm{b}} = \mathbb{E}_{\mathbf{H}} \left\{ Q\left(\sqrt{2\gamma_{\mathrm{b}}}\right) \right\}. \tag{4.7}$$

Thus, $\bar{E}_{\mathrm{b}}$ for any configuration and a given BER requirement can be obtained by inverting (4.7). Substituting in (4.6), the total energy required to complete a transmission of L bits is given by $E_{\mathrm{t}} = LE_{\mathrm{b,t}}$.

4.2.2.2 Optimized Variable-Rate MQAM

As suggested in [CGB04], by optimizing the rate (constellation size) of the communication system over the transmission distance we may be able to decrease the total required energy, especially for STBC-based systems supporting higher constellation sizes than SISO. This allows the system to shorten the transmission time without violating the BER requirement, reducing the break-even distance at which the STBC-based systems outperform the SISO. It should be clarified that rate optimization over the transmission distance is different from adaptive modulation systems (e.g., [WS95; CG01; CWC07]), where the constellation size is varied according to the short-term or the long-term fading rate of the channel. In this part, we assume MQAM modulation of constellation size b bits per symbol and a symbol rate of R_{s} (equal to the modulation bandwidth) so that the bit rate $b \cdot R_{\mathrm{s}}$ depends on the chosen modulation. Consequently, in Configurations A and C we have $R_{\mathrm{b}} = bR_{\mathrm{s}}$. However, in Configurations B and D, the half-rate TS STC results in $R_{\mathrm{b}} = bR_{\mathrm{s}}/2$ requiring two times the circuit energy consumption $P_{\mathrm{c}}/R_{\mathrm{b}}$ with respect to SISO. Notice also that in Configuration B we have $\mathbf{H} = [h_1 \ h_2]$ and $\gamma_{\mathrm{b}} = \frac{\max(|h_1|^2, |h_2|^2)}{2} \frac{\bar{E}_{\mathrm{b}}}{N_0}$. In Configuration D, the TS STC is combined with receive antenna selection obtaining $\mathbf{H} = \begin{bmatrix} h_{11} & h_{12} \\ h_{21} & h_{22} \end{bmatrix}$ and $\gamma_{\mathrm{b}} = \frac{\max_{i,j\in\{1,2\}}\{|h_{ij}|^2\}}{2} \frac{\bar{E}_{\mathrm{b}}}{N_0}$.

With MQAM modulation, $\bar{E}_{\mathrm{b}}$ is defined by the target BER and the underlying

constellation size $b \geq 2$ according to the following relationship [Pro00][1]

$$P_{\mathrm{b}} \approx \mathbb{E}_{\mathbf{H}} \left\{ \frac{4}{b} \left(1 - \frac{1}{2^{b/2}} \right) Q \left(\sqrt{\frac{3b}{2^b - 1} \gamma_{\mathrm{b}}} \right) \right\}. \tag{4.8}$$

As in [CGB04], substituting $\bar{E}_{\mathrm{b}}$ and R_{b} into (4.6), we can find by brute-force search for any configuration the modulation size that minimizes $E_{\mathrm{b,t}}$ at a certain distance d. Similarly, the total energy to transmit L bits is $E_{\mathrm{t}} = LE_{\mathrm{b,t}}$.

4.2.3 Cooperative Systems

We compare the above techniques with a system where two single-antenna nodes cooperate in order to transmit a classical (full-rate) 2×1 Alamouti signal structure to a single-antenna receive node (Figure 4.2, Configuration E) *assuming the ideal condition of perfectly synchronized transmission between the cooperating wireless sensor nodes.* We have $\mathbf{H} = [h_1 \ h_2]$ and $\gamma_{\mathrm{b}} = \frac{|h_1|^2 + |h_2|^2}{2} \frac{\bar{E}_{\mathrm{b}}}{N_0}$. The total energy consumption E_{t} for the long-haul communication, i.e., the communication between the two transmit nodes and the receive node, is found as in the non cooperative system in both fixed and variable rate cases. Notice here that $N_{\mathrm{RF}}^{\mathrm{Rx}} = 1$ whereas $N_{\mathrm{RF}}^{\mathrm{Tx}} = 2$, i.e., the number of RF chains on the transmitter side is doubled with respect to configurations A-D.

In this system we also need to take into account the energy lost for local data exchange on the transmitter side. Prior to transmitting the information sequence according to the Alamouti structure, the cooperating nodes need to exchange their information bits using different time slots (we assume that each node has $L/2$ bits to send). For local transmissions, we assume a ζ-law power loss with AWGN [CGB04]. The total energy cost per bit for local information flow, denoted as E_ℓ, can be calculated according to the result obtained for SISO communication links in AWGN channels in [CGB05, Equation (10)] assuming the cooperating nodes separated by distance d_ℓ. Notice that in the variable-rate case, the modulation (of constellation size b_ℓ bits per symbol) is optimized for the local transmission as well. The total energy consumption in order to transmit L bits in the cooperative approach is given by $E_{\mathrm{coop,t}} = L(E_\ell + E_{b,\mathrm{t}})$.

4.3 Performance Evaluation

4.3.1 Total Energy Consumption Performance Analysis

To simulate the proposed non cooperative STBC and antenna selection schemes for single-radio sensor nodes, we use the circuit and system parameters given in [CGB04, Table I]. The parameters correspond to the circuitry of a typical WSN radio at the operating frequency $f_{\mathrm{c}} = 2.5$ GHz in the ISM band according to [CGB05; Lee98; SML+02; WPS+00; SXK97], as described and used in the literature for WSNs (e.g., [CGB04; Jay06; Jay07; XC07]). For example, the drain efficiency is given by $\eta_{\mathrm{drain}} =$

[1] We consider negligible the error in (4.8) when b is odd [CGB04].

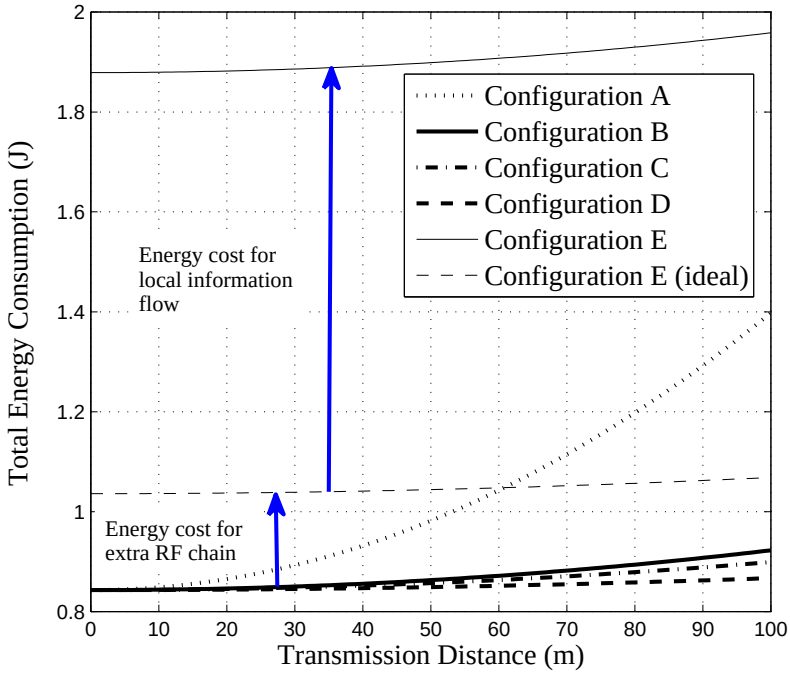

Figure 4.3: Total energy consumption for fixed-rate BPSK modulation under Rayleigh fading and $\beta = 2$. Configurations A-D: Non cooperative cases with the proposed Alamouti and / or receive antenna selection, Configuration E: Cooperative 2×1 Alamouti (Figure 4.2).

0.35, which is a practical value for class-A RF power amplifiers (due to the linearity requirement for amplifying MQAM signals, class-A power amplifiers are usually used) [Lee98]. The target BER is 10^{-3}, $L = 40$ Kb, $B = 10$ KHz and the power supply is $V_{\text{dd}} = 3$ V. At such operating frequency and voltage, a SPDT RF switch has a typical insertion loss of around 0.35 dB. We assume pure Rayleigh fading (i.e., $\sigma = 0$ dB) and $\beta = 2$. The results for the fixed-rate system ($R_{\text{b}} = 10$ Kb/s) are given in Figure 4.3, where we see that the proposed non-cooperative space-time techniques (Configurations B-D) outperform the conventional SISO system (Configuration A) when $d \geq 9$ m. On the other hand, the cooperative 2×1 Alamouti (Configuration E) results in tremendous energy expenditure owing to a) the extra circuit energy consumption and b) the energy cost for local information flow. The latter, however, is exacerbated by the suboptimality of the low-rate BPSK modulation for the small-range local communication. Even if we ignore the energy cost for the local transmissions (ideal Configuration E), the energy cost is still significant and the corresponding break-even distance with respect to SISO rises to $d = 62$ m.

Regarding the variable-rate communication, Figure 4.4 shows how the total energy consumption depends on the constellation size for various transmission distances for Configuration B (TS STC at the transmitter and antenna selection at the receiver). It

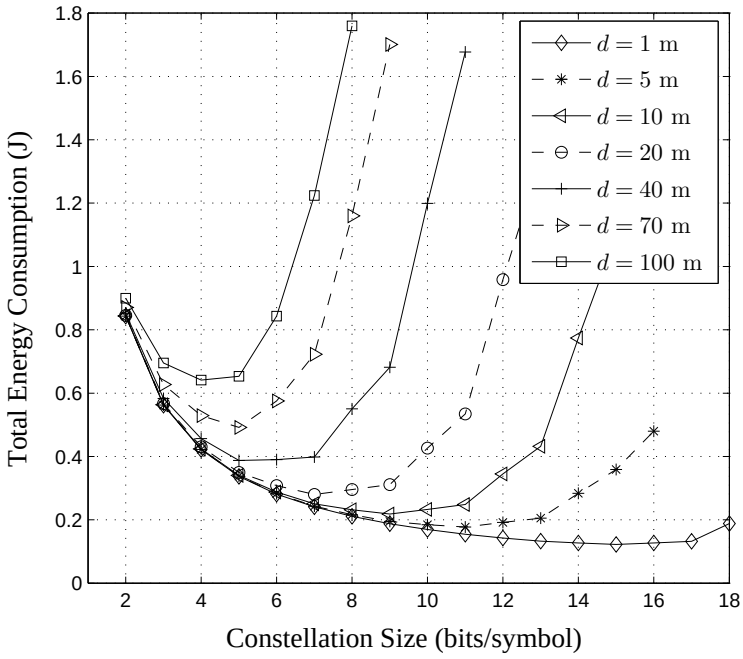

Figure 4.4: Total energy consumption versus MQAM constellation sizes at different transmission distances d for Configuration B (TS STC at the transmitter and antenna selection at the receiver) under Rayleigh fading and $\beta = 2$.

is clear from Figure 4.4 that there is an optimal constellation size for each transmission distance for which the total energy is minimized. Table 4.1 summarizes these optimal constellation sizes for each Configuration and transmission distance d. The results indicate that the proposed non-cooperative space-time techniques (Configurations B-D) can support higher data rates with respect to SISO (Configuration A) and to cooperative Alamouti (Configuration E) to decrease the transmission time without increasing the transmission energy. Some of the numbers in Table 4.1 are not practical, especially the ones at very small distances. However, these numbers will be helpful in providing us with insights into the theoretical capabilities of the different configurations regarding energy efficiency.

Figure 4.5 shows the simulation results for the optimized multimode case. For the local transmission in the cooperative scheme (Configuration E) we assume $\zeta = 3.5$ and $d_\ell = 1$ m, whereas the optimal constellation size is found as $b_\ell = 16$ bits/symbol. From Figure 4.5, it is obvious that the diversity techniques (Configurations B-E) are further enhanced with respect to SISO since they can support higher constellation sizes. Although the cooperative 2×1 Alamouti (Configuration E) performs better than the non-cooperative half-rate TS STC (Configuration B), we can observe that the non-cooperative Configurations C and D outperform the cooperative Configuration E in terms of the total energy consumption.

Table 4.1: Optimized MQAM Constellation Size (bits / symbol) under Rayleigh Fading and $\beta = 2$

d (m)	1	5	10	20	40	70	100
Configuration A	12	6	5	4	4	2	2
Configuration B	15	11	9	6	5	5	4
Configuration C	15	10	9	7	5	4	4
Configuration D	16	13	10	9	7	5	5
Configuration E	14	10	8	6	5	4	3

In Figure 4.6, we have plotted the energy efficiency (energy savings) of the different space-time schemes (Configurations B-E) with respect to SISO (Configuration A) for variable-rate MQAM under Rayleigh fading and various path-loss parameters β. We can notice from Figure 4.6 that the energy savings offered by the space-time schemes grow rapidly as β increases. Figure 4.6 also shows that those efficiencies are achieved at shorter distances for large β values (i.e., the critical distances decrease), since transmission energy becomes significant at shorter distances for large β values. We can also observe that the proposed non-cooperative schemes (Configurations C-D) result in greater energy-savings compared to cooperative Alamouti (Configuration E), as in Figure 4.5, although these savings are less pronounced as β increases. A similar trend has been observed for fixed-rate BPSK, however in this case the Configurations B-D exhibit greater energy savings, as in Figure 4.3.

Figure 4.7 depicts the energy efficiency of Configurations B-E with respect to SISO (Configuration A) for variable-rate MQAM and for $\beta = 2$ under Rayleigh fading as well as under shadowed Rayleigh fading with $\sigma = 8$ dB. We can observe that the curves shift to the left under the composite shadowed Rayleigh channel, similarly to the effect of larger β values. Thus, the energy savings offered by the space-time schemes increase when shadowing is added in the model. Figure 4.7 also shows that those efficiencies are achieved at shorter distances under the composite channel, since transmission energy becomes significant at shorter distances under the compound effect of Rayleigh fading and shadowing. Similar results have been observed for different values of β, in all having the non-cooperative Configurations C-D outperform the cooperative 2×1 Alamouti.

Finally, by comparing the Configurations C and D, we notice that in a scenario where *both* of the two communicating sensor nodes are equipped with a switched-antenna system, the benefit of the proposed modified Alamouti code together with antenna selection (under fixed-rate BPSK) is marginal over only using antenna selection (e.g., Figure 4.3), whereas the combination of TS STC with antenna selection performs almost as well as antenna selection in a variable-rate MQAM setting with respect to the total energy consumption (Figure 4.5-4.7). This may lead to the result that, under such a scenario and spatially independent fading conditions, energy saving benefits may result from transmitting over only one of the two antennas while letting the receiver perform antenna selection.

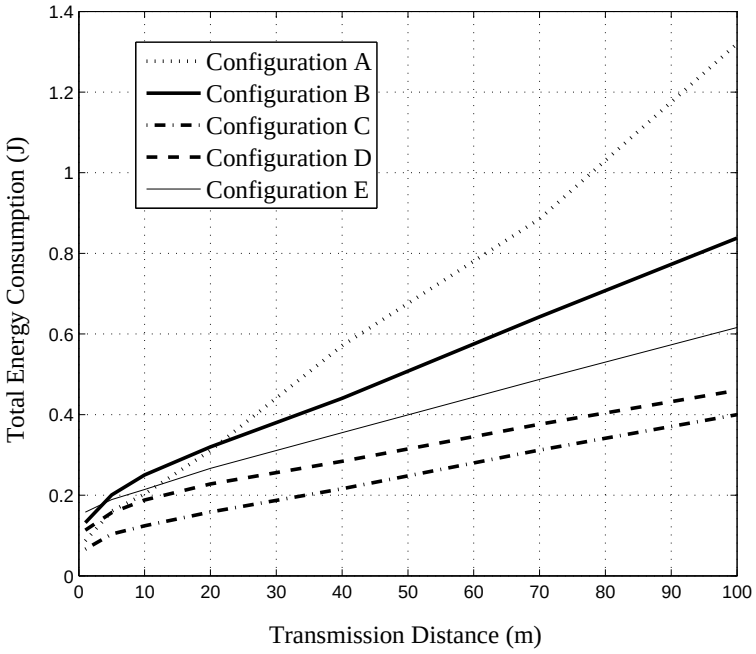

Figure 4.5: Total energy consumption for optimized variable-rate MQAM modulation under Rayleigh fading and $\beta = 2$. Configurations A-D: Non cooperative cases with TS STC and / or receive antenna selection, Configuration E: Cooperative 2×1 Alamouti (Figure 4.2).

Remarks:

It should be emphasized that in this work the focus is on low-cost energy-constrained wireless devices, thus, the different space-time schemes are mainly evaluated in terms of their energy consumption. The impact on the energy consumption of the TS STC (compared to a full-rate code) is twofold:

(a) Circuit energy consumption [equations (4.5)-(4.6)]: Although, the TS STC requires a single RF frontend ($N_{\mathrm{RF}}^{\mathrm{Tx}} = 1$) compared to the two-RF cooperative Alamouti requiring two frontends ($N_{\mathrm{RF}}^{\mathrm{Tx}} = 2$), under the half-rate TS STC and for a given constellation size b, the node's circuitry is used twice the time per bit $[2 \cdot 1/(bR_{\mathrm{s}})$ s/bit] compared to the SISO or to a full-rate code $[1/(bR_{\mathrm{s}})$ s/bit].

(b) Transmission energy consumption: The TS STC also affects the energy consumed for transmission requiring increased average energy per bit $\bar{E}_{\mathrm{b}}$ for a target bit rate and for a given BER specification compared to the 2×1 Alamouti code. This is illustrated in Figure 4.8 depicting the error performance versus the required $\bar{E}_b/N_0$ for various MQAM modulations. (10^6 channel realizations where taken under Rayleigh fading as well as under shadowed Rayleigh fading; for the log-normal

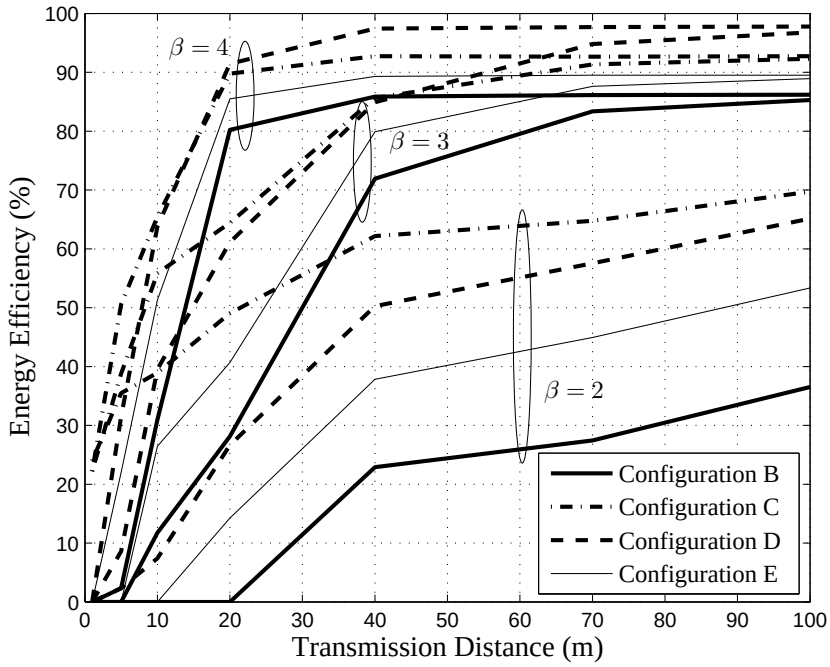

Figure 4.6: Energy efficiency of diversity techniques (Configurations B-E) with respect to SISO (Configuration A) for variable-rate MQAM under Rayleigh fading and various β.

shadowing, the standard deviation of the associated Gaussian random variable is equal to 8 dB.) It can be noted that the TS STC results in about $1-1.5$ dB increase in the required $\bar{E}_b/N_0$ compared to classical Alamouti for a given target BER. This increase is more important for large distances, where the transmission energy is the dominant term in the total energy consumption.

We should also keep in mind that the cooperative 2×1 Alamouti incurs some circuit and transmission energy consumption for the local transmissions.

It should be noted that all these effects in the energy consumption are taken into account when optimizing the constellation size aiming at energy efficiency minimization in variable-rate MQAM systems (Section 4.2.2 and Section 4.3.1).

4.3.2 Total Delay Performance Analysis

As the energy efficiency is the major goal of the analysis of this chapter, the figures hitherto focus on plotting the total energy consumption or the energy efficiency with respect to SISO versus the transmission distance or versus the constellation size, for various configurations and under different channel conditions, such as Rayleigh fading, shadowed Rayleigh fading, and for different path loss exponents. On top of these, the

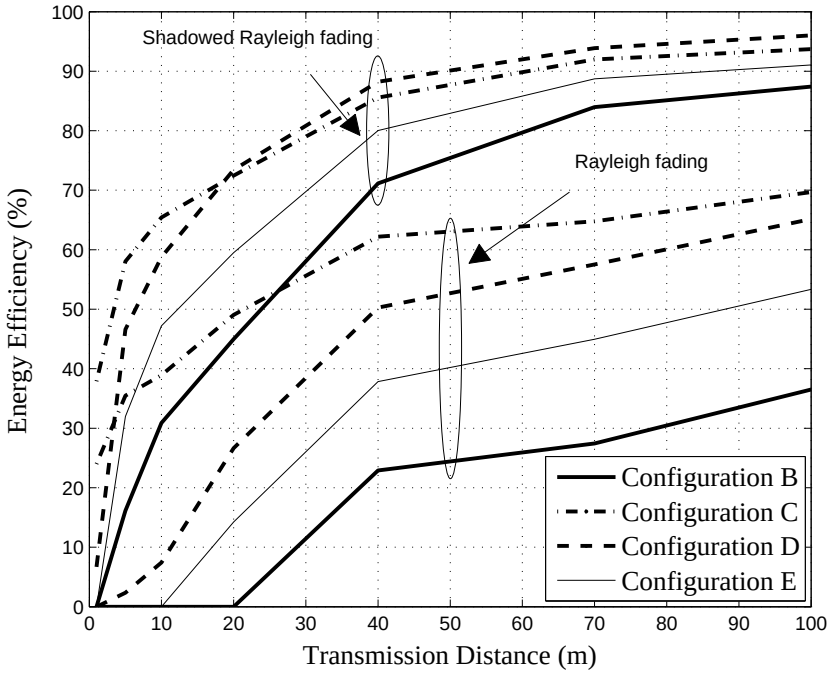

Figure 4.7: Energy efficiency of diversity techniques (Configurations B-E) with respect to SISO (Configuration A) for variable-rate MQAM under Rayleigh fading and shadowed Rayleigh fading with $\sigma = 8$ dB ($\beta = 2$).

optimal constellations size versus the transmission distance under variable-rate MQAM is given in Table 4.1.

Other figures of merit of interest include the throughput and the total delay, i.e., the total transmission delay required by a certain scheme. The suggested non-cooperative TS STC is a half-rate space-time code. In general, the throughput is given by

$$\text{Throughput} = \frac{\text{Number of bits to be transmitted}}{\text{Total delay}} = \frac{L}{\text{Total delay}}, \tag{4.9}$$

where the number of bits to be transmitted (prior to space-time coding) is L and the total delay is the total transmission delay required by a certain scheme. For a fixed transmission bandwidth B, we have assumed that the symbol period $T_s = 1/R_s$ is approximately $T_s \approx (1/B)$. For the non-cooperative schemes, the delay for transmitting L bits when the transmission is at full rate [e.g., SISO (Configuration A), receive antenna selection (Configuration C), Configurations B and D with the proposed modified 2×1 Alamouti] is denoted by $T_{\text{non-coop, full-rate}}$ and is given by

$$T_{\text{non-coop, full-rate}} = T_s \cdot L/b. \tag{4.10}$$

Similarly, the delay for transmitting L bits when the transmission is at half rate (e.g.,

Configurations B and D with TS STC), denoted by $T_{\text{non-coop, half-rate}}$, is equal to

$$T_{\text{non-coop, half-rate}} = 2 \cdot T_{\text{s}} \cdot L/b, \tag{4.11}$$

because the half-rate TS-STC requires double the transmission time to transmit L bits for a given constellation size. Therefore, from equations (4.9) and (4.10) the throughput in case of full-rate non-cooperative schemes is equal to $\frac{L}{T_{\text{s}} \cdot L/b} = bR_{\text{s}}$, whereas from equations (4.9) and (4.11) the throughput in case of half-rate non-cooperative schemes is equal to $\frac{L}{2T_{\text{s}} \cdot L/b} = bR_{\text{s}}/2$. Therefore, under the half-rate TS-STC, the throughput is half with respect to SISO or to a full-rate space-time block code (STBC) for a given constellation size (*see* Section 4.1, Section 4.2.2).

Also, the total delay for the cooperative 2×1 Alamouti (Configuration E) includes the delay for both the long-haul transmission and the local transmission, assuming that each cooperating node has $L/2$ bits to send. Accordingly, the delay for transmitting L bits is given by

$$T_{\text{coop}} = T_{\text{s}} \cdot L/b \ + \ T_{\text{s}} \cdot L/b_{\ell}, \tag{4.12}$$

where b_{ℓ} is the constellation size (in bits per symbol) used for the local transmissions whereas, from equations (4.9) and (4.12), the throughput is given by $\frac{L}{T_{\text{s}} \cdot L \cdot (1/b_{\ell} + 1/b)} = R_{\text{s}}(b \cdot b_{\text{l}})/(b + b_{\ell})$.

The delay performance comparison among the Configurations A-E is plotted in Figure 4.9 for various path loss exponents β and for $B = 10$ KHz and $L = 40$ Kb (as in Section 4.3.1). The comparison is for optimized variable-rate MQAM, i.e., in the equations (4.10)-(4.12) the constellation size used is the one that results from the energy consumption minimization as explained in Sections 4.2.2 and 4.3.1. For the cooperative 2×1 Alamouti (Configuration E) *we have assumed the ideal condition of perfectly synchronized transmission between the cooperating wireless sensor nodes.* As expected, from Figure 4.9 it can be seen observed that the non-cooperative Configurations B and D are the least delay efficient strategies due to the half-rate nature of the TS STC. Moreover, when the transmission distance becomes large and for $\beta = 3$ or $\beta = 4$ (Figure 4.9(b)-4.9(c)), the transmission energy becomes dominant such that the optimized constellation for all Configurations is 4-QAM. As a result, the delay caused after a transmission distance threshold value will be the same for Configurations A and C (equal to 2 sec). The cooperative Alamouti (Configuration E), however, incurs some extra delay for local information flow, whereas Configurations B and D have double the transmission delay with respect to Configurations A and C due to the half-rate TS STC (equal to 4 sec).

Similar results can be inferred for shadowed Rayleigh fading with $\sigma = 8$ dB (Figure 4.10). It can be concluded that the non-cooperative Configuration C exhibits quite advantageous delay performance. Taking also into account the favorable energy consumption characteristics of Configuration C, similarly to Section 4.3.1, it can be concluded that in a scenario where both of the two communicating sensor nodes are equipped with a switched-antenna system and under spatially independent fading conditions, the communicating pair may benefit by transmitting over only one of the

two antennas while letting the receiver perform AS.

4.4 Conclusions

In this final chapter, we have shown that non cooperative space-time communication is possible for wireless sensor networks via reduced-complexity architectures and space-time codes. More importantly, aside from significant total energy savings, the need for any kind of node synchronization can be avoided with the proposed schemes.

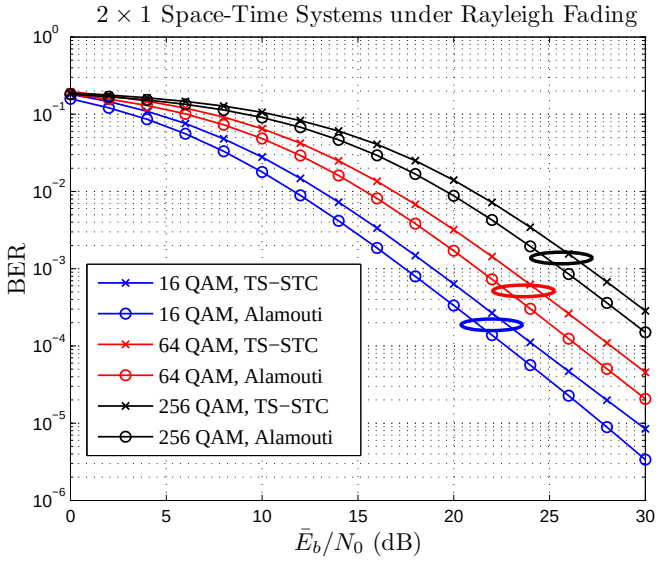

(a)

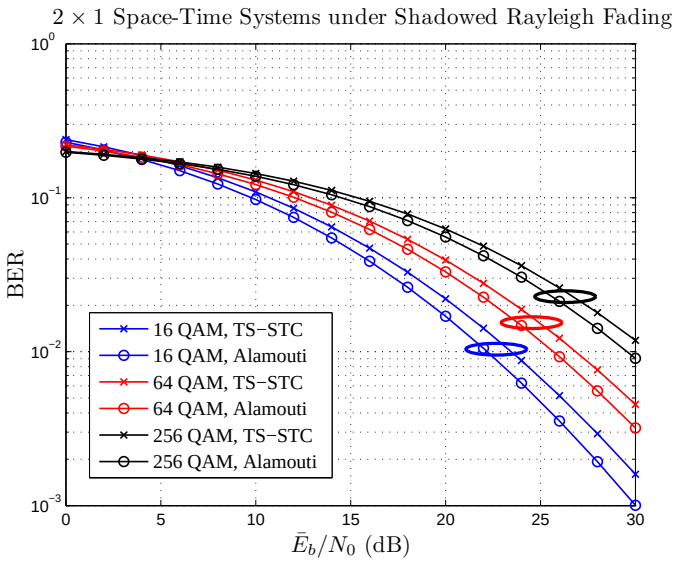

(b)

Figure 4.8: BER for MQAM under (a) Rayleigh fading and (b) shadowed Rayleigh fading based on equation (4.8).

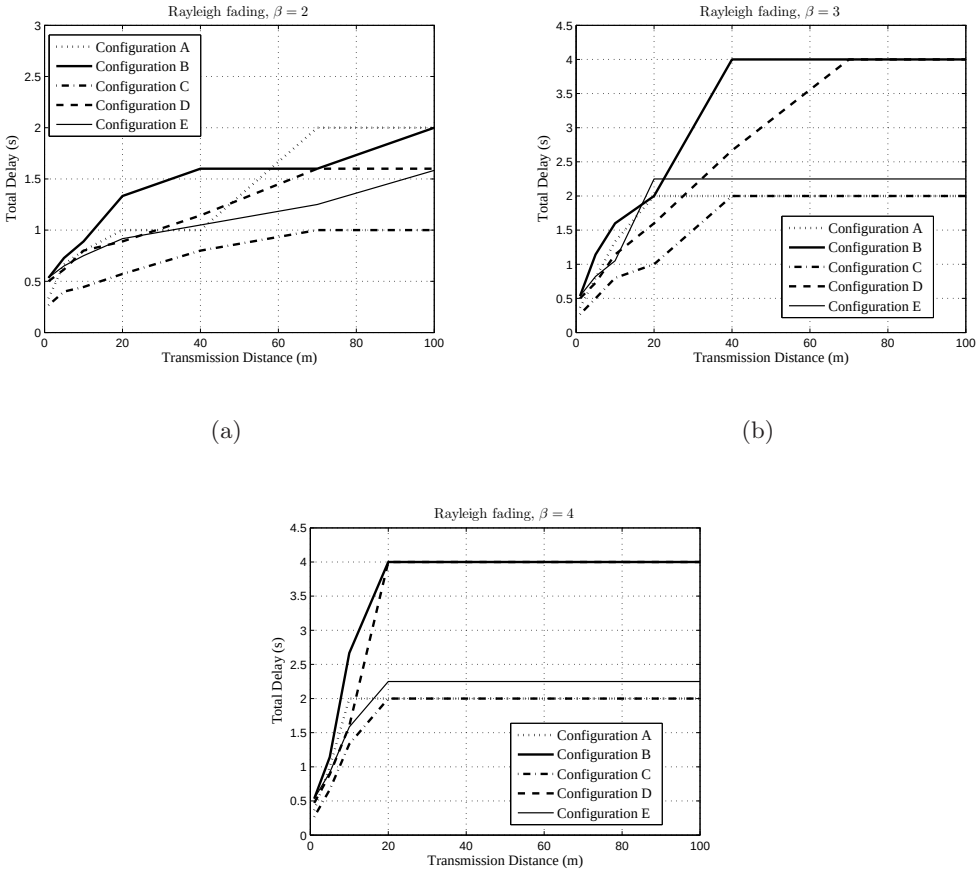

Figure 4.9: Total delay over transmission distance d under Rayleigh fading for variable-rate MQAM and for (a) $\beta = 2$, (b) $\beta = 3$, and (c) $\beta = 4$. Configurations A-D: Non cooperative cases with TS STC and / or receive AS, Configuration E: Cooperative 2×1 Alamouti.

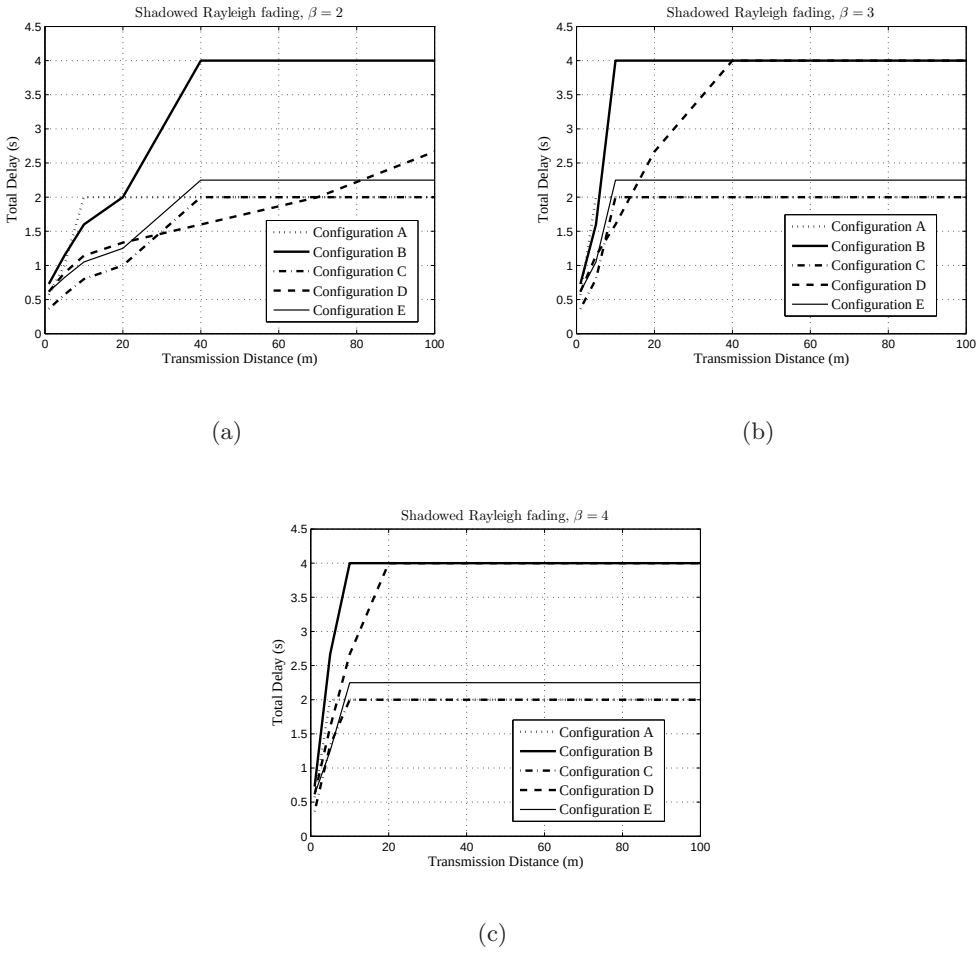

Figure 4.10: Total delay over transmission distance d under shadowed Rayleigh fading ($\sigma = 8$ dB) for variable-rate MQAM and for (a) $\beta = 2$, (b) $\beta = 3$, and (c) $\beta = 4$. Configurations A-D: Non cooperative cases with TS STC and / or receive AS, Configuration E: Cooperative 2×1 Alamouti.

4. NON-COOPERATIVE SPACE-TIME COMMUNICATION FOR ENERGY EFFICIENCY IN SENSOR NETWORKS

5

Epilogue

In this thesis, reduced-complexity wireless transceiver architectures and corresponding techniques have been developed for space-time systems ranging from point-to-point MIMO and multiuser diversity setups to CR and WSN applications.

Chapter 2 introduced MAMP antenna arrays for MIMO and multiuser diversity systems. Specifically, Section 2.1 presented an adaptive MAMP array capable of changing its correlation and matching properties according to the structure of the channel using tunable passive elements. The adaptive MAMP array adapts to the CDI requiring a low-rate feedback from its receiver. Specific adaptive MAMP antenna systems were evaluated under different channel propagation conditions, showing performance gains over classical all-active antenna systems. Further, the proposed adaptive MAMP antenna array addresses the limitations of portable radios regarding size and cost permitting an efficient usage of the spare transmit antennas according to future wireless standards. On the other hand, Section 2.2 proposed SC via optimized realistic receive antenna architectures for compact low-cost UTs in multiuser environments. It has been shown that the proposed compact S-UCA or S-PA antenna systems are able to achieve performance gains (in terms of average throughput) comparable to widely spaced antennas, by properly optimizing the antenna loading conditions for both antenna efficiency and diversity.

Chapter 3 mainly dealt with CR aspects. Section 3.2 provided an overview of the spatial spectrum sensing design challenges for CRs employing OSA. Furthermore, we have proposed novel low-profile frequency-agile antennas for users mobile terminals. The E3SPAR antenna, unlike the classical ESPAR, exploits the mutual coupling between the parasitic elements and the central active one for tuning the operational subband rather than for maximizing the SINR. The resonant frequency is varied in a predetermined fashion by properly controlling the varactor diodes, a task not intended by the classical approach of using the ESPAR antennas with relatively larger inter-element spacing merely for beamsteering applications. Moreover, the narrowband beampatterns are controlled in the analogue domain allowing the tunable cognitive antenna system to exploit the precious spatial resource. Section 3.3 described directional spectrum sensing using such single-radio switched-beam E3SPAR antennas where PU

signal detection is performed on each antenna pattern. The antennas loading conditions have been optimized for maximum average beamforming gain in the beampattern look direction. The simulation results have shown that the average beamforming gain of the beam response can improve the probability of detection of the energy detector by enhancing the SNR at the receiver side. Moreover, by selectively combining the sensing results from the K weakly correlated beampatterns, diversity gains can be added to the cognitive radio system performance. The last part of the chapter (Section 3.4) used the reduced-complexity wireless $(K+1)$-element ESPAR system to proposed orthogonal precoding for suppressing the interference toward a maximum of K single-antenna users. The proposed technique requires a single-radio antenna, whereas the parasitic elements require no extra RF hardware making it a viable option for small terminals where size, cost, and DC power consumption are major constraints.

Finally, Chapter 4 developed a novel modified Alamouti scheme suitable for smart antenna wireless sensor prototypes comprised of a single RF chain. This scheme along with other smart single-radio diversity techniques were shown to exhibit significant circuit and transmission energy savings for WSNs compared to cooperative diversity and traditional SISO configurations. The approach is in accordance with the global green energy effort imposing a need for energy-efficient wireless devices and helps prolong the battery lifetime of energy-constrained sensor nodes.

6

Appendix

Impedance Matrix Calculation

We consider the standard case of arrays comprised of thin half-wavelength dipoles, separated by a distance d. The array can be modeled by an impedance matrix $\mathbf{Z}$. An approached expression of the dipoles self-impedance is given by the impedance of a half-wavelength long isolated dipole [Har78]:

$$\langle \mathbf{Z} \rangle_{ii} = 30 \left[\ln (2\pi n \gamma) - \mathrm{Ci}\,(2\pi n) + \mathrm{j}\,\mathrm{Si}\,(2\pi n) \right], \tag{6.1}$$

where γ is the Euler constant ($\gamma = 0.5772156649...$) and Si and Ci are the sine and cosine integral functions defined as follows

$$\mathrm{Si}\,(x) = \int_0^x \frac{\sin(t)}{t} \cdot dt\,, \tag{6.2}$$

$$\mathrm{Ci}\,(x) = \int_\infty^x \frac{\cos(t)}{t} \cdot dt = \gamma + \ln x + \int_0^x \frac{\cos(t) - 1}{t} \cdot dt\,. \tag{6.3}$$

The coupling-impedance terms $\langle \mathbf{Z} \rangle_{ij} = \mathcal{R}_{ij} + \mathrm{j}\mathcal{X}_{ij},\ \ i \neq j$ are calculated using the induced electromotive force method [KM02]

$$\mathcal{R}_{ij} = \frac{\eta_\mathrm{f}}{4\pi} \left[2\,\mathrm{Ci}\,(u_0) - \mathrm{Ci}\,(u_1) - \mathrm{Ci}\,(u_2) \right] \tag{6.4}$$

$$\mathcal{X}_{ij} = -\frac{\eta_\mathrm{f}}{4\pi} \left[2\,\mathrm{Si}\,(u_0) - \mathrm{Si}\,(u_1) - \mathrm{Si}\,(u_2) \right], \tag{6.5}$$

where $u_0 = \kappa d$, $u_1 = \kappa \left(\sqrt{d^2 + \ell^2} + L \right)$, $u_2 = \kappa \left(\sqrt{d^2 + \ell^2} - L \right)$, $\eta_\mathrm{f} = 120\pi$ is the free-space impedance, $\kappa = 2\pi/\lambda$ is the wavenumber and $L = \lambda/2$ is the dipole length.

Bibliography

[aJHL03] H. Shin and J. H. Lee. Capacity of multiple-antenna fading channels: spatial fading correlation, double scattering, and keyhole. *IEEE Transactions on Information Theory*, 2003. 22

[AKH05] A. H. Al-Ka'bi and J. Homer. Parameters computation of the extended Suzuki mobile fading channel of type II. *IEEE Workshop on Signal Processing Advances in Wireless Communications (SPAWC)*, 2005. 96

[AKPP09a] O. N. Alrabadi, A. Kalis, C. B. Papadias, and R. Prasad. Aerial modulation for high order PSK transmission schemes. *1st International Conference on Wireless Communications, Vehicular Technology, Information Theory and Aerospace & Electronic Systems Technology (Wireless VITAE)*, 2009. 82

[AKPP09b] O. N. Alrabadi, A. Kalis, C. B. Papadias, and R. Prasad. A universal encoding scheme for MIMO transmission using a single active element for PSK modulation schemes. *IEEE Transactions on Wireless Communications*, 2009. 17, 55, 58, 81, 91

[Ala98] S. M. Alamouti. A simple transmit diversity technique for wireless communications. *IEEE Journal on Selected Areas in Communications*, 1998. 90

[ALP04] D. Avidor, J. Ling, and C. Papadias. Jointly opportunisitic beamforming and scheduling for downlink packet access. *IEEE International Conference on Communications (ICC)*, 2004. 34

[Alr11] O. N. Alrabadi. MIMO communication using single feed antenna arrays. *PhD Dissertation, Aalborg Universitet*, 2011. 8, 35, 45

[APCK12] O. N. Alrabadi, J. Perruisseau-Carrier, and A. Kalis. MIMO transmission using a single RF source: Theory and antenna design. *IEEE Transactions on Antennas and Propagation*, 2012. 49

[APK+09] O. N. Alrabadi, C. B. Papadias, A. Kalis, N. Marchetti, and R. Prasad. MIMO transmission and reception techniques using three-element ESPAR antennas. *IEEE Communications Letters*, 2009. 17

BIBLIOGRAPHY

[BA08] E. Beres and R. Adve. Selection cooperation in multi-source cooperative networks. *IEEE Transactions on Wireless Communications*, 2008. 9

[Bai08] R. Bains. On the usage of parasitic antenna elements in wireless communication systems. *PhD Thesis, Norwegian University of Science and Technology*, 2008. 9

[BB82] P. Bhartia and I. J. Bahl. A frequency agile microstrip antenna. *Antennas Propagation Society International Symposium*, 1982. 17

[BCC04] D. Bliss, A. Chan, and N. Chang. MIMO wireless communication channel phenomenology. *IEEE Transactions on Antennas and Propagation*, 2004. 22

[BFBS02] S. Bellofiore, J. Foutz, C. A. Balanis, and A. S. Spanias. Smart-antenna system for mobile communication networks. Part 2. Beamforming and network throughput. *IEEE Antennas and Propagation Magazine*, 2002. 1

[BGN00] R. H. Byrd, J. C. Gilbert, and J. Nocedal. A trust region method based on interior point techniques for nonlinear programming. *Mathematical Programming*, 2000. 32, 43

[BKSK10] V. Barousis, A. G. Kanatas, N. D. Skentos, and A. Kalis. Pattern diversity for single RF user terminals in multiuser environments. *IEEE Communications Letters*, 2010. 35

[BRJ08] V. Blaschke, T. Renk, and F. K. Jondral. A cognitive radio receiver supporting wide-band sensing. *IEEE International Conference on Communications (ICC) Workshops*, 2008. 59

[Bro58] E. T. Browne. Introduction to the Theory of Determinants and Matrices. *University of North Carolina*, 1958. 22

[BS07] R. Bosisio and U. Spagnolini. On the sum-rate of opportunistic beamforming schemes with multiple antennas at the receiver. *IEEE International Conference on Communications (ICC)*, 2007. 34, 45

[Caf98] R. E. Caflisch. Monte Carlo and quasi-Monte Carlo methods. 1998. 25

[CCV01] M. Chiani, A. Conti, and R. Verdone. Partial compensation signal-level-based up-link power control to extend terminal battery duration. *IEEE Transactions on Vehicular Technology*, 2001. 95

[CG01] S. T. Chung and A. J. Goldsmith. Degrees of freedom in adaptive modulation: A unified view. *IEEE Transactions on Communications*, 2001. 97

[CGB04] S. Cui, A. J. Goldsmith, and A. Bahai. Energy-efficiency of MIMO and cooperative MIMO techniques in sensor networks. *IEEE Journal on Selected Areas Communications*, 2004. 2, 3, 89, 90, 95, 97, 98

[CGB05] S. Cui, A. J. Goldsmith, and A. Bahai. Energy-constrained modulation optimization. *IEEE Transactions on Wireless Communications*, 2005. 95, 98

[CL09] C. Chang and Y. Lee. Opportunistic beamforming systems with diversity combining. *7th International Conference on Information, Communications and Signal Processing*, 2009. 34

[CO07] B. Clerckx and C. Oestges. *MIMO Wireless Communication, From Real-World Propagation to Space-Time Code Design*. 2007. 20, 21, 22

[Com02] Federal Communications Commission. Spectrum Policy Task Force Report (ET Docket no. 02-135). 2002. 53

[CS03] G. Caire and S. Shamai. On the achievable throughput of a multiantenna Gaussian broadcast channel. *IEEE Transactions on Information Theory*, 2003. 33

[CT06] T. M. Cover and J. A. Thomas. Elements of Information Theory. 2006. 22

[CWC07] A. Conti, M. Z. Win, and M. Chiani. Slow adaptive M-QAM with diversity in fast fading and shadowing. *IEEE Transactions on Communications*, 2007. 97

[DAS03] F. F. Digham, M.-S. Alouini, , and M. K. Simon. On the energy detection of unknown signals over fading channels. *IEEE International Conference on Communications (ICC)*, 2003. 74

[DAS07] F. F. Digham, M.-S. Alouini, and M. K. Simon. On the energy detection of unknown signals over fading channels. *IEEE Transactions on Communications*, 2007. 70, 74

[DCBV07] D. Dardari, A. Conti, C. Buratti, and R. Verdone. Mathematical evaluation of environmental monitoring estimation error through energy-efficient wireless sensor networks. *IEEE Transactions Mobile Computing*, 2007. 91, 96

[DM10] K.-L. Du and W. H. Mow. Affordable cyclostationarity-based spectrum sensing for cognitive radio with smart antennas. *IEEE Transactions on Vehicular Technology*, 2010. 70

[Erc04] V. Erceg. TGn channel models: IEEE 802.11 standard contribution 802.11-03/940r4. 2004. 24, 80

[EYT91] Y. Ebine, Y. Yamada, and T. Takahash. Study of vertical space diversity for land mobile radio. *Electronics and Communications in Japan*, 1991. 16

[Fei08] Y. Fei. Compact MIMO terminals with matching networks. *PhD Thesis, The University of Edinburgh*, 2008. 18

[FFLT08] Y. Fei, Y. Fan, B. K. Lau, and J. Thompson. Optimal single-port matching impedance for capacity maximization in compact MIMO arrays. *IEEE Transactions on Antennas and Propagation*, 2008. 16

[FGJF08] F. Fazel, A. Grau, H. Jafarkhani, and F. De Flaviis. Space-time block coded reconfigurable MIMO communication system using ORIOL antennas. *IEEE Wireless Communications and Networking Conference (WCNC)*, 2008. 91

[Fos96] G. J. Foschini. Layered space-time architecture for wireless communication in a fading environment when using multi-element antennas. *Bell Laboratories Technical Journal*, 1996. 23

[FTH+99] B. H. Fleury, M. Tschudin, R. Heddergott, D. Dahlhaus, and K. Ingeman Pedersen. Channel parameter estimation in mobile radio environments using the SAGE algorithm. *IEEE Journal on Selected Areas in Communications*, 1999. 24

[Gar91] W. A. Gardner. Exploitation of spectral redundancy in cyclostationary signals. *IEEE Signal Processing Magazine*, 1991. 70

[GF98] M. J. Gans and G. J. Foschini. Limits of wireless communication in a fading environment when using multiple antennas. *Wireless Personal Communications*, 1998. 1, 16

[GHH+08] P. Gardner, M. R. Hamid, P. S. Hall, J. Kelly, F. Ghanem, and E. Ebrahimi. Reconfigurable antennas for cognitive radio: Requirements and potential design approaches. *IET Seminar on Wideband, Multiband Antennas and Arrays for Defence or Civil Applications*, 2008. 54, 59, 60

[GJMS09] A. Goldsmith, S. A. Jafar, I. Maric, and S. Srinivasa. Breaking spectrum gridlock with cognitive radios: An information theoretic perspective. *Proceedings of the IEEE*, 2009. 2, 53

[GNP03] D. Gore, R. Nabar, and A. Paulraj. *Introduction to Space-Time Wireless Communications*. 2003. 22, 23, 89, 97

[GR00] I. S. Gradshteyn and I. M. Ryzhik. Table of Integrals, Series, and Products. *6th ed. San Diego, CA: Academic*, 2000. 74, 75

[GRJF05] A. Grau, J. Romeu, L. Jofre, and F. De Flaviis. On the polarization diversity gain using the ORIOL antenna in fading indoor environments. *IEEE Antennas and Propagation Society International Symposium*, 2005. 90

[Har78] R. F. Harrington. Reactively controlled directive arrays. *IEEE Transactions on Antennas and Propagation*, 1978. 113

[Hay05] S. Haykin. Cognitive radio: Brain-empowered wireless communications. *IEEE Journal of Selected Areas in Communications*, 2005. 2, 53

[HDL07] S. Huang, Z. Ding, and X. Liu. Non-intrusive cognitive radio networks based on smart antenna technology. *IEEE Global Telecommunications Conference (GLOBECOM)*, 2007. 70

[HKCK97] P. S. Hall, S. D. Kapoulas, R. Chauhan, and C. Kalialakis. Microstrip patch antenna with integrated adaptive tuning. *10th International Conference on Antennas and Propagation*, 1997. 17

[HM71] R. F. Harrington and J. R. Mautz. Theory of characteristic modes for conducting bodies. *IEEE Transactions on Antennas and Propagation*, 1971. 50

[HNT+07] N. Honma, K. Nishimori, Y. Takatori, A. Ohta, and S. Kubota. Proposal of compact MIMO terminal antenna employing Yagi-Uda array with common director elements. *IEEE Antennas and Propagation Society International Symposium*, 2007. 17

[HSB+06] M. A. Hein, R. Stephan, K. Blau, C. Volmer, and J. Weber. Miniaturized antenna arrays using decoupling networks with realistic elements. *IEEE Transactions on Microwave Theory and Techniques*, 2006. 16, 35

[IWF02] T. Itoh, Y. Wang, and J. D. Fredrick. A smart antenna receiver array using a single RF channel and digital beamforming. *IEEE Transactions on Microwave Theory and Techniques*, 2002. 9

[Jay06] S. K. Jayaweera. Virtual MIMO-based cooperative communication for energy-constrained wireless sensor networks. *IEEE Transactions on Wireless Communications*, 2006. 2, 89, 90, 95, 98

[Jay07] S. K. Jayaweera. V-BLAST-based virtual MIMO for distributed wireless sensor networks. *IEEE Transactios on Communications*, 2007. 98

[JM05] M. A. Jensen and M. L. Morris. Modeling front-end signal coupling in MIMO systems. *IEEE Wireless Communications and Applied Computational Electromagnetics*, 2005. 3

BIBLIOGRAPHY

[Kay98] S. M. Kay. Fundamentals of Statistical Signal Processing: Detection Theory. *Prentice Hall*, 1998. 70

[KD05] A. Kalis and T. Dimitriou. Fast routing in wireless sensor networks using directional transmissions. *International Journal on Mobile Network Design and Innovation*, 2005. 94

[KEH+08] J. Kelly, E. Ebrahimi, P. S. Hall, P. Gardner, and F. Ghanem. Combined wideband and narrowband antennas for cognitive radio applications. *IET Seminar on Cognitive Radio and Software Defined Radios: Technologies and Techniques*, 2008. 60

[KKOC10] A. Kounoudes, A. Kalis, T. Onoufriou, and A. G. Constantinides. Smart wireless sensor technology for continuous health monitoring of structures. *International Conference on Bridge Maintenance, Safety, and Management (IABMAS)*, 2010. 90, 93

[KM02] J. D. Kraus and R. J. Markhefka. Antenna for all applications. *3rd ed. Upper Saddle River, NJ: McGraw Hill*, 2002. 113

[Kos02] V. I. Kostylev. Energy detection of a signal with random amplitude. *IEEE International Conference on Communications (ICC)*, 2002. 70, 75

[KSP+02] J. Kermoal, L. Schumacher, K. Pedersen, P. Mogensen, and F. Frederiksen. A stochastic MIMO radio channel model with experimental validation. *IEEE Journal on Selected Areas in Communications*, 2002. 22

[LB03] R. G. Lorenz and S. P. Boyd. Robust minimum variance beamforming. *37th Asilomar Conference on Signals, Systems and Computers*, 2003. 82

[LCL05] X. Li, M. Chen, and W. Liu. Application of STBC-encoded cooperative transmissions in wireless sensor networks. *IEEE Signal Processing Letters*, 2005. 2, 3, 89, 90

[Lee98] T. H. Lee. The Design of CMOS Radio-Frequency Integrated Circuits. *Cambridge, U.K.: Cambridge University Press*, 1998. 98, 99

[LGL10] H. Liu, S. Gao, and T. Hong Loh. Frequency agile small smart antenna. *4th European Conference on Antennas and Propagation (EuCAP)*, 2010. 9

[LK04] D. Leang and A. Kalis. Smart SensorDVB: Sensor network development boards with smart antennas. *International Conference on Communications, Circuits, and Systems (ICCCAS)*, 2004. 90, 93

[LOKM05] B. K. Lau, S. M. S. Ow, G. Kristensson, and A. F. Molisch. Capacity analysis for compact MIMO systems. *IEEE Vehicular Technology Conference (VTC)*, 2005. 16

[LPB00] P. Laspougeas, P. Pajusco, and J.-C. Bic. Radio propagation in urban small cells environment at 2 GHz: Experimental spatio-temporal characterization and spatial wideband channel model. *IEEE Vehicular Technology Conference (VTC)*, 2000. 29

[LPL06] D. Livezey, A. Pham, and C. Lu. On the feasibility of CMOS multiband phase shifters for multiple-antenna transmitters. *IEEE Microwave and Wireless Components Letters*, 2006. 7

[LRWW98] J. C. Lagarias, J. A. Reeds, M. H. Wright, and P. E. Wright. Convergence properties of the Nelder-Mead simplex method in low dimensions. *Society of Industrial and Adaptive Mathematics (SIAM) J. Optimization*, 1998. 75, 84

[lte] 3rd Generation partnership project. 17, 28

[mat] The Mathworks, Natick MA. 32, 43, 84

[MKAL06] A. F. Molisch, G. Kristensson, J. B. Andersen, and B. K. Lau. Impact of matching network on bandwidth of compact antenna arrays. *IEEE Transactions on Antennas and Propagation*, 2006. 3, 16, 35, 45

[MT10] R. Mohammadkhani and J. S. Thompson. Adaptive matching for compact MIMO systems. *7th International Symposium on Wireless Communication Systems (ISWCS)*, 2010. 47

[Nar06] R. Narasimhan. Transmit antenna selection based on outage probability for correlated MIMO multiple access channels. *IEEE Transactions on Wireless Communications*, 2006. 23, 24

[OG00] T. Ohira and K. Gyoda. Design of electronically steerable passive array radiator (ESPAR) antennas. *IEEE Antennas and Propagation Society International Symposium*, 2000. 7, 17, 55, 56, 58, 81

[OHW+03] H. Ozcelik, M. Herdin, W. Weichselberger, J. Wallace, and E. Bonek. Deficiencies of 'Kronecker' MIMO radio channel model. *Electronic Letters*, 2003. 22

[OI04] T. Ohira and K. Iigusa. Electronically steerable parasitic array radiator antenna. *Electronics and Communications in Japan*, 2004. 55

[Orp08] S. J. Orphanides. Electromagnetic Waves and Antennas. *Rutgers University*, 2008. 4

[OY06] T. H. ODonnell and A. D. Yaghjian. Electrically small superdirective arrays using parasitic elements. *IEEE Antennas and Propagation Society International Symposium*, 2006. 61, 63

BIBLIOGRAPHY

[PBRP+98] C. Puente-Baliarda, J. Romeu, R. Pous, J. Ramis, and A. Hijazo. Small but long Koch fractal monopole. *Electronics Letters*, 1998. 94

[PDL06] L. Petit, L. Dussopt, and J. Laheurte. MEMS-Switched parasitic-antenna array for radiation pattern diversity. *IEEE Transactions on Antennas and Propagation*, 2006. 4, 68

[Pin07] D. Pinchera. The adaptive MIMO antenna: A novel low-cost reconfigurable array for MIMO systems. *PhD Thesis, University of Cassino*, 2007. 8

[PKP07] M. Pun, V. Koivunen, and H. V. Poor. Opportunistic scheduling and beamforming for MIMO-SDMA downlink systems with linear combining. *IEEE International Symposium on Personal, Indoor and Mobile Radio Communications (PIMRC)*, 2007. 34, 43

[Poz94] D. M. Pozar. The active element pattern. *IEEE Transactions on Antennas and Propagation*, 1994. 18

[Poz05] D. M. Pozar. Microwave Engineering. *John Wiley & Sons*, 2005. 40

[Pro00] J. G. Proakis. Digital Communications. *4th ed. New York: McGraw-Hill*, 2000. 98

[Ree02] J. H. Reed. Software radio: a modern approach to radio engineering. *A division of Pearson Education Inc.*, 2002. 18, 19

[RHR96] O. Rostbakken, G. S. Hilton, and C. J. Railton. An adaptive microstrip patch antenna for use in portable transceivers. *IEEE Vehicular Technology Conference (VTC)*, 1996. 17

[RK89] R. Roy and T. Kailath. ESPRIT-Estimation of signal parameters via rotational invariance techniques. *IEEE Transactions on Acoustics, Speech and Signal Processing*, 1989. 24

[RK05] K. Rosengren and P.-S. Kildal. Radiation efficiency, correlation, diversity gain and capacity of a six-monopole antenna array for a MIMO system: theory, simulation and measurement in reverberation chamber. *IEE Microwaves, Antennas and Propagation*, 2005. 19, 20

[RS01] A. Ranheim and T. Svantesson. Mutual coupling effects on the capacity of multielement antenna systems. *IEEE International Conferene on Acoustics Speech and Signal Processing (ICASSP)*, 2001. 16

[SA05] M. K. Simon and M.-S. Alouini. Digital Communication over Fading Channels. *John Wiley & Sons*, 2005. 44

[Sch04] R. W. Schlub. Practical realization of switched and adaptive parasitic monopole radiating structures. *PhD Thesis, Griffith University*, 2004. 20, 21

[SCL+09] C. Stevenson, G. Chouinard, Z. Lei, W. Hu, S. Shellhammer, and W. Caldwell. IEEE 802.22: The first cognitive radio wireless regional area network standard. *IEEE Communications Magazine*, 2009. 54, 59

[SFGK00] D. S. Shiu, G. J. Foschini, M. J. Gans, and J. M. Kahn. Fading correlation and its effect on the capacity of multielement antenna systems. *IEEE Transactions on Communications*, 2000. 21, 36, 79

[SH05] M. Sharif and B. Hassibi. On the capacity of MIMO broadcast channels with partial side information. *IEEE Transactions on Information Theory*, 2005. 2, 34

[SHMM11] H. Sarvanko, M. Hoyhtya, M. Matinmikko, and A. Mammela. Exploiting spatial dimension in cognitive radios and networks. *6th International ICST Conference on Cognitive Radio Oriented Wireless Networks and Communications (CROWNCOM)*, 2011. 70

[SHOK04] C. Sun, A. Hirata, T. Ohira, and N.C. Karmakar. Fast beamforming of electronically steerable parasitic array radiator antennas: theory and experiment. *IEEE Transactions on Antennas and Propagation*, 2004. 7, 17, 55, 57, 58, 81, 83

[SJJS00] Q. H. Spencer, B. D. Jeffs, M. A. Jensen, and A. L. Swindlehurst. Modeling the statistical time and angle of arrival characteristics of an indoor multipath channel. *IEEE Journal in Selected Areas on Communications*, 2000. 26, 28, 29

[SML+02] M. Steyaert, B. De Muer, P. Leroux, M. Borremans, and K. Mertens. Low-voltage low-power CMOS-RF transceiver design. *IEEE Transactions on Microwave Theory and Techology*, 2002. 98

[SN04] S. Sanayei and A. Nosratinia. Antenna selection in MIMO systems. *IEEE Communications Magazine*, 2004. 8

[SPM06] F. Schettino, D. Pinchera, and M. D. Migliore. Improving channel capacity using adaptive MIMO antennas. *IEEE Transactions on Antennas and Propagation*, 2006. 8, 17

[SST06] W. L. Schroeder, P. Schmitz, and C. Thome. Miniaturization of mobile phone antennas by utilization of chassis mode resonances. *German Microwave Conference*, 2006. 50

[SXK97] P. J. Sullivan, B. A. Xavier, and W. H. Ku. Low voltage performance of a microwave CMOS Gilbert cell mixer. *IEEE Journal on Solid-Sate Circuits*, 1997. 98

[Tan06] N. Tanzi. Varactor-tuned coupled resonator front-end bandpass filters for cognitive radio applications. *IEEE Radio and Wireless Symposium*, 2006. 59

[TAPP10a] E. P. Tsakalaki, O. N. Alrabadi, C. B. Papadias, and R. Prasad. An adaptive reactance-assisted antenna system for the MIMO uplink. *17th IEEE International Conference on Electronics, Circuits, and Systems (ICECS)*, 2010. 12

[TAPP10b] E. P. Tsakalaki, O. N. Alrabadi, C. B. Papadias, and R. Prasad. Enhanced selection combining for compact single rf user terminals in multiuser diversity systems. *IEEE International Symposium on Personal, Indoor, and Mobile Radio Communications (PIMRC)*, 2010. 12, 34, 45

[TAPP10c] E. P. Tsakalaki, O. N. Alrabadi, C. B. Papadias, and R. Prasad. Spatial spectrum sensing for cognitive radios via miniaturized parasitic antenna systems. *5th International ICST Conference on Cognitive Radio Oriented Wireless Networks and Communications (CROWNCOM)*, 2010. 9, 12, 70, 81

[TAPP10d] E. P. Tsakalaki, O. N. Alrabadi, C. B. Papadias, and R. Prasad. Spatial spectrum sensing for wireless handheld terminals: Design challenges and novel solutions based on tunable parasitic antennas [dynamic spectrum management]. *IEEE Wireless Communications Magazine*, 2010. 9, 11, 12, 34, 70, 81

[TAPP11a] E. P. Tsakalaki, O. N. Alrabadi, C. B. Papadias, and R. Prasad. Adaptive reactance-controlled antenna systems for MIMO applications. *IET Microwave Antennas & Propagations Journal, Special issue on RF/Microwave Communication Subsystems for Emerging Wireless Technologies*, 2011. 11, 12

[TAPP11b] E. P. Tsakalaki, O. N. Alrabadi, C. B. Papadias, and R. Prasad. Analogue orthogonal precoding using reduced complexity transceivers. *IEEE International Symposium on Antennas and Propagations*, 2011. 12

[TAPP12a] E. P. Tsakalaki, O. N. Alrabadi, C. B. Papadias, and R. Prasad. Non cooperative space-time communication for energy efficiency in sensor networks. *IEEE Transactions on Communications*, 2012. 11, 12

[TAPP12b] E. P. Tsakalaki, O. N. Alrabadi, C. B. Papadias, and R. Prasad. Reduced-complexity radio architectures for enhanced receive selection combining in

multiuser diversity systems. *International Journal of Antennas and Propagation, Special Issue on MIMO Antenna Design and Channel Modeling*, 2012. 11, 12

[Tel99] I. E. Telatar. Capacity of multi-antenna gaussian channels. *Wireless Personal Communications*, 1999. 1

[Thi04] D. V. Thiel. Switched parasitic antennas and controlled reactance parasitic antennas: A systems comparison. *IEEE Antennas and Propagation Society Symposium*, 2004. 34, 40

[TLV05] A. M. Tulino, A. Lozano, and S. Verdu. Impact of antenna correlation on the capacity of multi-antenna channels. *IEEE Transactions on Information Theory*, 2005. 3, 16

[TS88] J. Tsao and B. D. Steinberg. Reduction of sidelobe and speckle artifacts in microwave imaging: The CLEAN technique. *IEEE Transactions on Antennas and Propagation*, 1988. 24

[TWdCR12] E. P. Tsakalaki, D. Wilcox, E. de Carvalho, and C. B. Papadias T. Ratnarajah. Spectrum sensing using single-radio switched-beam antenna systems. *7th International ICST Conference on Cognitive Radio Oriented Wireless Networks and Communications (CROWNCOM)*, 2012. 11, 12, 81

[TZNZ09] K. H. Teo, H. Zhang, Y. N. Nakache, and J. Zhang. Space-time-frequency sensing of RF spectrum in cognitive radios. *United States Patent 7610036*, 2009. 58, 61

[VA87] R. Vaughan and J. B. Andersen. Antenna diversity in mobile communications. *IEEE Transactions on Vehicular Technology*, 1987. 39, 40, 44

[VA03] R. Vaughan and J. B. Andersen. Channels, Propagation and Antennas for Mobile Communications. *IEE Electromagnetic Waves Series, Institution of Electrical Engineers*, 2003. 72

[Vau98] R. Vaughan. Switched parasitic elements for antenna diversity. *IEEE Transactions on Antennas and Propagations*, 1998. 8, 18, 34

[VG06] D. Veronesi and D. L. Goeckel. Multiple frequency offset compensation in cooperative wireless systems. *IEEE Global Communications Conference (GLOBECOM)*, 2006. 3

[VP07] M. Vu and A. Paulraj. MIMO wireless linear precoding. *IEEE Signal Processing Magazine*, 2007. 20

BIBLIOGRAPHY

[VTL02] P. Viswanath, D. Tse, and R. Laroia. Opportunistic beamforming using dumb antennas. *IEEE Transactions on Information Theory*, 2002. 2, 34

[VY03] B. Vucetic and J. Yuan. Space-Time Coding. *Wiley InterScience*, 2003. 89, 90, 92

[Whe47] H. A. Wheeler. Fundamental limitations of small antennas. *Proceedings of the Institute of Radio Engineers (IRE)*, 1947. 63

[WIK04] Y. Wang, T. Itoh, and S. Kim. A compact realization of antenna arrays for mobile communications. *IEEE Vehicular Technology Conference (VTC)*, 2004. 9

[WJ04] J. W. Wallace and M. A. Jensen. Termination-dependent diversity performance of coupled antennas: Network theory analysis. *IEEE Transactions on Antennas and Propagation*, 2004. 16

[WJ09] J. W. Wallace and M. A. Jensen. Sparse power angle spectrum estimation. *IEEE Transactions on Antennas and Propagations*, 2009. 24

[WMNO06] R. A. Waltz, J. L. Morales, J. Nocedal, and D. Orban. An interior algorithm for nonlinear optimization that combines line search and trust region steps. *Mathematical Programming*, 2006. 32, 43

[WPS+00] S. Willingham, M. Perrott, B. Setterberg, A. Grzegorek, and B. McFarland. An integrated 2.5 GHz frequency synthesizer with 5 s settling and 2 Mb/s closed loop modulation. *IEEE International Solid-State Circuits Conference (ISSCC)*, 2000. 98

[WS95] W. T. Webb and R. Steele. Variable rate QAM for mobile radio. *IEEE Transactions on Communications*, 1995. 97

[xbo] Wireless measurement system MICA2. *Crossbow Technology Inc., 1421 McCarthy Boulevard, Milpitas, CA 95035*. 94

[XC07] K. Xu and D. Chizuni. A V-BLAST based virtual MIMO transmission scheme for sensor network lifetime maximization. *IEEE Vehicular Technology Conference (VTC)*, 2007. 98

[YA09] T. Yucek and H. Arslan. A survey of spectrum sensing algorithms for cognitive radio applications. *IEEE Communication Surveys and Tutorials*, 2009. 2, 58, 59, 60, 70

[YBO+01] K. Yu, M. Bengtsson, B. Ottersten, D. McNamara, P. Karlsson, and M. Beach. Second order statistics of NLOS indoor MIMO channels based on 5.2 GHz measurements. *IEEE Global Communications Conference (GLOBECOM)*, 2001. 22

[YG06a] T. Yoo and A. Goldsmith. On the optimality of the multi-antenna broadcast scheduling using zero-forcing beamforming. *IEEE Journal on Selected Areas in Communications*, 2006. 33

[YG06b] T. Yoo and A. Goldsmith. On the optimality of the multi-antenna broadcast scheduling using zero-forcing beamforming. *IEEE Journal on Selected Areas in Communications*, 2006. 82

[ZJ05] L. Zan and S. A. Jafar. Combined opportunistic beamforming and receive antenna selection [cellular downlink applications]. *IEEE Wireless Communications and Networking Conference*, 2005. 34

[ZLLZ10] R. Zhang, T. Lim, Y.-C. Liang, and Y. Zeng. Multi-antenna based spectrum sensing for cognitive radios: A GLRT approach. *IEEE Transactions on Communications*, 2010. 2, 70

[ZLPH09] Y. Zeng, Y.-C. Liang, E. C. Y. Peh, and A. T. Hoang. Cooperative covariance and eigenvalue based detections for robust sensing. *IEEE Global Communications Conference (GLOBECOM)*, 2009. 2, 70